Inaugural-Dissertation

zur Erlangung der Doktorwürde der Naturwissenschaftlich-Mathematischen Gesamtfakultät der Ruprecht-Karls-Universität Heidelberg

vorgelegt von
Diplom-Physiker Stefan Knauf
aus Rom

Tag der mündlichen Prüfung: 19. Juli 2011

Numerical simulations for ball bearings considering fluid-structure interaction problems and non-Newtonian fluids with a free boundary

Gutachter: Prof. Dr. Dr. h.c. Rolf Rannacher

Gutachter: Prof. Dr. Dr. h.c. mult. Willi Jäger

Abstract

In this thesis a novel approach for the simulation of elastohydrodynamic problems is established. It is novel in modeling the fluid as non-Newtonian with a free boundary and considering fluid-structure interaction at the same time.
We present a robust numerical algorithm for the simulation of problems of such type. Furthermore, we analyze the difficulties and propose some improvements for treating the free boundary as well as the non-Newtonian flow numerically. We adress modeling aspects and model uncertainties with respect to material models, parameters and experimental investigations.
For validation, we compare the numerical approximations with a widely accepted analytic approximation from engineering literature and achieve a reasonable accuracy. We conclude by bringing the thesis in relation with interesting further points of investigation on the basis of the established methods which rely on the novel modeling in this thesis.

Zusammenfassung

In dieser Arbeit wird ein neuartiger Ansatz zur Simulation von elastohydrodynamischen Problemen vorgestellt. Dieser Ansatz ist neuartig, da das Fluid als nicht-Newtonisch und mit freiem Rand modelliert wird und gleichzeitig Fluid-Struktur-Interaktion betrachtet wird.
Wir stellen einen robusten numerischen Algorithmus für die Simulation solcher Probleme vor. Weiterhin analysieren wir die Schwierigkeiten und schlagen einige Verbesserungsmöglichkeiten bei der Simulation von nicht-Newtonischen Fluiden sowie freien Randwertproblemen vor. Modellierungsaspekte und Modellunsicherheiten bezüglich der Materialgleichungen, Parameter und der experimentellen Untersuchungen werden thematisiert.
Für Zwecke der Validierung werden die numerischen Lösungen mit einer in der ingenieurswissenschaftlichen Literatur weit verbreiteten und akzeptierten Näherung verglichen und man stellt eine gute Übereinstimmung fest. Wir diskutieren die erreichten Ergebnisse und schlagen auf dieser Basis weitere interessante Themen für künftige Arbeiten vor, die auf der neuartigen Modellierung dieser Arbeit beruhen.

Contents

Chapter 1

Introduction

In this thesis numerical methods are presented for the simulation of lubrication flow and fluid-structure interaction in ball bearings. This is known in literature as "elastohydrodynamic" lubrication problem. We consider a generalized Newtonian fluid modelled by a Navier-Stokes system with pressure-dependent viscosity. Furthermore a method will be presented, allowing not to fix a constant underlying domain in the beginning, but to consider a free boundary value problem. Instead of neglecting the important aspect of fluid-structure interaction or to treat it with simple ad-hoc models, we use a fundamental fluid-structure interaction formulation derived from basic continuum mechanical laws. Former work in this field of research has thereby tended to base all studies on considerably simplified models. For instance, in most cases an approximation for thin lubrication films, called Reynolds' equation, is used instead of the Navier-Stokes equations. In addition in most former work available in literature at most one of the above aspects, non-Newtonian flow, fluid-structure interaction or free boundary value problems is considered. To the knowledge of the author, the present thesis is the first one to consider *all* aspects at the same time.
In addition, no simplification with respect to geometry is done but the equations will be solved on the complicated ball bearing domain (in two dimensions).
All of the generalizations and allowed pathologies of the problem stated above lead to difficulties of very distinct nature.

- The fluid domain in a ball bearing possesses a free boundary, its shape is not known a priori. In distinction to most other work on lubrication problems this aspect will be covered in this thesis and is described in chapter 2. In

this context we propose a new fully implicit manner of discretization and verify it with a simple benchmark example. For the simulations concerning the ball bearing it turns out that the free boundary has only small impact on the local balance of forces so that it can indeed in some situations be justified to neglect it. There is yet an indirect influence on the system which will be explained. As we are not interested in complex models for its own sake we will also sometimes neglect the free boundary. However the methodology of this thesis is different to other work in that simplifications of the model are only performed if numerical tests indicate them to be well justified.

- The non-Newtonian character of the fluid leads to mathematical difficulties when we try to formulate a well-posed problem. At this point there is a gap between mathematical theory and those fluid models used and preferred in applications. The resulting difficulties in this context and a comparison between theoretically well-founded models, for which a proof of existence is known and the ones from applications will be given in chapter 3. This chapter depicts an attempt to diminish this gap: Different regularizations of the problem leading to its numerical solvability will be presented and their precise effect on the numerical scheme will be tested.

- In a ball bearing, locally very high pressure arises leading to a deformation of the surrounding structure. Often this fact is neglected at all and, if not, mostly simple and imprecise models for the balance of forces between structure and fluid are used. This stems from the fact that already for the fluid the thin film approximation, Reynolds' equation, is adopted. Therefore information about forces on the fluid are difficult to retrieve. The present thesis is, to the knowledge of the author, the first one considering a fluid-structure interaction problem based on fundamental models without simplifications for fluid and structure in the context of elastohydrodynamics. The fluid has a viscosity depending on pressure, concerning the structure we deal with a (nonlinear) material model of St.-Venant-Kirchhoff type. The numerical treatment of fluid-structure interaction problems on its own is a subject of current research, in this specific case of application there exist further different problems and details worth considering which will be reviewed in chapter 4.

- The domain on which the fluid equations for the physical processes in a ball

bearing are posed has an extremely anisotropic shape. The film thickness of the surrounding fluid is at most of the order of some μm whereas the radius of the ball amounts to some mm. This results in a high imbalance in the volume of the fluid and the structure domain respectively. In order to perform a discretization we need a grid which at least roughly accounts for this extreme geometry. The generation of such a grid with some size and shape regularity at any rate requires a lot of work. Furthermore the necessity for anisotropic mesh cells causes a variety of problems for the numerical scheme. These difficulties will be brought up at several instances throughout this thesis though they are not accessible directly to a true "solution". As long as we keep to work on the real physical domain without rude simplifications we have to deal with such problems. Related questions will be subject of chapter 5.

- Any realistic modeling of fluids in ball bearings will inevitably lead to equations for which no rigorous mathematical theory of existence and uniqueness of solutions is available. Therefore it is especially important in this field to be able to judge the quality of the numerical approximation. Firstly we will compare our simulations with one reference problem for which also experimental data can be found in literature and achieve a high degree of agreement. Secondly we show simulation results for a ball bearing. For this purpose a precise definition of the problem, the geometry and all relevant parameters is necessary and will be explicated in chapter 6.

- In this thesis a novel approach to elastohydrodynamic lubrication is presented. The results in the context of existing methods as well as interesting questions for further research are discussed in chapter 7.

In this thesis all of the problem aspects stated above as well as strategies for its solution will be considered and analyzed. Simplifications of the model will only be made if they show up as insignificant for the quantitative results of the numerical approximation. On this basis we can compare with a widely accepted analytical approximation also confirmed by experiments and we will find a high degree of accordance. The model we use is more complex and more fundamental than in previous work. This will lead to a variety of scientific fields playing a role for modeling and simulation such as non-Newtonian fluids, free boundary value problems and fluid-structure interaction formulations. In this spirit the present

Figure 1.1: Ball bearing.

thesis is representing a cross-sectional piece of work which shows what kinds of simulations are possible on current computers with modern methods.

1.1 Introduction to ball bearings

Ball bearings are complex technical devices which are used wherever two bodies rotating relative to each other have to be supported. The range of applications spans from hard disk drives in computers to aircraft turbines and momentum wheels for satellites, the latter being of special interest in the present thesis. Ball bearings usually consist of a cylinder called "bearing mandrel" which is fixed in the reference frame of the observer. In addition there is a cylinder with a larger radius surrounding the mandrel and rotating relative to it. In figure 1.1 the mandrel with the balls is depicted, the outer ring will be the rotating part.
In simple journal bearings only a lubricating fluid resides in the middle of the two concentric cylinders. In contrast, in ball bearings balls are used to support the rotating cylinder. In order to prevent friction and wear the balls and cylinders are also usually lubricated by a mineral oil.
Since the beginning of the use of ball bearings these components are subject to research in engineering sciences in theoretical as well as experimental fields. During the last 40 years by the advent of more and more powerful computers the possibility of numerical simulations has come up as well. The additional use of numerical simulations in this domain is essential because in ball bearings a variety of processes is present, coupling to one another in a highly nonlinear way. This is

limiting the explanatory power of analytic methods, although for some quantities analytical approximations exist which are astonishingly precise. We will compare our results to some analytical approximations which are known in literature to be good approximations for experimental data [Křupka *et al.* (2005)]. Nevertheless these analytical laws can always only answer some distinct questions whereas numerical methods are more flexible and cover a broader variety of possible problems.

In this chapter we give an overview of the relevant processes in a ball bearing and its mathematical treatment. The subject of this thesis is somehow in a border area between numerical analysis and engineering science. Therefore we will present the precise mathematical models to the reader interested more in mathematical aspects. For the reader interested in the physics of ball bearings we will describe the system with its geometry and all relevant parameters. In addition, literature related to physical modeling of processes in elastohydrodynamics will be indicated. In this introduction we will address all aspects in a short manner and the reader is referred to the later individual chapters where more details can be found. The main numerical difficulties and their solution shall be described to a degree of precision that the reader should be enabled to conduct simulations for ball bearings himself if interested in doing so.

In the following, always one single ball in a ball bearing will be considered neglecting possible interaction between two different balls or any other process in which several balls play a role at the same time. In general such processes coupling different balls may occur but we focus on the microscopic aspects in elastohydrodynamics.

This thesis has been established in cooperation with the company *Rockwell Collins Germany* (RCD) from Heidelberg. Below ball bearings manufactured by this company for use in momentum wheels in satellites are of special interest. Consequently several aspects related to this particular situation are specifically relevant, indeed a thorough understanding of the microscopic processes in a ball bearing is not necessary for many industrial applications. For ball bearings used in satellites a higher precision and running smoothness as well as long durability is needed. This is why a more detailed analysis is useful in this application.

All results presented in this thesis are two-dimensional. Indeed a ball bearing does not posses a cylindrical symmetry, therefore the situation is in principle fully three-dimensional. However, the two-dimensional numerical model yields accurate results. The technical difficulties as well as computation times would

increase enormously for three dimensions. In this sense the two-dimensional numerical simulation is a well-justified compromise between accuracy and technical difficulties.

1.2 Fluid flow in ball bearings

The motion of fluids is often modeled by the Navier-Stokes equations. The basic underlying assumption herein is that all volume under consideration is much larger than the mean free path of a particle in the fluid and the size of the molecules. In this case it is appropriate to assume that any small, physically "infinitesimal" volume still contains a huge number of particles so that it is not necessary to distinguish single particles. Instead we use smooth functions $v \in \mathcal{C}^\infty(\mathbb{R}^2)$, $p \in \mathcal{C}^\infty(\mathbb{R})$ for the description of velocity and pressure [Landau & Lifšic (2007)]. At this point we mention directly that this usually uncritical assumption can become delicate in the case of ball bearings. There is experimental data [Křupka *et al.* (2005)] where the film thickness is only of the order of several nm and thus of similar size as the molecules and their mean free path. In literature from engineering sciences it is usually assumed that down to film thicknesses larger than $10nm$ a continuum assumption is reasonable, see [Szeri (2000)]. In this thesis always higher film thicknesses are considered so that we use exclusively continuum mechanical models. However it would be highly interesting and challenging to consider the border region where single-particle effects become important. Since such studies would require very different methods and approaches both from a modeling point of view as for numerical analysis we leave this point open for further research.
In general in lubrication problems we deal with laminar flow, thus Reynolds numbers are always very small. Consequently Stokes' equations are in principle a valid approximation, at least at low pressure. We are mostly interested in stationary processes throughout this thesis. We therefore remark that any linearization or even neglecting the transport term does not change the results considerably.
Basic continuum mechanical assumptions [Landau & Lifšic (2007)] lead to the postulation of a symmetric tensor $\sigma \in \mathbb{R}^{2\times 2}_{sym}$, called the Cauchy stress tensor depending on velocity v and pressure p. On a domain Ω with boundary Γ the equations of balance of forces read

$$-\nabla \cdot \sigma(p, v) = f \qquad \text{in} \quad \Omega.$$

If we consider incompressible fluids to begin with in addition we postulate the constraint

$$\nabla \cdot v = 0 \qquad \text{in} \quad \Omega.$$

As boundary condition we have in general parts of the boundary where we either prescribe a given velocity g or exert boundary forces h on the fluid

$$\begin{aligned} v &= g \qquad \text{on} \quad \Gamma_D, \\ \sigma n &= h \qquad \text{on} \quad \Gamma_N. \end{aligned}$$

Here Γ_D and Γ_N denote parts of the boundary where Dirichlet or Neumann type boundary conditions are prescribed. For the case that (compatible) Dirichlet conditions are posed on the entire boundary we require that the pressure has zero mean value $\int_\Omega p \, \mathrm{dx} = 0$.
If we assume that the Cauchy stress $\sigma(p, v)$ is depending on $D(v) = \nabla v + (\nabla v)^T$ and p in a linear way, we end up with Stokes' equations with the following expression for the Cauchy stress

$$\sigma(p, v) = -pI + \mu D(v). \tag{1.1}$$

Herein μ is a material constant called "dynamic viscosity".
The assumption of a constant viscosity is valid for low pressure. However it is not necessary for a consistent model that the viscosity is constant, see [Franta *et al.* (2005)] for a discussion. In lubrication flow the pressure often reaches values as high as $1GPa$ in parts of the domain and is close to ambient pressure elsewhere. Under these circumstances viscosity has to be modeled as a function of pressure. Furthermore a fluid at such conditions is no more completely incompressible. Fluid models with constant viscosity are called "Newtonian", if viscosity is a function of $D(v)$ or p the models are called "generalized Newtonian" or "non-Newtonian".
There are many generalizations of Stokes' equations with pressure dependent viscosity. Instead of equation (1.1) we consider more general models for the fluid with the following expression for the stress

$$\sigma(p, v) = -pI + \mu(p, |D|)D(v).$$

The form of $\mu(p, |D|)$ is mostly given by fitting parameterized functions to experimental data. They can usually not be derived from physical principles directly.

One of the most common relationship between pressure and viscosity is called "Barus" equation and reads

$$\mu(p, |D|) = \mu_0 \exp(\alpha p). \tag{1.2}$$

Barus' equation is often used in engineering science however there is *no* theory of existence of solutions to fluid models where the viscosity *only* depends on pressure, see [Franta *et al.* (2005)]. A certain well-posed dependence of the viscosity on the shear rate $|D|$ is needed in theoretical analysis in order to control the velocity gradient. So in this context it is crucial that in equation (1.2) there is no dependence on the shear rate at all. Even if instead of the exponential function a well-behaved bounded, but non-constant function is taken, no existence can be shown easily. Of course the unbounded character makes theoretical and numerical analysis even more challenging. The range of models for which there is a proof of existence of a solution is small and uses rather artificial pressure-viscosity functions to make the proof work. In some sense there exists a gap between theory and applications at this point: The models allowing a rigorous mathematical analysis with proof of existence are too restrictive for practical purposes. On the other hand for the models people tend to use in applications, up to now no mathematical theory is available for the well-posedness of the resulting problems. In general the shape of the lubricant flow domain has to be considered as additional unknown because its boundary is changing due to the capillary and curvature related boundary forces. Therefore the fluid phase has to be modeled as a *free* boundary value problem. For free boundary value problems there also exist only few restrictive existence results even in the case of Stokes' equations, see e.g. [Schweizer (1996)]. For the even more complex system of a non-Newtonian flow with a free boundary no theory exists at all to the knowledge of the author.

1.3 Elastic deformation in ball bearings

In ball bearings the motion of the fluid together with the shape of the fluid domain lead to high forces. Locally, these forces are high enough to deform the surrounding steel. The resulting change in the fluid domain couples back to the fluid motion so that a fluid-structure interaction problem results. This explains the name of the discipline "elastohydrodynamics". We now specify the different spatial dimensions, see also figure 1.2. Note that figure 1.2 does not reflect the

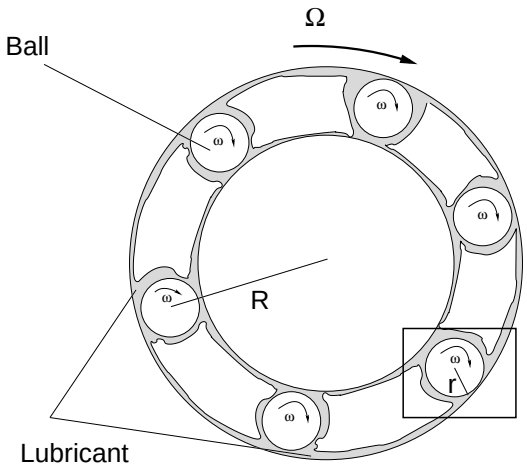

Figure 1.2: Scheme of balls in a ball bearing.

correct ratio of the different length scales on purpose for better visualization.

The radius of the circle on which the center of mass of a ball is moving, denoted R in figure 1.2, is in $[1, 10]$ cm. A typical radius of a ball in a ball r bearing is in $[0.1, 1]$ cm. This size is very large compared to the typical film thickness. This ranges from $10nm$ to $1\mu m$ in the case of "starvation" lubrication which means that very small amounts of lubricant are used. The change in film thickness stems from the deformation of the ball so that the latter is in the same range as the film thickness and thus also small compared to the radius of the ball. The deformation of the ball being of the same order of magnitude as the film thickness results in the fact that it cannot be neglected. Since deformation is indeed small compared to the ball however a linear elastic model may be used. The most common material for ball bearings is steel which can be described as a compressible material using a St.Venant-Kirchhoff model. Since the derivation of such a model is standard and can be found in many textbooks [Braess (2007)] we directly write the governing equations for the deformation $\hat{u}$

$$\begin{aligned} -\hat{\nabla} \cdot (\hat{J}\hat{\sigma}\hat{F}^{-T}) &= \hat{\rho}\hat{f} \qquad \text{in} \quad \hat{\Omega}, \\ \text{with} \quad \hat{\sigma} &= \hat{J}^{-1}\hat{F}\left(\lambda tr(\hat{E})I + 2\mu\hat{E}\right)\hat{F}^T, \\ \hat{F} = I + \hat{\nabla}\hat{u}, \quad \hat{J} = \det\hat{F}, \quad \hat{E} &= \frac{1}{2}\left(\hat{F}^T\hat{F} - I\right). \end{aligned} \tag{1.3}$$

In equations (1.3) the hat on the appearing variables indicates a constant fixed domain which is used for the Lagrangian description of structural deformations. We also pose boundary conditions g, h on the Dirichlet and Neumann part of the

boundary as in the case of the fluid problem.

$$\begin{aligned} \hat{u} &= g \qquad \text{on} \quad \hat{\Gamma}_D, \\ \hat{\sigma}\hat{n} &= h \qquad \text{on} \quad \hat{\Gamma}_N. \end{aligned}$$

As mentioned above also the linearization of these equations with respect to deformation can be considered a valid approximation.
Apart from the fluid flow there exists another cause for deformation in ball bearings. Usually ball bearings are pre-loaded with some exterior force by means of spring-like mechanical structures. Therefore the bearing surfaces are pressed together and the pre-loading force is a variable parameter in experiments. Pre-loading always leads to some flattening of the ball in a static situation without rotation. In such a static situation due to pre-loading also a high pressure arises in the bearing. Treatment of pre-loading is not a simple task from a modeling point of view. Experimental data shows some dependence on the load [Křupka *et al.* (2005)] which seems not always to be decisive. We will elaborate all aspects related to deformation of the ball and pre-loading in chapter 4.2 and 4.3.
In addition to these reasons for deformation the ball may also undergo a rigid translation influencing the film thickness.

1.4 Fluid-structure interaction in ball bearings

In a ball bearing the lubrication flow leads to locally very high pressure which deforms the surrounding steel and couples back again to the fluid. Therefore any model with fixed geometry will be inaccurate, instead we have to consider fluid-structure interaction. In this introductory section we will show the resulting equations, a detailed derivation will be postponed to chapter 4.
In this thesis we will stick to the most robust numerical method for the simulation of fluid-structure interaction problems, namely the monolithic "Arbitrary Eulerian Lagrangian method" (ALE). It will also be derived in chapter 4 or see [Hron & Turek (2006)]. Here we just remark that we formulate a system of equations on a domain $\hat{\Omega}$ consisting of a fluid domain $\hat{\Omega}_f$ and structure domain $\hat{\Omega}_s$. On this domain there exists a boundary Γ_{fs} between fluid and structure where the local balance of forces will be fulfilled implicitly as a natural (nonlinear) boundary condition for the weak formulation derived later. We indicate quantities in the structural domain with an index s, in the fluid domain with an index f. The

system of equations then reads

$$
\begin{aligned}
-\hat{\nabla}\cdot(\hat{J}\hat{\sigma}_s\hat{F}^{-T}) &= \hat{\rho}_s\hat{f} && \text{in } \hat{\Omega}_s,\\
\hat{v} &= \hat{F}^{-T}\hat{v}_0, && \text{in } \hat{\Omega}_s,\\
\hat{\sigma}_s &= \hat{J}^{-1}\hat{F}\left(\lambda tr(\hat{E})I + 2\mu\hat{E}\right)\hat{F}^T,\\
\hat{F} = I + \hat{\nabla}\hat{u}, \quad \hat{J} = \det\hat{F}, \quad \hat{E} &= \frac{1}{2}\left(\hat{F}^T\hat{F} - 1\right),\\
\hat{J}\hat{\rho}\left(\hat{F}^{-1}(\hat{v})\cdot\hat{\nabla}\right)\hat{v}\hat{F} - \hat{\nabla}\cdot\left(\hat{J}\hat{\sigma}_f(\hat{p},\hat{v})\hat{F}^{-T}\right) &= \hat{\rho}_f\hat{f} && \text{in } \hat{\Omega}_f,\\
\hat{\nabla}\cdot(\hat{J}\hat{F}^{-1}\hat{v}) &= 0 && \text{in } \hat{\Omega}_f,\\
\hat{\sigma}_f(\hat{p},\hat{v}) = -\hat{p}I + \mu(\hat{p})\left(\hat{\nabla}\hat{v}\hat{F}^{-1} + \hat{F}^{-T}(\hat{\nabla}\hat{v})^T\right), \mu(p) &= \mu_0\exp(\alpha p). && (1.4)
\end{aligned}
$$

The fluid and the structure fulfill their proper boundary conditions on parts of the boundary which are not an interface between fluid and structure as in the sections above

$$
\begin{aligned}
\hat{v} &= g \quad \text{on} \quad \hat{\Gamma}_f,\\
\hat{u} &= h \quad \text{on} \quad \hat{\Gamma}_s.
\end{aligned}
$$

The coupling happens via the boundary condition on the interface. On this boundary $\hat{\Gamma}_{fs}$ we postulate a balance of forces

$$
\hat{J}\hat{\sigma}_s\hat{F}^{-T}\hat{n} = \hat{J}\hat{\sigma}_f\hat{F}^{-T}\hat{n} \quad \text{on} \quad \hat{\Gamma}_{fs}. \tag{1.5}
$$

This whole formulation is given on an undeformed reference domain therefore transformations are used which appear as factors related to $\hat{\nabla}\hat{u}$ such as $\hat{F}$ and $\hat{J}$, the specific form will be derived later. In practice the reference domain often consists of the domain at the initial state.
Formulating a weak formulation of equation (1.4) is not straight forward especially due to the boundary conditions for the different components at the interface. This will be subject of chapter 4.2.
The convective term $\left(\hat{F}^{-1}(\hat{v})\cdot\hat{\nabla}\right)\hat{v}\hat{F}$ can be neglected in equation (1.4) in lubrication flows. However the resulting fluid-structure interaction problem will be nonlinear due to the nonlinear boundary condition on $\hat{\Gamma}_{fs}$ and the transformation. This holds even for linear models for the structure *and* the fluid. Certainly, the fluid itself has to be modeled in a nonlinear way due to the pressure dependent viscosity.

1.5 Comparison with previous work in elastohydrodynamics and goal of the thesis

As mentioned before we use more complete models in this thesis than in most of the previously existing pieces of work. We will now substantiate this assertion with a comparison. Furthermore we will specify the aim of this thesis.
In [Křupka *et al.* (2005)] Reynolds' equation is used together with a non-Newtonian compressible fluid. The non-Newtonian model is however treated in a non-consistent way, see [Rajagopal & Szeri (2003)]. The use of Reynolds' equation constitutes a severe reduction of the model in comparison with a generalized Navier-Stokes model considered in this thesis. At high pressure in the elastohydrodynamic regime the sorrounding structure becomes deformable. This fact is often neglected, in [Křupka *et al.* (2005)] it is modelled by a simple integral formula for the lateral pressure. In our work we consider a full fluid-structure interaction problem without continuum mechanical simplifications. In addition there is no free boundary of the fluid in [Křupka *et al.* (2005)] in contrast to this work.
A similar approach as in [Křupka *et al.* (2005)] is presented e.g. in [Jubault (2002)] and [Jubault *et al.* (2003)]. Again a simplified elastic model is used. These publications show besides interesting experimental results.
In [Gwynllyw *et al.* (1996)] a full generalized Newtonian fluid is considered instead of Reynolds' equation. In this case the fluid domain is however fixed and thus the structure is assumed to be rigid. Due to the different geometry there is no free boundary neither.
In [Olaru & Gafitanu (1993)] an analytical theory is developped for the free-boundary aspect of a ball-bearing but it is based on simple geometric considerations. Furthermore the analytic approximation is presumably not valid for all relevant sets of parameters. Fluid-structure interaction is completely neglected.
The elastohydrodynamic film thickness is one of the most important quantities in ball bearings. Whenever it is close to zero, a breakdown of the fluid film is possible. Damage of the bearing may happen in such cases, therefore the film thickness is such an important quantity. This is why there are also many analytical approximations and lots of experiments dealing with film thickness in ball bearings. Most of the literature cited above is also considering this parameter.
Througout this thesis we will derive a method to simulate the elastohydrodynamic film thickness in ball bearings. We will compare the results of the sim-

ulation with an analytical approximation widely used in literature. There is a reasonable accuracy in the regions of parameters where the analytical theory is valid. The numerical method presented in this work will be more flexible with respect to changes of parameters than analytical approximations. In addition it will be based on fundamental continuum mechanical principles. The most important result will be the prediction of the film thickness. Also other quantities are interesting and can be determined by means of the numerical algorithm such as pressure profiles or forces on the ball. The film thickness is of special importance because it may predict a collapse of the fluid film and thus bearing failure.
From a methematical point of view we propose a way to deal with pressure-dependent viscosities numerically. We achieve robustness so that we are able to perform simulations in a wide range of relevant physical parameters. In addition we propose a fully implicit discretization of the free-boundary value problem for the lubricant flow.

Chapter 2

Free boundary value problems in lubrication flow

This chapter is about free boundary value problems and their numerical simulation. Since in ball bearings good mass preserving properties of the numerical algorithm are needed, we analyze the algorithms with respect to this issue in detail. Two stable and one stabilized discretization will be compared. It turns out that stable discretizations have much better properties for such problems than stabilized ones. We propose a new fully implicit scheme for the simulation of flow with a free boundary which is based on weak imposition of boundary values. The resulting algorithm is then stable for arbitrarily large time-steps in contrast to previous discretizations proposed in literature.

2.1 Formulation of the free boundary value problem

Ball bearings consist of balls and the bearing unit made of steel as well as a lubricating fluid. Assuming for the moment that the parts made of steel are rigid we know a priori the position of the interface between steel and fluid. However the fluid also possesses a free boundary on the inlet and outlet. On the free boundary there are thus forces due to the surface tension of the fluid. The free surface will therefore depend on the inflow speed and the material parameters and evolve in time until it reaches a stationary setting.

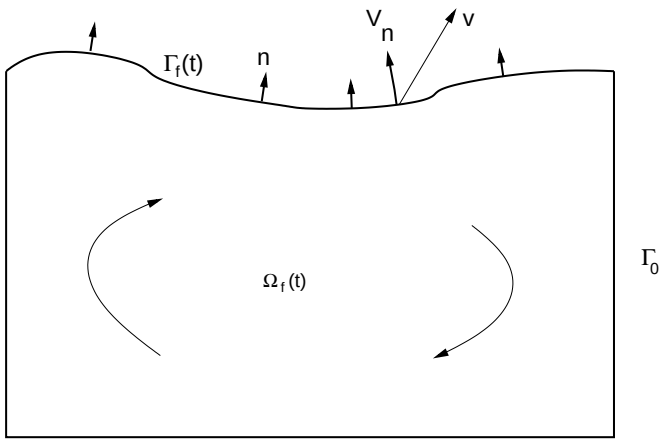

Figure 2.1: Scheme of a free boundary value problem with fixed boundary Γ_0, free boundary $\Gamma_f(t)$, exterior normal n, fluid velocity v and velocity of the boundary V_n.

The following derivation will be two-dimensional but all relations can be formally extended to three dimensions.
The most common model for surface tension forces is to assume that they are proportional to the local curvature of the free surface κ. For the Navier-Stokes equations with a time dependent domain $\Omega_f(t)$ and a free boundary $\Gamma_f(t)$ which moves with an associated velocity field V_n we pose the following problem derived in [Bänsch (2001)]. The tangential and normal vector at the boundary are denoted t and n respectively.

Problem 2.1. *Let v_0 be initial data, Ω_0 the initial domain. Find v, p and $\Omega_f(t)$ such that*

$$\begin{aligned}
\rho\partial_t v + \rho(v\cdot\nabla)v - \nabla\cdot\sigma(p,v) &= \rho f \quad \text{in} \quad \Omega_f(t),\\
\nabla\cdot v &= 0 \quad \text{in} \quad \Omega_f(t),\\
\sigma(p,v) = -pI + \mu D(v), \quad D(v) &= \nabla v + (\nabla v)^T,\\
v(\cdot,0) &= v_0,\\
\Omega_f(0) &= \Omega_0,\\
V_n = n(vn) \quad &\text{on} \quad \Gamma_f(t),\\
v = 0 \quad &\text{on} \quad \Gamma_0,\\
\sigma t = 0 \quad &\text{on} \quad \Gamma_f(t),\\
\sigma n = \gamma\kappa n \quad &\text{on} \quad \Gamma_f(t).
\end{aligned} \tag{2.1}$$

The fixed boundary is here denoted Γ_0, γ is the constant material parameter of surface tension. The existence of a solution to the system of equations (2.1) is

far from self-evident but has to be postulated a priori. Even with small initial data and smooth initial domains a change in topology may happen when for example droplets develop and separate from the main fluid phase. Furthermore cusps or similar pathologies may occur at the free boundary in the course of time. This problem is very fundamental, in [Bänsch (2001)] and the reference therein the interested reader finds more on these theoretical questions. In [Schweizer (1996)] a proof of existence is given in a specialized situation with some additional assumptions. Often in theoretical analysis it is assumed that the free boundary is given as graph of a function which is a severe restriction and usually not physical. The free boundary shall be a sharp interface so that no fluid particle is allowed to cross the free boundary. This modelling assumption does not hold exactly in real lubrication flows since evaporization may occur. For the moment however we stick to this assumption. It follows that if a non-zero normal component of the fluid velocity on the boundary exists, the interface moves in the normal direction.

$$V_n = n(vn) \qquad \text{on} \quad \Gamma_f(t).$$

Here V_n is the velocity of the free boundary itself. This serves as boundary condition for the evolution of the interface in equations (2.1).
We will now derive a formulation for the curvature which is well suited for numerical treatment as well as theoretical analysis. It involves the Laplace-Beltrami operator and its relation to curvature which we derive in the following, see [Delfour & Zolésio (2001)] and the references therein for a detailed derivation.

Definition 2.1 (Tangential gradient)**.** *Let F be $\in \mathcal{C}^1(U, \mathbb{R})$ where $U \subset \mathbb{R}^2$ is an open set which contains Γ. The tangential gradient is then defined as*

$$\overline{\nabla} F := \nabla F - \frac{\partial F}{\partial n} n.$$

We also need the tangential gradient of vector valued functions.

Definition 2.2 (Tangential Jacobian)**.** *Let F be $\in \mathcal{C}^1(U, \mathbb{R}^2)$ where $U \subset \mathbb{R}^2$ is an open set which contains Γ. The tangential Jacobian is defined componentwise as*

$$(\overline{D} F)_{ij} := (\overline{\nabla} F_i)_j. \tag{2.2}$$

Definition 2.3 (Tangential divergence)**.** *With the above notation and Dv as usual Jacobian the tangential divergence is defined as*

$$\overline{\nabla} \cdot v := tr\left[\overline{D} v - Dv n^T n\right]. \tag{2.3}$$

We define the Laplace-Beltrami operator in a nearby manner as tangential divergence of the tangential gradient.

Definition 2.4 (Laplace-Beltrami Operator)**.** *The Laplace-Beltrami operator* $\overline{\Delta}$ *is defined as*

$$\overline{\Delta} v := \overline{\nabla} \cdot \overline{\nabla} v. \tag{2.4}$$

More details on the background of these definitions with respect to differential geometry can be found in [Delfour & Zolésio (2001)].

Proposition 2.1 (Curvature)**.** *There holds for the identity mapping* $id : \Gamma \to \Gamma$ *with* κ *as curvature*

$$\overline{\Delta} id|_\Gamma = \kappa n. \tag{2.5}$$

Proof. A proof can be found in [Eschenburg & Jost (2007)]. □

In order to derive a weak formulation we need partial integration.

Proposition 2.2 (Partial Integration)**.** *For closed curves* Γ *and smooth test functions* ϕ *there holds*

$$\int_\Gamma \overline{\Delta} id|_\Gamma \phi \; dx = - \int_\Gamma \overline{\nabla} id|_\Gamma \overline{\nabla} \phi \; dx. \tag{2.6}$$

Proof. A proof can be found in [Gallot *et al.* (2004)]. □

With these definitions and relations we are able to formulate a variational formulation of the free boundary value problem (2.1). As in the case of fluid-structure interaction later in this thesis we transform the actual domain $\Omega(t)$ to the initial domain. We use a method known as "Arbitrary Lagrangian Eulerian" (ALE) which will be described in detail in chapter 4.2. For the derivation how to transform scalar, vector- or tensor valued fields on moving domains we also refer to [Dunne (2007)] where additional formulas and details on calculus can be found. The most important difference to fluid-structure interaction problems considered later in this thesis stems from the fact that there is no structure, just a transformation function which has only physical meaning on the free boundary. In

equation (2.1) we have the boundary conditions for the deformation u at the moving boundary

$$\partial_t u|_\Gamma = V_n = (vn)n.$$

These boundary values are extended to the whole fluid domain by means of harmonic extension.
In the following we will need to transform the normal on a moving boundary. For this purpose we give a formula for the transformation of the exterior normal.

Proposition 2.3 (Transformation of the exterior normal)**.** *Let $\hat{\Gamma}$ be the boundary of the domain $\hat{\Omega}$ with exterior normal $\hat{n}$ and $\hat{u}$ be a diffeomorphism from $\overline{\hat{\Omega}}$ on $\overline{\Omega}$. On the boundary of Ω which is denoted Γ the exterior normal is n. We denote $\hat{F} := I + \hat{\nabla}\hat{u}$.*
It holds

$$n(x) = n\left(\hat{x} + u(\hat{x})\right) = \frac{\hat{F}(\hat{x})^{-T}\hat{n}(\hat{x})}{||\hat{F}(\hat{x})^{-T}\hat{n}(\hat{x})||}.$$

We also use the short notation

$$n = \frac{\hat{F}^{-T}\hat{n}}{||\hat{F}^{-T}\hat{n}||}.$$

Proof. The formula follows immediately by application of the chain rule and normalization. □

We will in the following consider the discretization of equation (2.1) by means of finite elements of which the precise definition is given in chapter 5. In time we use a standard implicit Euler scheme.

Problem 2.2 (Discrete formulation of the free boundary value problem, explicit treatment of the curvature)**.** *Let the interval $[0, T]$ be divided in m equidistant time-steps of size dt. For $n \in \{0, ..., m-1\}$*

1. *find* $v_h^n := v_h(t^n)$, $u_h^n := u_h(t^n) \in V_h$, $p_h^n := p_h(t^n) \in X_h$ *such that*

$$\begin{aligned}
\frac{1}{dt}(\hat{J}_h^{n+1}\hat{\rho}\hat{v}_h^{n+1}, \phi) + \left(\hat{J}_h^{n+1}\hat{\rho}(\hat{v}_h^{n+1} - \partial_t \hat{u}_h^{n+1}) \cdot \hat{\nabla}\hat{v}_h^{n+1}, \phi\right) \\
+ \left(\hat{J}_h \hat{\sigma}(\hat{p}_h^{n+1}, \hat{v}_h^{n+1})\hat{F}_h^{-T,n+1}, \hat{\nabla}\phi\right) = \\
\frac{1}{dt}(\hat{J}_h^n \hat{\rho} v_h^n, \phi) + (\hat{\rho} f^{n+1}, \phi) + \gamma < \kappa n, \phi >_{\Gamma_n} \\
\left(\hat{\nabla} \cdot (\hat{J}_h^{n+1}\hat{v}_h^{n+1}\hat{F}_h^{-1,n}), \chi\right) = 0 \\
(\hat{\nabla}\hat{u}_h^{n+1}, \hat{\nabla}\psi) = 0
\end{aligned}$$

for all $\phi, \psi \in V_h$, $\chi \in X_h$.

2. *update the boundary*

$$\hat{u}_h^{n+1} = \hat{u}_h^n + dt(\hat{n}_h^n \cdot \hat{v}_h^n)\hat{v}_h^n \qquad \text{on} \quad \hat{\Gamma}$$

For the Neumann boundary condition in the variational formulation of the fluid (2.1) we use the above definitions and obtain

$$\int_{\Gamma(t)} \kappa n \phi = \int_{\Gamma(t)} \overline{\Delta} id|_{\Gamma(t)} \phi = -\int_{\Gamma(t)} \overline{\nabla} id|_{\Gamma(t)} \overline{\nabla}\phi.$$

The transformation of the tangential gradient $\hat{\overline{\nabla}}$ can be easily computed with the transformation laws derived in chapter 4. It holds

$$\overline{\nabla} = \nabla - n\nabla n = \hat{F}^{-1}\hat{\nabla} - \frac{\hat{F}^{-T}\hat{n}}{||\hat{F}^{-T}\hat{n}||}\hat{F}^{-1}\hat{\nabla}\frac{\hat{F}^{-T}\hat{n}}{||\hat{F}^{-T}\hat{n}||}.$$

Consequently we obtain the boundary condition on the reference domain in the form

$$\begin{aligned}
\int_{\Gamma(t)} \overline{\nabla} id|_{\Gamma(t)} \overline{\nabla}\phi = \int_{\hat{\Gamma}} \Bigg[\left(\hat{F}^{-1}\hat{\nabla} - \frac{\hat{F}^{-T}\hat{n}}{||\hat{F}^{-T}\hat{n}||}\hat{F}^{-1}\hat{\nabla}\frac{\hat{F}^{-T}\hat{n}}{||\hat{F}^{-T}\hat{n}||} \right) id_{\hat{\Gamma}} \\
\left(\hat{F}^{-1}\hat{\nabla} - \frac{\hat{F}^{-T}\hat{n}}{||\hat{F}^{-T}\hat{n}||}\hat{F}^{-1}\hat{\nabla}\frac{\hat{F}^{-T}\hat{n}}{||\hat{F}^{-T}\hat{n}||} \right) \phi \Bigg].
\end{aligned}$$

Before stating the discrete systems we comment on the discretization of the curvature term

$$\sigma n = \gamma \kappa n \qquad \text{on} \quad \Gamma_f(t).$$

The formulation using the Laplace Beltrami operator is in summary particularly advantageous because there is no need of evaluating the curvature, only the exterior normal is needed. By using partial integration the order of derivatives needed

is only one, instead of two when discretizing the curvature directly. Sometimes in engineering literature the curvature is indeed directly evaluated on a discrete level. However for many discretizations the boundary is not smooth and a node-wise evaluation of the curvature is not defined directly. In fact there are also methods to recover a node-wise curvature on polygonal domains but these methods can be understood as (twice) numerical differentiation. Furthermore the implementation of such an evaluation of the curvature is cumbersome.
The exterior normal we need is neither defined in a node-wise sense. In the subsequent we will show a method to approximate it nevertheless with the right order of convergence under mesh refinement.
The discrete variational formulation is fully explicit with respect to the movement of the boundary since its new position *only* depends on data of the last time-step. Such a discretization therefore leads to a conditional stability, e.g. the algorithm is only stable for small time-steps. In addition temporal and spatial discretization are coupling, any refinement of the spatial grid requires also smaller time-steps. This effect has shown up in the simulations conducted in this thesis and is also well known in literature. In [Brackbill *et al.* (1991)] a qualitative as well as quantitative analysis is given with a result for the stability condition

$$\Delta t < \sqrt{\frac{h^3 \rho}{\gamma}}.$$

The first step to overcome this restriction is a semi-implicit treatment of the curvature terms. This method was proposed in [Bänsch (2001)] and it consists of evaluating parts of the curvature terms at the new time-step. If we consider the curvature term on the boundary

$$< \overline{\nabla} id_{\Gamma_f}, \overline{\nabla} \phi >_{\Gamma} \tag{2.7}$$

we write for the new position of the boundary

$$\Gamma^{n+1} = \Gamma^n + dt(v^{n+1} \cdot n^n) n^n$$

and insert this new position in equation (2.7).
We thus introduce a coupling to the velocity field at the new time-step. The following semi-implicit system results.

Problem 2.3 (Discrete semi-implicit formulation of the free boundary value problem)**.** *Let the interval* $[0, T]$ *be divided in* m *equidistant time-steps of size* dt*. For* $n \in \{0, ..., m-1\}$

1. *find* $v_h^n := v_h(t^n)$, $u_h^n := u_h(t^n) \in V_h$, $p_h^n := p_h(t^n) \in X_h$ *such that*

$$\frac{1}{dt}(\hat{J}_h^{n+1}\hat{\rho}\hat{v}_h^{n+1}, \phi) + \left(\hat{J}_h^{n+1}\hat{\rho}(\hat{v}_h^{n+1} - \partial_t \hat{u}_h^{n+1}) \cdot \hat{\nabla}\hat{v}_h^{n+1}, \phi\right)$$
$$+ \left(\hat{J}_h\hat{\sigma}(\hat{p}_h^{n+1}, \hat{v}_h^{n+1})\hat{F}_h^{-T,n+1}, \hat{\nabla}\phi\right) =$$
$$\frac{1}{dt}(\hat{J}_h^n\hat{\rho}v_h^n, \phi) + (\hat{\rho}f^{n+1}, \phi) + \gamma < \overline{\nabla}\left(id_{\Gamma_n} + dt(v_h^{n+1} \cdot n^n)n^n\right), \overline{\nabla}\phi >_{\Gamma^n}$$
$$\left(\hat{\nabla} \cdot (\hat{J}_h^{n+1}\hat{v}_h^{n+1}\hat{F}_h^{-1,n}), \chi\right) = 0$$
$$(\hat{\nabla}\hat{u}_h^{n+1}, \hat{\nabla}\psi) = 0$$

   for all $\phi, \psi \in V_h$, $\chi \in X_h$.

2. *update the boundary*

$$\hat{u}_h^{n+1} = \hat{u}_h^n + dt(\hat{n}_h^n \cdot \hat{v}_h^n)\hat{v}_h^n \qquad \text{on} \quad \hat{\Gamma}$$

In problem (2.3) only the velocity field of the fluid is evaluated at the new time-step, all integration is performed on the domain of the old time-step. Indeed the domain and thus the normal is fixed throughout one time-step and updated explicitely.

The semi-implicit term in problem (2.3) allows considerably larger time-steps in practice. For many kinds of applications the still-present coupling of mesh-size and time-step does not show up since for other reasons small time-steps are needed anyway. A typical case are the Navier-Stokes equations with higher Reynolds number. In such dynamical situations the convective term in the Navier-Stokes equations requires small time-steps anyway.

Indeed the conditional stability is still present and not corrected completely in the semi-implicit scheme as shown by numerical experiments in [Hysing (2006)]. This makes the method somehow unattractive for local mesh refinement which we are interested in for simulations for elastohydrodynamics.

In all previous variants of discretization the integration happens on the domain of the old time-step. The reason is that the evolution of the free boundary is given as Dirichlet data and hence considered as known boundary values in each time-step. Since the curvature is based on evaluation of the normal at the boundary it can be only evaluated explicitely either. We overcome this problem in imposing the boundary values only *weakly*. Consequently we are able to formulate the position of the free boundary implicitly. Recall that in (2.2) the boundary values are given as

$$u_h^{n+1} = u_h^n + dt(n_h^n \cdot v_h^n)v_h^n \qquad \text{on} \quad \Gamma.$$

We impose these boundary values weakly using Nitsche's method [Nitsche (1971)]. In such a way one can consider the new position at the boundary as an additional unknown quantity in each time-step instead of imposing it. For this purpose we add a boundary term with a small parameter ϵ

$$\frac{1}{h\epsilon}\left\langle u_h^{n+1} - (u_h^n + dt(v_h^{n+1}n^{n+1})n^{n+1}, \phi\right\rangle.$$

Here h denotes the local mesh-size. We have therewith introduced an additional nonlinear boundary condition for the transformation. As a result we recover a fully implicit formulation

Problem 2.4 (Discrete implicit formulation of the free boundary value problem)**.** *Let the interval $[0,T]$ be divided in m equidistant time-steps of size dt. For $n \in \{0,...,m-1\}$ find $v_h^n := v_h(t^n)$, $u_h^n := u_h(t^n) \in V_h$, $p_h^n := p_h(t^n) \in X_h$ such that*

$$\begin{aligned}
\frac{1}{dt}(\hat{J}_h^{n+1}\hat{\rho}\hat{v}_h^{n+1}, \phi) + \left(\hat{J}_h^{n+1}\hat{\rho}(\hat{v}_h^{n+1} - \partial_t\hat{u}_h^{n+1})\cdot\hat{\nabla})\hat{v}_h^{n+1}, \phi\right) \\
+ \left(\hat{J}_h\hat{\sigma}(\hat{p}_h^{n+1}, \hat{v}_h^{n+1})\hat{F}_h^{-T,n+1}, \hat{\nabla}\phi\right) = \\
\frac{1}{dt}(\hat{J}_h^n\hat{\rho}v_h^n, \phi) + \gamma < \overline{\nabla}id_{\Gamma^{n+1}}, \overline{\nabla}\phi >_{\Gamma^{n+1}} + (\hat{\rho}f^{n+1}, \phi) \\
+\frac{1}{h\epsilon}\left\langle u_h^{n+1} - (u_h^n + dt(v_h^{n+1}n^{n+1})n^{n+1}, \phi\right\rangle_{\Gamma^{n+1}} \\
\left(\hat{\nabla}\cdot(\hat{J}\hat{v}_h^{n+1}\hat{F}_h^{-1,n}), \chi\right) = 0, \\
(\hat{\nabla}\hat{u}_h^{n+1}, \hat{\nabla}\psi) = 0. \qquad (2.8)
\end{aligned}$$

for all $\phi, \psi \in V_h$, $\chi \in X_h$.

After all this formulation is most appropriate when we are interested in stationary limits. In this case it is possible to choose in principle arbitrarily large time-steps. However due to the additional nonlinearity there is also a limit for the time-steps arising from slow convergence of nonlinear iterations. In general it can be stated that it is indeed favorable and less costly to work with the implicit algorithm at a larger time-step. The higher number of nonlinear iterations is more than compensated by the possibility of larger time-steps.
In the case of ball bearings we are in the present thesis only interested in stationary limits. Due to the much higher complexity inherently instationary processes are not in our focus. When dealing with them we would also as a first step have to be able to solve stationary problems efficiently.

	Curvature	Domain
Explicit	explicit	explicit
Semi-implicit (Bänsch)	semi-implicit	explicit
Implicit	implicit	implicit

Table 2.1: Different types of discretization for free boundary value problems.

We summarize the different types of discretization for the sake of clearness in table 2.1.

2.2 Numerical results under explicit and semi-implicit treatment of the free boundary

In order to validate and compare the above methods we firstly describe the benchmark example given in [Bänsch (2001)]. It consists in two dimensions of an ellipsoid with semiaxis $r_1 = 1$, $r_2 = 1.2$ where the non-constant curvature of the boundary leads to oscillatory behaviour if viscous damping is small enough. In this example the Reynoldsnumber is $Re = 300$, allowing indeed oscillations. In configurations for ball bearings the Reynoldsnumber is usually much smaller ≤ 1 so that no oscillations occur and larger time-steps are useful. This is the situation where the fully implicit method is advantageous.
Figure 2.2 shows the velocity field at different instances in time. In order to derive a quantitative comparison we consider the change in volume of the ellipsoid in the course of time as well as the tip position. During the tests for this comparison we also considered the entire kinetic energy of the fluid but it seemed to be less sensitive with respect to different types of discretizations. Therefore we omit this quantity here. Recall that for an incompressible fluid an analytical solution would of course show no change in volume at all whereas kinetic energy decreases in a viscous fluid.
In figure 2.3 some simulation results for the free boundary of the lubricant in a ball bearing are shown. The simulations are based on the same discretization methods presented above. For validation purposes the oscillating bubble is chosen as a more simple benchmark problem.
In figure 2.4 the position of the tip of the oscillating bubble is depicted for small time-steps at the beginning of the simulation. Later the mass loss throughout

Figure 2.2: Oscillating bubble at different instances in time.

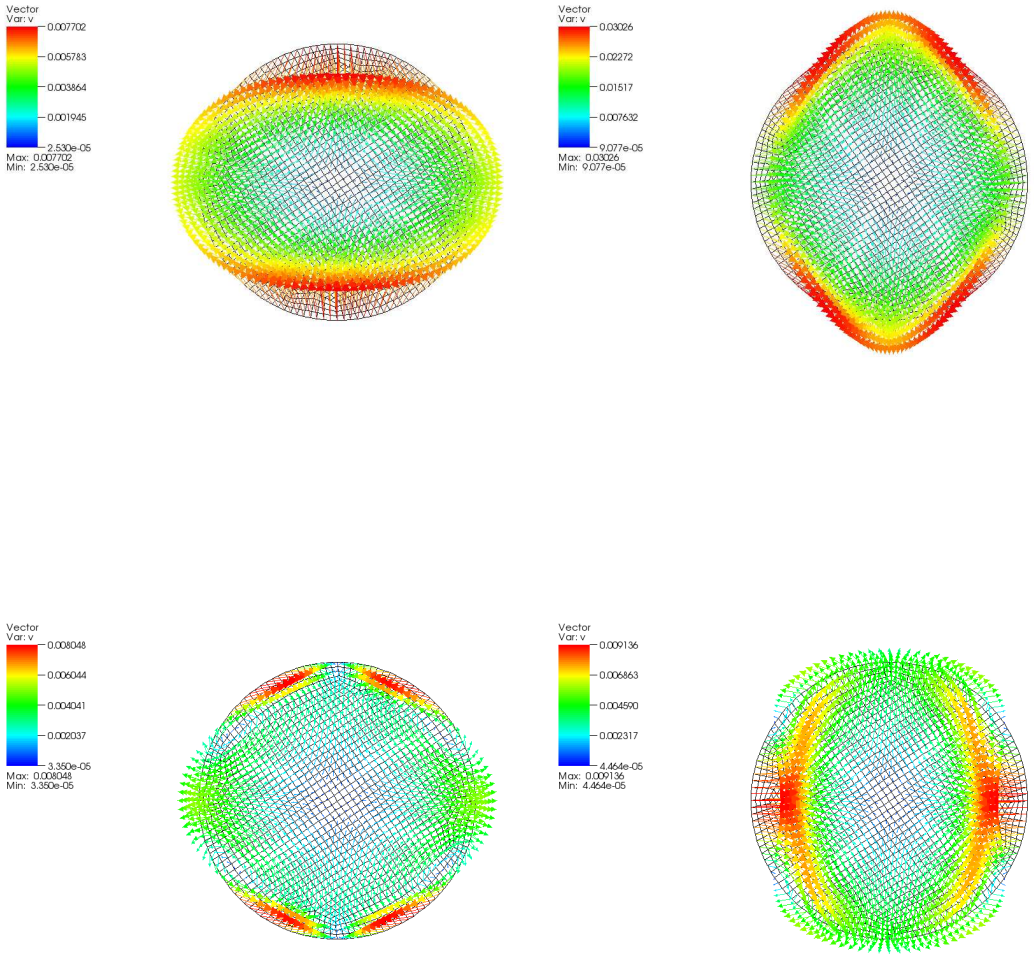

this interval in time will be measured and compared for different discretizations. In figure 2.5 the position of the tip of the oscillating bubble is depicted for approximately one period of the oscillation.

In order to analyse in the following the numerical results we have to presuppose the precise definition of finite element spaces which is given in chapter 5.
We thus continue with directly discussing the properties of the discretizations and the numerical results. In this context we firstly discuss the reasons for a loss of mass on a discrete level. Later on we confirm the statements with numerical experiments.
In principle there are the following reasons for errors in mass-conservation:

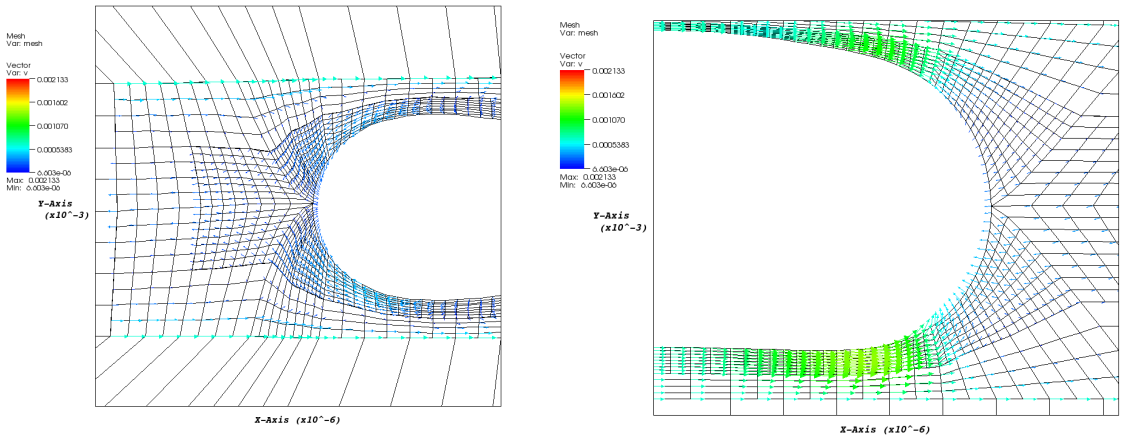

Figure 2.3: Lubricant in ball bearing with free boundary.

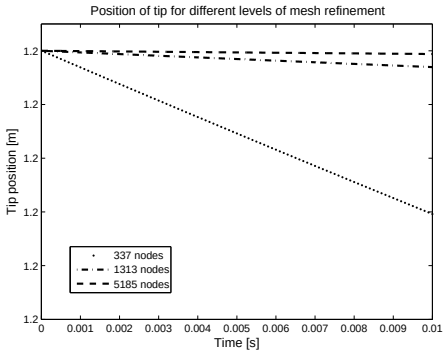

Figure 2.4: Position of tip of the oscillating bubble for three levels of mesh refinement in the course of time.

- Error in the approximation of the normal:
  The discrete normal determines the evolution of the free boundary because of the boundary condition for the transformation

$$\Gamma^{n+1} = \Gamma^n + dt(n_h^n \cdot v_h^n)n_h^n \qquad \text{on} \quad \Gamma_f. \tag{2.9}$$

  It follows that any error in the approximation of the normal leads to an error in mass-conservation. In the benchmark example under consideration the reference domain has ellipsoidal shape and hence an analytically known normal. Due to proposition (2.3) the error in the approximation of the normal is given by the order of approximation of $\hat{\nabla}\hat{u}$. When using one of the methods with explicit treatment of the boundary, the boundary values for the transformation are given as Dirichlet data. Therefore they are evaluated

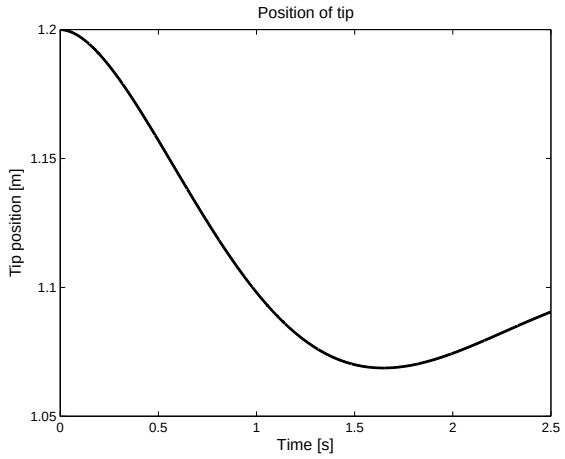

Figure 2.5: Position of tip for the oscillationg bubble for longer time interval on fixed mesh.

in nodes that is a pointwise manner. For the free boundary value problem there are no rigorous pointwise error estimates available. If we neglegt the coupling between the transformation and the fluid we can expect the error of the transformation to behave like in the case of a Laplace equation with Dirichlet data. We assume that the pointwise evaluation does not degrade the order of convergence compared to mean errors as it is often seen in practical applications. Under this assumption we expect an order of approximation of $O(h)$ in the case of (stabilized) Q_1 elements, when using Q_2 elements the order is $O(h^2)$, see chapter 5 and the references therein. Recall that the inf-sup-stable elements used in this thesis are the Q_2Q_1 Taylor-Hood element as well as the $Q_2P_1^{disc}$ element, both using Q_2 elements for the transformation. The error in the approximation of the normal can be improved when using stabilized Q_1 elements by approximating *only* the normal with Q_2 elements. This increases the order of approximation to $O(h^2)$ and will also be discussed and confirmed by numerical experiments in more detail in the following.

- Approximation in the incompressibility constraint:
  Stabilized elements as well as the Q_2Q_1 Taylor-Hood element are mass-preserving only in a *global* way. Only the $Q_2P_1^{disc}$ element using a discontinuous pressure is mass-preserving cell-wise. However we only consider the global error in the volume of the domain, hence *all* discretizations should in principle preserve this quantity when working with an exact normal. On a

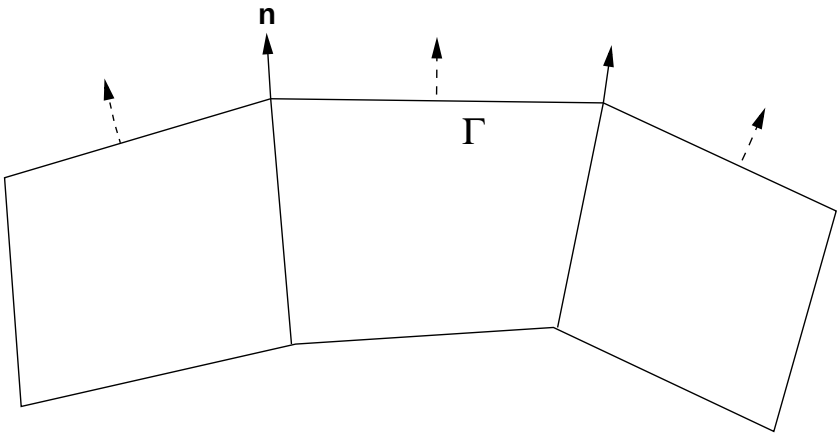

Figure 2.6: Approximation of the normal when using Q_1-elements.

continuous level the incompressibility constraint is equivalent to preserving mass due to the Gauss theorem but on a discrete level this only holds up to an error of $O(h^2)$.

- Evolution of the boundary in time:
  The transformation at the boundary of the domain is given by equation (2.9). This expression is a first order approximation in time. Recall that expression (2.9) has to be evaluated in a pointwise manner when prescribing Dirichlet data for the numerical approximation.

In the benchmark example the entire boundary of the domain is a free boundary for the flow.
We will now study the different discretizations with respect to the different causes of error in domain size. Firstly we consider the error in the approximation of the normal. In the case of using a Q_1 discretization the boundary of the discrete domain is polygonal, see figure 2.6. In case of Q_2 elements it is a piecewise quadratic polynomial. Since we need a pointwise evaluation of the normal in the case of explicit treatment of the boundary we face the problem to define it in a nodal way. For this purpose we use averaging over adjacent edges weighted by edge length. If we call the edges e with length $|e|$ we thus define the normal at the node K with the set of adjacent edges $E(K)$ as

$$n_h^K = \frac{\sum_{e \in E(K)} n_h^e |e|}{|| \sum_{e \in E(K)} n_h^e |e| ||}.$$

The normal on an edge is of course also well defined for Q_1 elements except at end points. We check the node-wise approximation by comparing it to an analytical

Number of nodes	Normal Q1	Normal Q2
89	0.414192	0.366243
337	0.169722	0.091408
1313	0.083528	0.025255
5185	0.042307	0.006545
20609	0.021281	0.001657

Table 2.2: Convergence of the normal in the case of Q_1- as well as Q_2-elements.

normal field. Therefore we use the initial reference domain with ellipsoidal shape and thus known normal. We consider the error between the numerical approximation for the normal and the analytical one. As a measure for the error we take.

$$e_h = ||n_h - n||_{L^2(\Gamma)}$$

where $n = (n^x, n^y)^T$ denotes the analytical and $n_h = (n_h^x, n_h^y)^T$ the discrete normal. Results are given in table 2.2 and perfectly show linear and accordingly quadratic behaviour. Having confirmed the error in the approximation of the normal we pursue by considering mass-conservation. We start with the semi-implicit methods with explicit treatment of the transformation at the boundary. The surface tension forces are however coupling to the flow field in an implicit way. Since we are for the moment not considering time discretization we choose a small time-step neglecting the error belonging to time discretization. This time-step will be larger for the stabilized methods since they lead to considerably larger errors related to spatial discretization. For the $Q_1Q_1 - Lps$ element we take $\Delta t = 1.0^{-4}s$ and conduct 10.000 time-steps on three levels of mesh refinement and measure the change in volume of the domain. For the stable elements Q_2Q_1 Taylor-Hood and $Q_2P_1^{disc}$ we choose $\Delta t = 1.0^{-6}s$ and 50.000 time-steps.

In order to have a fair comparison we have to consider on each level of mesh refinement the error in comparison to the initial state. The initial state itself approximates the ellipsoidal shape with a rate of $O(h^2)$ to the analytical value of the initial domain-size $|\Omega| = \pi r_1 r_2$ with $r_1 = 1.0$ and $r_2 = 1.2$.
Recall that the semi-implicit discretization and the fully explicit do not differ in the treatment of the transformation at the boundary so that we do not consider them separately. Later on we also analyze the fully implicit method on one fixed grid with different time-steps to detect the error coming from time discretization.

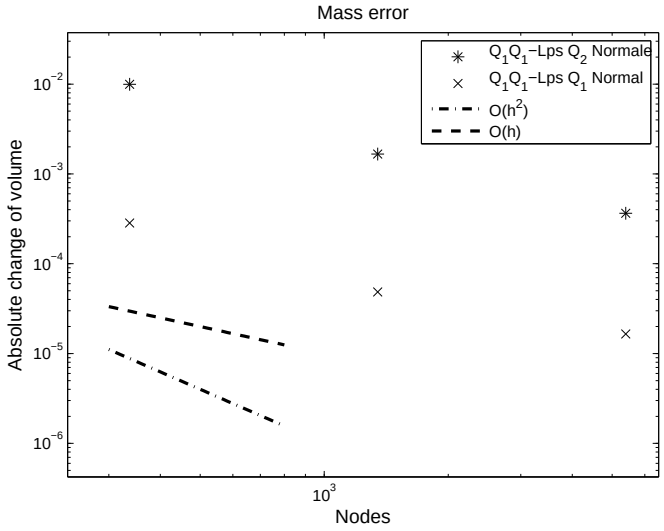

Figure 2.7: Order of convergence of the mass error for stable discretizations.

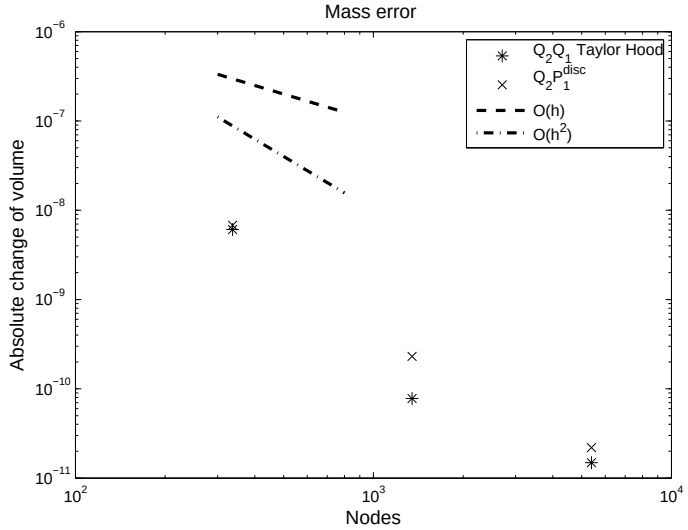

Figure 2.8: Order of convergence of the mass error for stabilized discretizations.

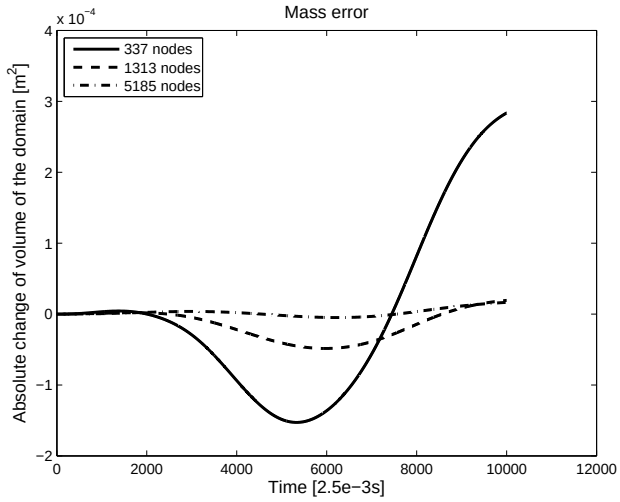

Figure 2.9: Mass error in the course of time (stabilized elements), $Q_1Q_1 - Lps$ with Q_1 normal

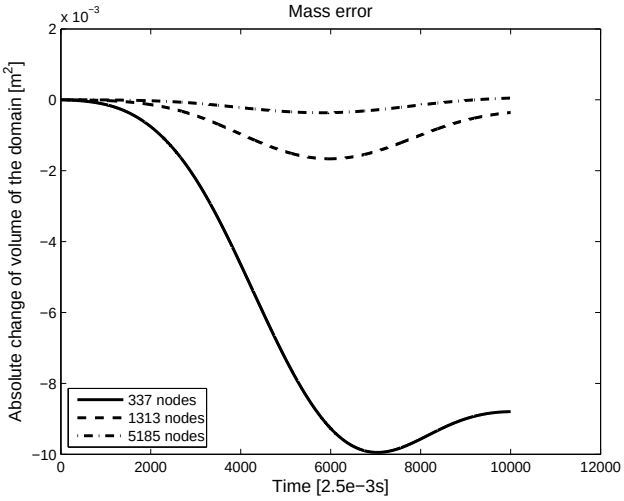

Figure 2.10: Mass error in the course of time (stabilized elements) $Q_1Q_1 - Lps$ with Q_2 normal

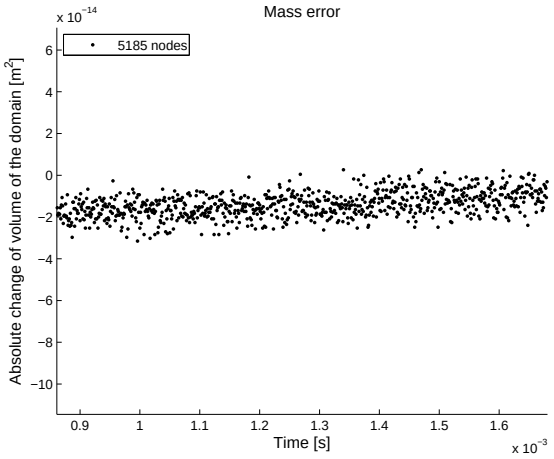

Figure 2.11: Detailed course of the mass error for the stable $Q_2P_1^{disc}$ element. The stochastic nature of the mass-error becomes visible.

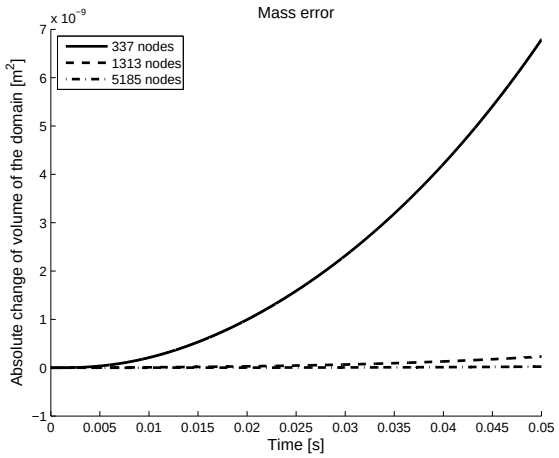

Figure 2.12: Mass error in the course of time $Q_2P_1^{disc}$.

In figure 2.7 and 2.8 the experimental order of convergence for different discretization is shown. The expectations stated above are in general confirmed. For the stabilized Q_1 element the order of convergence in case of a Q_1 approximation of the normal is approximately linear. By using a Q_2 interpolation for the normal this order can be increased to approximately quadratic convergence, the order being indeed slightly smaller than one or two respectively.

For the stable elements the error is considerably smaller. The order of convergence is also close to quadratic. Considering the much smaller error $\sim 10^{-10}$, stable elements seem to be preferable in comparison with stabilized ones when discretizing free boundary value problems. However the cell-wise mass-preserving

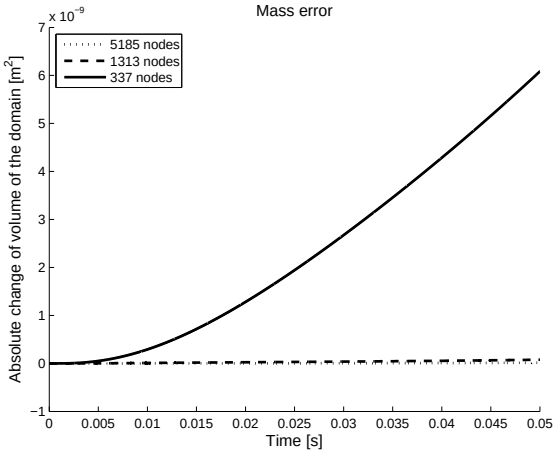

Figure 2.13: Mass error in the course of time Q_2Q_1.

element shows very similar behaviour compared to the stable but only globally mass preserving element. For both stable elements in practical applications the error due to time discretization will be dominant. This numerical example is precisely constructed to make the spatial error dominant by using very small time-steps on rather coarse grids. For the stabilized elements the error related to space discretization is dominant for a considerably larger range of time-steps.
In addition we show the mass error in the course of time for the stabilized discretization in figure 2.9 and figure 2.10 and for the stable one in figure 2.12 and figure 2.13. Figure 2.11 shows the mass error in a more detailed view.

2.3 Numerical results under fully implicit treatment of the boundary

There exists a stability bound for the time-step related to the mesh-size if the boundary is treated explicitly. This is an important drawback so that we have derived a fully implicit formulation above. It is a new method in the context of arbitrary Lagrangian-Eulerian transformations to the knowledge of the author. When using a fully implicit method, the time-step does not have to fulfill any stability condition. Due to the additional nonlinearity, nonlinear convergence may however become slow at large time-steps. In numerical applications slow convergence typically occurs at time-steps which are much larger than the stability bound for the semi-implicit scheme. Thus the implicit method is often favorable.

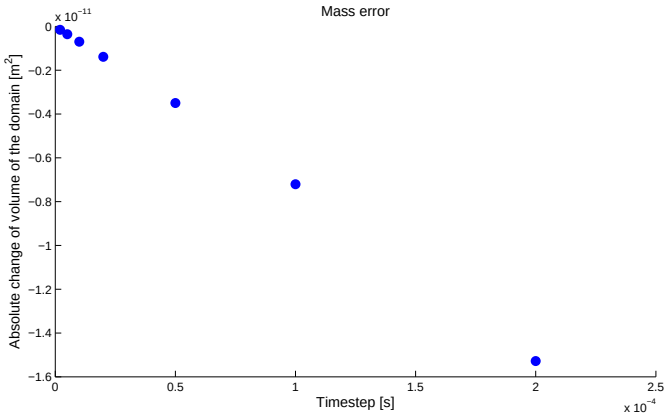

Figure 2.14: Order of convergence of the mass error for stable discretizations.

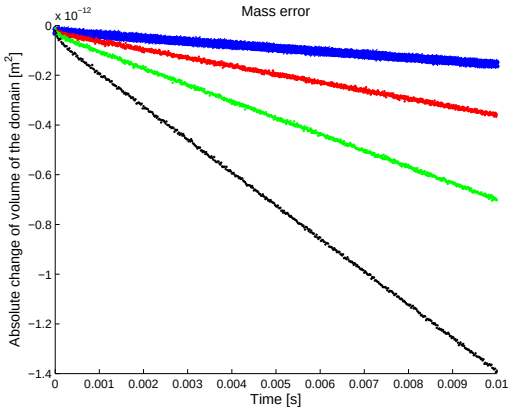

Figure 2.15: Mass error for stable discretizations and four different levels of mesh refinement.

Formula (2.9) for the evolution of the boundary is a first-oder approximation in time. We thus expect linear convergence of the mass error with respect to time discretization. In figure 2.14 we see the mass error depending on time for different levels of mesh refinement. Here we observe a clear tendency to a mass *loss*. This is different compared with the dominant spatial error where also positive errors occurred, see figure 2.11.

In figure 2.15 the mass error is plotted in the last time-step for different time-steps. Clearly linear convergence can be observed as expected.

When really large time-steps are required a linear order of convergence is unsatisfactory. It is however not straightforward to derive a second order accurate formulation. Therefore a different treatment of the free boundary would be necessary. Indeed the exact expression for the position of a point of the free boundary

at $\hat{x}$ in the reference configuration is

$$x = \hat{x} + \int_0^{\Delta t} (v(s) \cdot n(s))\, n(s) ds.$$

Formula (2.9) can be interpreted as an approximation of the integral with a box rule

$$\int_0^{\Delta t} (v(s) \cdot n(s))\, n(s) ds \sim \Delta t\, (v(0) \cdot n(0))\, n(0).$$

For the construction of a higher order method the integral would have to be approximated with a higher order integration formula.

Chapter 3

Numerical treatment of the pressure-dependent viscosity

This chapter will deal with the numerical approximation for flows with pressure-dependent viscosity. We briefly recall a theoretical existence result from literature and analyze two different ways of regularizing the problem. One approach will be to consider a slightly compressible fluid, the other one relies on cutting of the pressure-viscosity function at a certain value. The effect on the number of non-linear iterations in a benchmark example is studied. For both "regularizations" there is no proof for the existence of a solution on a continuous level. Later in the thesis both regularization methods will be applied for the simulation of elastohydrodynamic problems.

3.1 Pressure dependent viscosity in elastohydrodynamics

When modeling fluids with a continuum mechanical approach we postulate the existence of a stress tensor σ called Cauchy stress fulfilling

$$-\nabla \cdot \sigma(p, v) = f \qquad \text{in} \quad \Omega$$

where f denotes an exterior volumetric force. The physical properties of the fluid depend on the specific form of σ. For a physical model the tensor has to fulfill certain requirements. The usual assumption is that the stress of a fluid

shall only depend on pressure and on the symmetric part of the velocity gradient $D(v) = \nabla v + (\nabla v)^T$. A general formula for the stress is derived in [Hron *et al.* (2001)] and reads

$$\begin{aligned}
&\sigma = \alpha_0(p, \mathrm{I}_D, \mathrm{II}_D, \mathrm{III}_D)\mathrm{I} + \alpha_1(p, \mathrm{I}_D, \mathrm{II}_D, \mathrm{III}_D)D + \alpha_2(p, \mathrm{I}_D, \mathrm{II}_D, \mathrm{III}_D)D^2,\\
&D = \nabla v + (\nabla v)^T,\\
&\mathrm{I}_D = tr(D), \qquad \mathrm{II}_D = \frac{1}{2}\left([tr(D)]^2 - tr(D^2)\right), \qquad \mathrm{III}_D = det(D). \qquad (3.1)
\end{aligned}$$

For details on the underlying assumptions and a derivation we also refer to [Hron *et al.* (2001)] and the reference therein. Assuming that the stress depends on pressure and the velocity gradient in a linear way we find Stokes' equations

$$\sigma(p, v) = -pI + \mu D(v). \qquad (3.2)$$

Such a model with constant viscosity is called a "Newtonian" fluid. Lubrication flows in general do not obey such a model, but the viscosity μ is itself a function of pressure and the velocity gradient. In elastohydrodynamics the fluid is often modeled by a viscosity which only depends on pressure. However from a mathematical point of view there exists no theory of existence for such equations. For most theoretical results a certain dependence on the velocity gradient seems to be indispensable in order to control this quantity, see [Franta *et al.* (2005)].
Many fluids do not change their volume noticeably even under large pressure. This is modeled by an additional constraint for the velocity leading to the complete Stokes system on a domain Ω with boundary Γ

$$\begin{aligned}
-\nabla \cdot \sigma(p, v) &= f \qquad \text{in} \quad \Omega,\\
\nabla \cdot v &= 0 \qquad \text{in} \quad \Omega,\\
\sigma(p, v) = -pI + \mu D(v), &\qquad D(v) = \nabla v + (\nabla v)^T. \qquad (3.3)
\end{aligned}$$

Let us for the moment suppose that we have Dirichlet boundary conditions everywhere

$$v = 0 \quad \text{on} \quad \Gamma.$$

The value of the pressure is normalized by the condition

$$\int_\Omega p \, \mathrm{dx} = 0.$$

For the precise relationship between pressure and viscosity and or shear rate there exist a lot of models. Most of them which are used in engineering applications

contain at least as one part an exponential increase of viscosity with pressure

$$\mu = \mu_0 \exp(\alpha p). \tag{3.4}$$

This model is known as "Barus" equation after its original author.
As a consequence the value of the pressure itself, not only the gradient enters the equations. This is a remarkable difference in comparison to Stokes' equations (3.3). When considering a channel flow we can prescribe Dirichlet data everywhere together with a normalization of the pressure. Alternatively we can prescribe a Neumann type boundary condition on the outflow $\mu\partial_n v - pn = 0$. This is leading to a pressure normalization at the Neumann boundary.
If we compare both solutions only the pressure is shifted by a constant, the velocity fields are equal. In the case of the Barus material law both solutions would be completely different including the velocity fields. Consequently the precise way of imposing boundary conditions is absolutely crucial.
We remark at this point that in an incompressible fluid model the variable denoted "pressure" does not automatically play the role of the correspondent physical, thermodynamical variable. In a compressible fluid model there is an additional equation relating pressure and density. Consequently the equations do always depend on the absolute value of the pressure in this case. The pressure of an incompressible model is more subtle do interpret and does not have to be equivalent to the thermodynamical pressure. In fact incompressibility is an approximation based on the experimental observation that many fluids do not change their volume noticeably even when exerting large pressures. However exact incompressibility does not occur in nature and also in lubrication flows there is some change of volume under pressure. A model often used in engineering science for the density as a function of pressure is stated in [Křupka *et al.* (2000)] as

$$\rho(p) = \rho_0 \left(1 + \frac{ap}{1+bp}\right). \tag{3.5}$$

Here $a = 0.6\times10^{-9}[\frac{1}{Pa}]$ and $b = 1.7\times10^{-9}[\frac{1}{Pa}]$ are empirical parameters depending on the specific fluid under consideration. The constraint $\nabla \cdot v = 0$ is replaced by

$$\nabla \cdot (\rho v) = 0$$

in a stationary setting. In this thesis we stick to dealing with incompressible fluids anyway since changes in volume are quite small but the pressure-density relation (3.5) would introduce an additional nonlinearity. The changes in density with the given model and parameters would be insignificant.

3.2 Formulation of the regularized problem

There exist many different models for fluids in lubrication flow. Usually these models result from experiments. Different types of parameterized functions are fitted to match measurements for fluids under certain conditions. These models are often not very general within the meaning of applicability to different fluids. For different fluids, different empirical material models or at least different sets of parameters exist. Yet one fact is common for nearly all models coming from application: There exists no theory of existence for Stokes' equations if the viscosity as function of pressure and/or shear rate is plugged in.
Recently some effort has been made in order to derive a theory of existence for non-Newtonian fluids. The results do not cover the models coming from applications since there are restrictions for the increase of viscosity. Furthermore there exists no theory for fluids where the viscosity *only* depends on pressure as it is often the case for lubrication flow. A certain functional relation between velocity gradient and viscosity is needed theoretically in order to control the velocity gradient.
In order to motivate the regularizations we will propose later, we now cite a theoretical result given in [Franta *et al.* (2005)]. They propose a slightly compressible model with a small parameter ϵ determining the degree of compressibility. In their proof the parameter tends to zero recovering a fully incompressible model. In numerical simulations we will also use a simular term inspired by this theoretical piece of work but keep a finite value of the regularization.
For the proof a specific form of the viscosity is required.

Definition 3.1 (Admissible viscosity)**.** *Let the viscosity be of the form*

$$\nu_i(p, |D|^2) = (A + \gamma_i(p) + |D|^2)^{(r-2)/2} \tag{3.6}$$

where $A \in (0, 1]$ *and* $r \in (1, 2)$*, furthermore*

$$\gamma_1(p) = \left(1 + \alpha^2 p^2\right)^{-q/2},$$
$$\gamma_2(p) = \left(1 + \exp(\alpha p)\right)^{-q},$$
$$\gamma_3(p) = \begin{cases} \mu_0 \exp(-\alpha q p) & \text{if } p \geq 0, \\ 1 & \text{else.} \end{cases}$$

A viscosity of such form is called admissible if α *and* q *are positive and in addition some technical requirements on parameters are met, see [Franta* et al. *(2005)].*

With this definition we are now able to quote the existence result by [Franta *et al.* (2005)].

Theorem 3.1. *Let* $\Omega \subset \mathbb{R}^2$, $\frac{3}{2} < r < 2$ *and* $f \in W^{1,r}_{0,div}(\Omega)^2$.
Then there exists at least one weak solution such that $v \in W^{1,r}_{0,div}(\Omega)^2$, $p \in L^{r'}(\Omega)$

$$\int_\Omega [\nabla v] v\phi + \int_\Omega \nu(p, |D(v)|^2) D(v) \colon D(\phi) - \int_\Omega p \nabla \cdot \phi = < b, \phi > \quad \text{for all} \quad \phi \in W^{1,r}_{0,div}(\Omega)^2 \tag{3.7}$$

Proof. The proof as well as further references and background on existence theory for non-Newtonian fluids can be found in [Franta *et al.* (2005)]. □

As mentioned above the result is not directly applicable to lubrication problems. The most common model in this case is Barus' equation $\mu = \mu_0 \exp(\alpha p)$. This form of the viscosity is not admissible in the sense of the theorem since the term $|Dv|$ does not appear. Furthermore the term A in (3.6) would equal zero and the exponent p would equal two which both is not allowed. Even it these requirements were met the additional prerequisite on the size of parameters for admissible viscosities cannot be guaranteed in general.
In this thesis we consider Barus' law together with some regularizations introduced later on. Without regularization Barus' law leads to unbounded numerical approximations for realistic parameters and geometry. This could be a hint that this model indeed does not possess a solution on the continuous level.
The weak formulation of the generalized Stokes equations with pressure dependent viscosity reads

Problem 3.1 (Barus model)**.** *Find* $p \in L^2(\Omega)$, $v \in H^1(\Omega)^2$ *such that*

$$\begin{aligned} (\mu(p)\nabla v, \nabla \phi) - (p, \nabla \cdot \phi) &= (f, \phi), \\ (\nabla \cdot v, \chi) &= 0, \end{aligned}$$

for all $\chi \in L^2(\Omega)$, $\phi \in H^1(\Omega)^2$.

For the Barus model we would in principle set

$$\mu(p) = \mu_0 \exp(\alpha p).$$

However for $p \in L^2(\Omega)$ the resulting problem might not be well-posed. Also the numerical approximation in this case usually leads to unbounded solutions, we therefore consider two ways of regularizing the problem:

- Cutoff: We replace $\mu(p) = \mu_0 \exp(\alpha p)$ by a bounded expression

$$\mu(p) = \begin{cases} \mu_0 \exp(\alpha p) & \text{if } p < p_{max}, \\ \mu_0 \exp(\alpha p_{max}) & \text{else.} \end{cases}$$

  For the purpose of numerical approximation such a regularization does always lead to bounded solutions if p_{max} is sufficiently small. The existence of a continuous solution to this problem is however no easy question. The regularized problem does not fit in the theoretical framework cited above. Since the nonlinearity in the main part of the differential operator is still present in problem (3.1) there is also no other standard way to proof existence. Only numerical experience gives an indication that the regularized problem might indeed possess a solution.

- Artificial compressibility: We let the viscosity unchanged $\mu(p) = \mu_0 \exp(\alpha p)$ and change the divergence constraint with a small parameter ϵ such that

$$\nabla \cdot v + \epsilon \Delta p = 0.$$

  For the discretized problem we also observe that for sufficiently large ϵ there exists a solution. This type of regularization is closely related to the approximating problem of (3.7) in [Franta *et al.* (2005)]. In this reference a similar Laplacian term in the divergence constraint is added as an approximating problem. It is shown that there exists a weak solution also for the limit case of vanishing compressibility. We remark that also this regularization does not lead directly to the existence of a solution to the continuous problem. Again the Barus law for the viscosity does not fit in the framework of the existence theorem where the parameter ϵ tends to zero. The requirement for the admissible form of the viscosity is not met.

When using artificial compressibility as a method we *do not* make the parameter ϵ tend to zero on fine meshes. In doing so the problem would require more and more nonlinear iterations as the mesh becomes finer. This effect can be seen clearly in numerical simulations with e.g. the GLS-stabilized finite elements. This stabilization method adds a similar mesh-dependent term for stabilizing the linear systems arising from discretization.
Thus we will in our simulations keep a finite value for the regularization. Under high pressure in lubricant flow we know that the fluid is no more completely incompressible either. We remark that LPS-type stabilizations are not applicable

Regularization: ϵ	Drag	Lift	Nonlinear iterations
10^{-0}	0.014776020	-0.00000315	4
10^{-1}	0.063213262	0.000276081	3
10^{-2}	0.165761649	0.002033453	4
10^{-3}	0.293184182	0.005185094	8
9×10^{-4}	0.303288114	0.005408936	3
8×10^{-4}	0.318738514	0.005727693	4
7.5×10^{-4}	0.332383735	0.005984584	5
7.2×10^{-4}	0.349735928	0.006279133	5
7.15×10^{-4}	0.356868317	0.006390558	5
7.14×10^{-4}	0.359350505	0.006428111	3
7.13×10^{-4}	0.364035237	0.006497336	6
7.129×10^{-4}	0.365591922	0.006519875	5

Table 3.1: Influence of artificial-compressibility-regularization on functional values and nonlinear iterations.

for large pressure dependent viscosity as they lead to oscillations in pressure and singular matrices.
In a similar spirit we can add a pseudo time derivative in the divergence equation which often reduces the stiffness of the discrete system considerably. On the other hand in this case a sequence of problems has to be solved and slow convergence may occur. For completeness we show the regularized system with both types of regularization

Problem 3.2 (Discretized Barus model)**.** *Find $p_h \in X_h$, $v_h \in V_h$, such that*

$$
\begin{aligned}
(\mu(p_h)\nabla v_h, \nabla\phi) - (p_h, \nabla\cdot\phi) &= (f,\phi),\\
(\nabla\cdot v_h, \chi) + \epsilon(\nabla p, \nabla\chi) &= 0,\\
\mu(p) = \begin{cases} \mu_0 \exp(\alpha p) & \text{if } p < p_{max} \\ \mu_0 \exp(\alpha p_{max}) & \text{else} \end{cases},&
\end{aligned}
$$

for all $\chi \in X_h$, $\phi \in V_h$.

Furthermore the problem can be linearized around a known pressure $\overline{p}$ which leads to a linear problem with variable coefficient. Usually linearizations in the course of pseudo-time iterations unfortunately lead to instabilities in combination with the fluid-structure interaction problem which will later be presented. In

Regularization: p_{max}	Drag	Lift	Nonlinear iterations
0.1	0.074497934	0.000716068	3
1.0	0.213158154	0.003156162	12
1.5	0.276729261	0.004785104	7
2.0	0.350177004	0.006586801	9
2.2	0.396552027	0.007509716	34
2.3	0.427896474	0.008082925	7
2.35	0.446375737	0.008408280	5
2.4	0.467081760	0.008762729	6
2.45	0.490313214	0.009149471	5
2.5	0.516395084	0.009573050	6
2.55	0.545690978	0.010035351	6
2.6	0.578588485	0.010542554	5
2.65	0.615534779	0.011096559	6
2.7	0.657028002	0.011703898	6
2.75	0.703540965	0.012368441	6
2.8	0.755685136	0.013093591	6
2.85	0.814035110	0.013894010	6
2.9	0.879400872	0.014774989	7
2.95	0.952504082	0.015747731	6
3.0	1.034190477	0.016827420	6
3.05	1.125495881	0.018035291	6
3.1	1.227434498	0.019402558	7
3.15	1.341277730	0.020976851	8
3.2	1.468508715	0.022821164	8
3.25	1.610758352	0.025058006	9
3.3	1.770061663	0.027860784	9
3.35	1.949233912	0.031562927	8
3.4	2.152502767	0.036890980	8
3.45	2.387306132	0.045527795	10
3.5	2.661934172	0.058078256	19
3.55	2.970108081	0.072271659	10
3.551	2.977626574	0.072824349	11
Newtonian fluid	Drag	Lift	Nonlinear iterations
$\alpha = 0$	0.064372508	0.001604307	1

Table 3.2: Influence of cutoff-regularization on functional values and nonlinear iterations.

table 3.1 and 3.2 we show the influence of the two types of regularization on the nonlinear convergence as well as on the drag and lift on the cylinder in the flow. The domain corresponds to the benchmark problem of flow around a cylinder in two dimensions proposed by [Schäfer & Turek (1996)]. The pressure-viscosity coefficient is 1.6 and the viscosity at zero pressure is 0.01. The boundary conditions are the same as in [Schäfer & Turek (1996)] namely a parabolic inflow. In this specific situation, the discrete nonlinear algebraic systems can not be solved without a regularization. Newton's method will not converge, without damping it will explode, with strong damping it will stagnate. We consider two ways of regularizing the problem which actually lead to the solvability of the discrete systems. The numerical algorithm leading to the results shown in 3.2 is the following: The discretization consists of Q_1 elements for pressure and velocity with GLS-stabilization, see [Hughes *et al.* (1986)].
The problem was solved with initial value zero and the strongest regularization parameter in the beginning. This leads to 4 Newton iterations for the method of artificial compressibility and to 3 Newton iterations for cutoff regularization and is shown in table 3.1 and 3.2 as first entry.

Figure 3.1: Surface plot of pressure for two dimensional benchmark flow example without (l.) and with (r.) pressure dependent viscosity

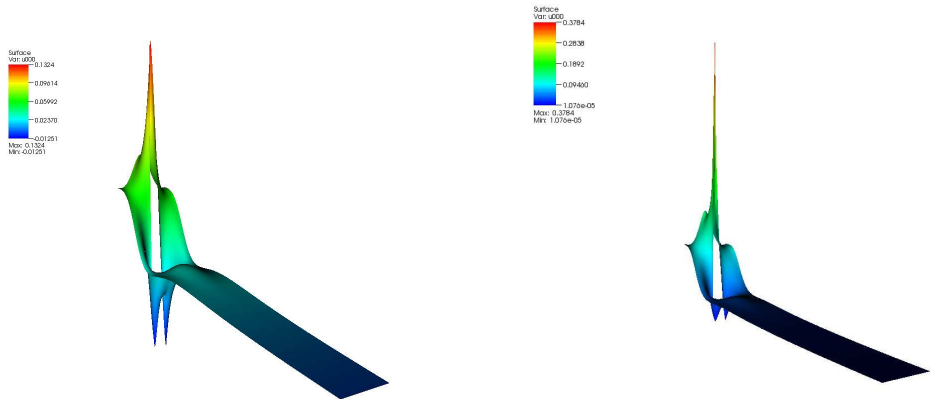

For the solution considering all other regularization parameters, the regularization was decreased and the last solution was taken as initial solution for the problem with smaller regularization. The number of nonlinear iterations is shown in table 3.1 and 3.2. For the Newtonian case we deal with a linear problem and only need one nonlinear iteration and no regularization, of course.
Both regularization strategies alter the problem in a way that the discrete equa-

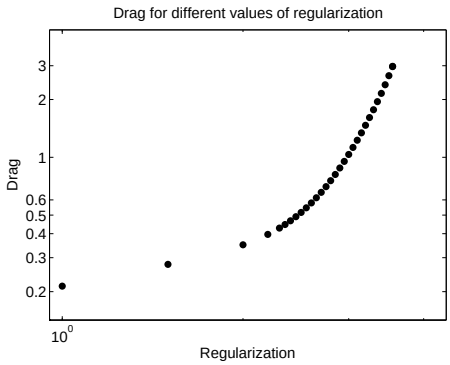

Figure 3.2: Drag depending on value of cutoff-regularization parameter.

tions become solvable for sufficiently strong regularization. However, when the regularization is decreasing, there exists a limit where the number of nonlinear iterations explodes and finally no convergence at all can be achieved. In practical applications we will therefore have to work with finite regularization parameters. The regularization with a cutoff of the exponential function leads to a non-convex and non-differentiable viscosity-pressure relationship. This explains the higher number of iterations generally needed for this method. One could also find a differentiable cutoff-function instead of equation (3.2). Some numerical experiments conducted by the author indicate that this is not leading to substantially different results.
In this example the pressure dependent viscosity is still very moderate compared to elastohydrodynamics, although the discrete equations can only be solved with regularization. The benchmark configuration leads to a maximum increase in viscosity by a factor of $\exp(\alpha p) = \exp(1.7 * 2.7) \sim \exp(4.5)$ whereas in ball bearings an increase of a factor $\exp(\alpha p) = \exp(2.4 \times 10^{-8} * 5 \times 10^{8}) \geq \exp(12)$ is not uncommon.

Figure 3.1 shows the somehow more pronounced pressure peak in the case of benchmark flow with pressure dependent viscosity. Without regularization typically the pressure peak will increase and become unbounded as α is increasing. At such a critical value of an exponent around 5 there seems to be a mesh dependent limit for convergence of the algorithm. It leads to more and more iterations as the regularization is decreased. This effect can be seen clearly in table 3.2: For an increase of the cutoff parameter from 3.5 to 3.55 it takes 10 Newton iterations to converge, for the subsequent increase from 3.55 to 3.551 it takes already 11 iterations although the difference in regularization is much smaller in the latter case. We believe that this can be considered as a numerical hint that no con-

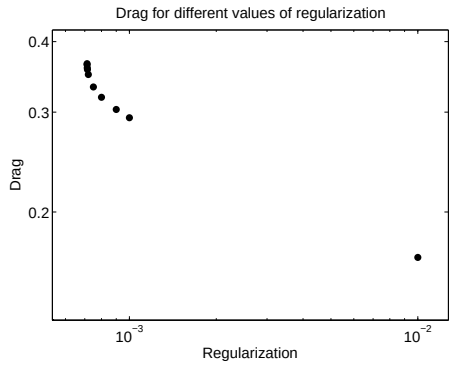

Figure 3.3: Drag depending on value of artificial-compressibility-regularization parameter.

tinuous solution exists for the unregularized problem. Such a conclusion can be also justified regarding figure 3.2 and figure 3.3. In both figures we observe that there seems to be no convergence for decreasing regularization but the slope of the drag becomes infinite for small regularizations at some point.

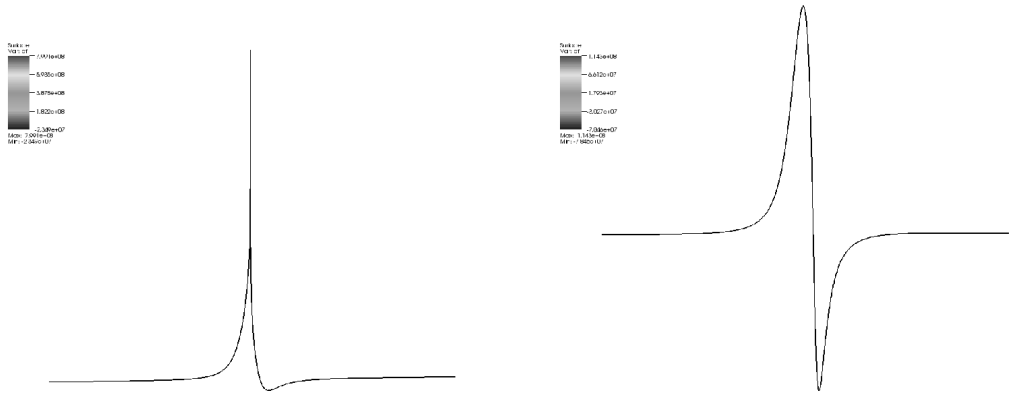

Figure 3.4: Simulation results of pressure profiles in a ball bearing with (l.) and without (r.) pressure dependent viscosity. For pressure dependent viscosity a huge pressure spike arises and the profile becomes highly unsymmetric compared to the Newtonian case. Note also the regions of negative pressure, the region of nearly constant pressure corresponds to zero pressure.

In figure 3.4 we show a typical pressure profile on a domain arising in simulations for ball bearings. Notice that the pressure becomes highly unsymmetric for the pressure dependent viscosity. The regions with high pressure are larger and the maximum value of the pressure is much higher. This leads to a net force on the surrounding structure which tends to increase the distance between ball and structure thus stabilizing the motion and preventing contact. We conclude that pressure dependent viscosities are absolutely crucial for realistic models for ball bearings. One of the main goals of this thesis was to present a method to simulate

the elastohydrodynamics film thickness in ball bearings. With the above remarks it becomes clear that this quantity is very sensitive with respect to pressure dependent viscosities. This fact also showed up in all numerical simulations. It is one of our principal observations that pressure dependent viscosities always play an important role in elastohydrodynamics. Therefore this effect should be included in any realistic model.

3.3 Cavitation

During the simulation of lubrication flow another problem arises: The pressure will in practically all situations and for all meaningful types of boundary conditions show regions with negative pressure. We emphasize that this problem can not be overcome by any physically motivated choice of boundary conditions. Indeed the fluid domain always has parts at the inflow and outflow with a "free boundary". We refer to chapter 3 for the derivation of the boundary condition at the free boundary. It reads

$$\sigma n = \gamma \kappa n.$$

This is enforcing a pressure normalization which in practice leads to a nearly vanishing pressure drop throughout the domain as in figure 3.4. We remark that in this situation the fluid motion is not driven by a pressure drop but by the no-slip condition at the boundary of the ball. The regions with negative pressure are caused by the curvature of the domain: Since the fluid domain consists of one converging and one diverging part it comes to high positive pressure in the first and to high negative pressure in the latter part. Indeed these pressure peaks are in a Newtonian model close to symmetric and only the pressure dependent viscosity leads to a strong increase in the positive part. In regions with small or negative pressure the pressure is only changed less significantly.
Yet negative values of the pressure are in general nothing extraordinary e.g. when using mean normal pressure $\int_\Omega p \, \mathrm{dx} = 0$ they always occur if the pressure does not happen to be constant. Here the situation is different since a pressure normalization at the outflow and inflow is given and yet the pressure reaches high negative values. In this situation it is clear that a fluid in reality will not be able to sustain this large negative pressure. Instead spontaneously gaseous or vacuum-like cavitation will appear in the fluid. In these regions the Navier-Stokes equations

are no longer a valid model but the cavitated region would need a different treatment. In [Sahlin *et al.* (2007)] it is modeled as a free boundary value problem. In [Nilsson & Hansbo (2008)] a cavitation model for Stokes' equations is presented which leads to a variational inequality in the divergence constraint.
However in huge parts of the engineering literature the problem of cavitation is not mentioned explicitly. Alternatively it is covered with post-processing or disregarding negative values of the pressure when evaluating functionals.
In experimental work cavitation is also rarely studied. In [Dhunput *et al.* (2007)] pressure profiles with cavitating regions are shown. However this publication deals with piston-rings and not with bearings directly. In [Dowson & Taylor (1979)] some further examples for cavitation are given. In this thesis no special cavitation model will be used. Where negative pressure arises in simulations which is the case practically always we let it stand without any further handling. In simulations for ball bearings the cavitating regions are small and the negative values of pressure are also much smaller than the maximum positive pressure as shown in figure 3.4. Consequently we neglect cavitation as physical phenomenon. However we will for the sake of completeness shortly comment on how cavitation could be included in elastohydrodynamic simulations leaving the implementation open for further research. Mathematical model equations are derived in [Nilsson & Hansbo (2008)] as follows:
Let K be the space of positive pressure

$$K = \{p \in L^2(\Omega) \quad | \quad p \geq 0\}.$$

The modified Stokes equations then read

Problem 3.3 (Stokes equations with cavitation)**.** *Find $v \in H^1(\Omega)^2$, $p \in K$, such that*

$$\begin{aligned}(\mu\nabla v, \nabla\phi) - (p, \nabla \cdot v) &= (f, \phi) \\ -(\nabla \cdot v, (p - q)) &\leq 0 \end{aligned} \tag{3.8}$$

for all $\phi \in H^1(\Omega)^2$, $q \in K$.

Problem (3.3) is the most fundamental cavitation model in the following sense:

- The solution does really fulfill $p \geq 0$ by construction.
- The solution coincides with a solution to Stokes' equations if the boundary conditions and right hand side already result in positive pressure everywhere.

We would be reasonable in requiring these two assumptions but in most cavitation models used in engineering literature they are not fulfilled.
In [Nilsson & Hansbo (2008)] the authors claim using an Uzawa algorithm for the solution of the discrete algebraic equations. Although this may be feasible for discretizations of Stokes' equations on a simple domain it will suffer from very slow (if at all) convergence on anisotropic domains in lubrication flow. Furthermore the generalization for solving fluid-structure interaction problems is not straightforward. Therefore it would be necessary to develop efficient solvers for treating equations (3.3) which is why we refrain from considering this model any further.
Another cavitation formulation which meets the above criteria when using the Reynolds equation is described in [Durany *et al.* (1996)]. This formulation is based on a free boundary value problem to model the cavitating region.
In order to give an idea of a typical approach to deal with cavitation in engineering literature we also describe such a model. In [Gwynllyw *et al.* (1996)] a change of the viscosity for negative pressure is proposed. For this purpose the pressure viscosity relation is also cut off for negative values in a smooth way

$$\begin{aligned} \mu(p) &= \mu_{min}(1 - g(p)) + \mu_0 \exp(\alpha p) g(p) \\ g(p) &= \frac{\psi(p-\delta)}{\psi(p-\delta) + \psi(p)} \\ \psi(p) &= \begin{cases} 0 & \text{if } p < 0 \\ exp(-1/p) & \text{if } p \geq 0. \end{cases} \end{aligned} \tag{3.9}$$

Therein equation (3.9) δ is a parameter of a minimal allowable pressure $\delta \sim 0$, for this purpose $10^3 Pa$ is a small value in lubrication flow.
Such a variation of the pressure-viscosity function will not lead to a solution which has positive pressure everywhere.
Furthermore the Navier-Stokes equations break down in cavitating regions which is not removed by merely changing the viscosity. Besides, numerical experiments with equation (3.9) indicate that the nonlinearity introduced thereby can be very problematic.
We cannot solve this problem entirely in the course of this thesis. When considering simulations for ball bearings negative pressure usually *does* appear but not in a quantitatively decisive way. If cavitation happens in real physical ball bearing systems is unclear, the number of experimental studies of this question in literature is small. As a consequence we neglect cavitation and let the solution stand with possibly occurring regions of negative pressure. In some cases especially when considering slow rotations cavitation can lead to a higher stiffness

of the entire system with fluid-structure interaction. This stems from the fact that in the cavitating region contact or at least close approach of the ball and the bearing will arrive. In these regions the mesh will consequently degenerate as described in detail in chapter 4. Since for very slow rotations the whole modeling including the generalized Navier-Stokes equations is questionable due to small film heights, we will not be considering this case and neglect cavitation.

3.4 Reynolds' equation

In this thesis all simulations are based on generalized Navier-Stokes equations. This is by no means the most common approach, contrarily in lubrication science Reynolds' equation is used almost exclusively. Since considering the Reynolds equation would be the most common starting point we will shortly comment on this possibility. Reynolds' equation reads in strong form

$$\partial_x \left(\frac{h^3}{\mu} \partial_x p \right) + \partial_y \left(\frac{h^3}{\mu} \partial_y p \right) = 6U \partial_x (\rho h) + 6h \partial_x U + 12V. \tag{3.10}$$

Here h is the film height usually given as an exterior parameter describing the geometry of the problem in consideration. The known, fixed velocity of the surrounding structure is denoted U and V respectively. Hence all terms on the right hand side of equation (3.10) are known. The equation can therefore be considered as a second order elliptic equation with (often strongly) varying coefficients.
For a detailed derivation of Reynolds equation we refer to [Szeri (2000)]. We yet state that Reynolds equation can be derived as an approximation of the Navier-Stokes equations with constant viscosity considering thin films. It will therefore be an accurate approximation for thin films. If the film thickness becomes too small the Navier-Stokes equations are not valid anymore and consequently also Reynolds' equation is no accurate model. In this case *all* analytical and numerical methos based on continuum assumptions are questionable. This includes also the models presented in this thesis, of course.
For high film thicknesses the scaling argument becomes a rough approximation and Reynolds' equation also breaks down. In equation (3.10) only the pressure is considered as unknown, all information about the velocity field is lost.
Also notice that the analytical approximation for elastohydrodynamic film thickness is derived from Reynolds' equation with the implied limitations stated below.
We now conclude in reasoning why in this thesis Reynolds equation is *not* con-

sidered.

- The film thickness can not simply be considered as unknown but has to be fixed before. In the case of high pressure lubrication this is unrealistic. Although there are heuristic approaches to deal with fluid-structure interaction in the framework of Reynolds' equation they rely on rough approximations, see e. g.[Křupka *et al.* (2000)]. Consequently the quality of such approximation is more questionable than using a more fundamental model based on the original continuum mechanical principles.

- Non-Newtonian fluid models can not be treated directly when considering Reynolds' equation. Indeed when deriving the Reynolds approximation viscosity is considered constant. If afterwards a variable viscosity is plugged in the equation, the derivation becomes inconsistent and violates the previously made assumptions. This is discussed in detail in [Rajagopal & Szeri (2003)] and can be overcome by a different derivation. In literature Reynolds' equation is though also often used in an inconsistent way. Also note that similar questions of existence like for Stokes' equations are open for the Barus pressure-viscosity model together with Reynolds' equation.

For testing reasons we also conducted simulations based on the Reynolds equation while establishing this thesis. When using Reynolds' equation in combination with pressure dependent viscosity the numerical solution of the algebraic equations also becomes a difficult task. In summary we refrain from using Reynolds equation.
Since the Navier-Stokes equations or its generalizations are no correct model for arbitrarily small volume there exist also different techniques for the simulation of very small films. In [Rajagopal & Szeri (2003)] molecular dynamics simulations are proposed for film thickness $\leq 10nm$. This method does not act on the assumption of continuous media but describes single particles and their stochastic interaction. It would be an interesting aspect to carry out simulations based on such a discrete model and to compare them with the results coming from the Navier-Stokes equations. Since molecular dynamics simulations require completely different numerical methods, this is difficult to put into practice at the same time and we leave this question open for further work.

Chapter 4

Fluid-structure interaction in elastohydrodynamics

In this chapter we will show a formulation of fluid-structure interaction problems suitable for a robust numerical discretization. This method is called "monolithic" because it poses one common set of equations for fluid and structure simultaneously. The interior of the fluid domain will undergo an arbitrary transformation, therefore we need to provide the equations of continuum mechanics on transformed domains.
We proceed with details on discretization and some aspects specific to the simulation of ball bearings like for example the treatment of pre-loading.

4.1 Derivation of the arbitrary Lagrangian Eulerian formulation

In ball bearings high pressure is prevailing leading to the deformation of the surrounding structure. Hence the domain of the lubricating flow cannot be considered as known a priori, not even if neglecting the free boundary at the inflow and outflow. Rather the deformation is responding and finally reaching a state fulfilling a balance of forces between the fluid and the structure. Thus we have to consider a fluid-structure interaction problem.
The coupling of the deformation with the fluid flow in lubrication flow is called elastohydrodynamic lubrication and is usually very pronounced. Even small

changes in the shape of the fluid domain lead to a large response in the pressure profile. Therefore it is suitable for numerical simulations to use also strongly coupled, implicit algorithms because of the stiffness of the discrete systems. We will in the subsequent describe such an implicit formulation and a numerical algorithm to find approximate solutions.

When dealing with fluid-structure interaction the dilemma is that the natural reference frame for a deformable structure is *Lagrangian* but for a fluid it is *Eulerian*. Indeed when modeling deformable structures we identify points in the domain with material points and consider their change of position under deformation. The change of the position of single particles is often not a very useful concept when dealing with fluids. For instance fluid particles may, depending on boundary conditions, enter or leave the flow domain under consideration. For fluids it is thus rather reasonable to consider the velocity field at a single fixed point in the domain. This difference in the underlying description has to be resolved somehow when dealing with fluid *and* structure at the same time. One way is to keep the natural Lagrangian description of the structure and to *transform* the fluid domain. The fluid is somehow also considered in a Eulerian domain but on a moving domain which is recovered by the actual configuration of a given reference state. We will now shortly derive this formulation, detailed calculations and proofs can be found in [Quarteroni (2004)].

Definition 4.1 (Regular Transformation)**.** *Let* $\hat{\Omega} \subset \mathbb{R}^2$ *be the reference domain,* $\Psi : \hat{\Omega} \times \mathbb{R}_+ \to \mathbb{R}^2$ *be a diffeomorphism* $\Psi(\cdot, t) \in \mathcal{C}^1(\overline{\hat{\Omega}}, \overline{\Omega})$, $\Psi(\cdot, t)^{-1} \in \mathcal{C}^1(\overline{\Omega}, \overline{\hat{\Omega}}) \quad \forall t$. *We call* Ψ *regular transformation if* $\det(\hat{\nabla}\Psi(\hat{x}, t)) > 0 \quad \forall \hat{x} \in \hat{\Omega}, \quad \forall t \geq 0$.

Definition 4.2 (Deformation)**.** *Let* Ψ *be a regular transformation. We call* $\hat{u} : \hat{\Omega} \to \mathbb{R}^2$, $\hat{u} = \Psi - Id$ *deformation.*

Below we denote the gradient of the transformation as $\hat{F}$, $\hat{F} = \hat{\nabla}\Psi$ the determinant of the deformation with $\hat{J} = \det(\hat{F})$. For the derivation of the differential equations we need the change of vector- and tensor-valued functions under transformation. We now show the formulas relating these quantities.

Proposition 4.1 (Scalar- and vector-fields under transformation)**.** *Let* $\hat{f} : \hat{\Omega} \times \mathbb{R}_+ \to \mathbb{R}$, $f : \Omega \times \mathbb{R}_+ \to \mathbb{R}$, $x_t = \psi(\hat{x}, t)$ *be differentiable with the property* $f(\Psi(\hat{x}, t)) = \hat{f}(\hat{x}, t) \quad \forall \hat{x}$ *in* $\hat{\Omega}$, $\forall t \geq 0$. *There holds*

$$\nabla f(x) = \hat{F}^{-T} \hat{\nabla} \hat{f}(\hat{x}).$$

For vector-valued differentiable function $\hat{g} : \hat{\Omega} \times \mathbb{R}_+ \to \mathbb{R}^2, \quad g : \Omega \times \mathbb{R}_+ \to \mathbb{R}^2$ *with* $g(\Psi(\hat{x}, t)) = \hat{g}(\hat{x}, t) \quad \forall \hat{x}$ *in* $\hat{\Omega}$, $\forall t \geq 0$ *there holds*

$$\nabla g(x) = \hat{F}^{-1} \hat{\nabla} \hat{g}(\hat{x}).$$

Proof. The assertion follows directly by applying the chain rule. □

The equations of continuum mechanics can be written in the form $\nabla \cdot \sigma = f$ where σ is a tensor of second order. We now consider the transformation of tensors. In literature the following transformation $\hat{\tau}$ of a tensor σ is called "Piola" transformation.

$$\hat{\tau}(\hat{x}) = \hat{J}(\hat{x}) \sigma(\hat{x}) \hat{F}(\hat{x})^{-T}$$

Proposition 4.2 (Divergence of the Piola transformation)**.** *For a differentiable tensor-field* $\sigma : \Omega \to \mathbb{R}^{2\times 2}_{sym}$ *there holds*

$$\hat{\nabla} \cdot \hat{\tau} = J \nabla \cdot \sigma \tag{4.1}$$

Proof. The proof is elementary and can be found for instance in [Quarteroni (2004)]. □

In this thesis we mostly deal with stationary situations. For completeness we will also consider time derivatives and their transformation.

Proposition 4.3 (Time derivatives)**.** *Let* Ψ *be a regular transformation* $\hat{f} : \hat{\Omega} \times \mathbb{R}_+ \to \mathbb{R}, \quad f : \Omega \times \mathbb{R}_+ \to \mathbb{R}$ *differentiable with the property* $f(\Psi(\hat{x}), t) = \hat{f}(\hat{x}, t) \quad \forall \hat{x} \quad in \quad \hat{\Omega}, \quad \forall t \geq 0$. *There holds*

$$\partial_t f = \partial_t \hat{f} - (\hat{F}^{-1} \partial_t \hat{\Psi} \cdot \hat{\nabla}) \hat{f}.$$

Proof. The proof is straightforward and can be found in [Quarteroni (2004)]. □

We will now show the equations describing the structure and the fluid. Ball bearings are usually made of steel. In experiments sometimes parts of the surrounding structure are made of sapphire. Relative deformations will be in general small. In

this case both materials can be modeled as St.-Venant-Kirchhoff material. The derivation of the equations is standard and can be found in [Braess (2007)]

$$\begin{aligned} \hat{\rho}_s \partial_t^2 \hat{u} - \hat{\nabla} \cdot (\hat{J} \hat{\sigma}_s \hat{F}^{-T}) &= \rho_s \hat{f} \qquad \text{in} \quad \hat{\Omega}_s, \\ \hat{\sigma}_s &= \hat{J}^{-1} \hat{F} \left(\lambda tr(\hat{E}) I + 2\mu \hat{E} \right) \hat{F}^T, \\ \hat{F} = I + \hat{\nabla} \hat{u}, \quad \hat{J} = \det(\hat{F}), \quad \hat{E} &= \frac{1}{2} \left(\hat{F}^T \hat{F} - 1 \right). \end{aligned} \tag{4.2}$$

The fluid is described as non-Newtonian and on a constant, undeformed domain $\hat{\Omega}_f$ there holds

$$\begin{aligned} \hat{\rho}_f \partial_t \hat{v} + \hat{\rho}_f [\hat{\nabla} \hat{v}] \hat{v} - \hat{\nabla} \cdot \hat{\sigma}_f(\hat{p}, \hat{v}) &= \hat{\rho}_f \hat{f} \quad \text{in} \quad \hat{\Omega}_f, \\ \hat{\nabla} \cdot \hat{v} &= 0 \quad \text{in} \quad \hat{\Omega}_f, \\ \hat{\sigma}_f(p, v) = -p\mathrm{I} + \mu D(v), \quad \mu(p) = \mu_0 \exp(\alpha p), \quad D(v) &= \nabla v + (\nabla v)^T. \end{aligned} \tag{4.3}$$

Thus we are in a position to formulate the fluid-structure interaction problem. In figure 4.1 we show a scheme of the basic situation. The domain has an outer boundary Γ_d where Dirichlet boundary conditions are posed for the structure. There is also a free boundary with a Neumann condition. Furthermore we have an interface between fluid and structure. Here we have to keep in mind that the boundary is moving. Applying Gauss' theorem to the Piola transformation (4.1) we obtain

$$\int_{\partial \hat{\Omega}} \hat{\tau} \hat{n} = \int_{\Omega} \nabla \cdot \sigma.$$

The equation of balance of forces on the fluid-structure interface is

$$\hat{J} \hat{\sigma_s} \hat{F}^{-T} n = \hat{J} \hat{\sigma_f} \hat{F}^{-T} n \quad \text{on } \hat{\Gamma}. \tag{4.4}$$

In both structural domains $\Omega_{s,1}$ and $\Omega_{s,2}$ the structure equation will be described in its natural Lagrangian framework. Together with (4.4) we will thus obtain a deformation up to the boundary Γ. The fluid domain will be transformed as sketched in figure 4.1. The values of the transformation of the fluid d on the boundary Γ are thus determined. In the interior of the fluid domain they have no physical relevance and can therefore be extended in an arbitrary way. This is why the resulting method is called *Arbitrary* Lagrangian Eulerian method. In this thesis the deformation will always be extended by a harmonic mapping. Consequently we obtain as equations for the deformation

$$\begin{aligned} \Delta \hat{d} &= 0 \text{ in } \hat{\Omega}_f, \\ \hat{d} = 0 \text{ on } \hat{\Gamma}_d, \quad \hat{d} &= \hat{u} \text{ on } \hat{\Gamma}. \end{aligned}$$

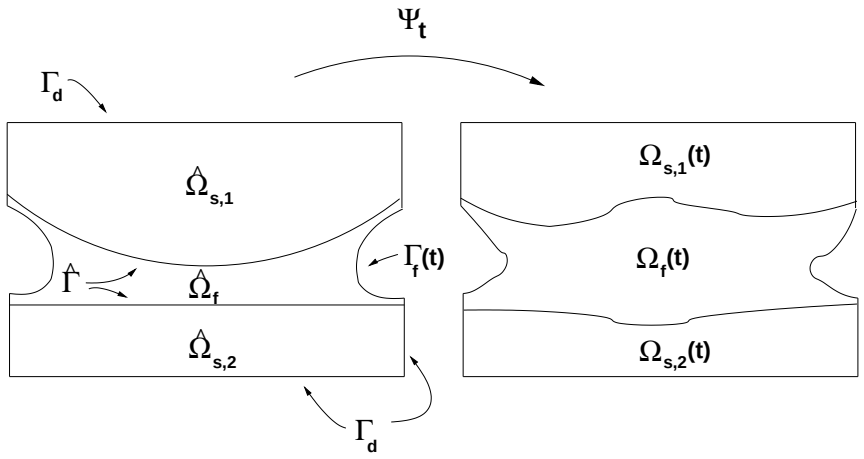

Figure 4.1: Scheme of a domain for a ball rotating in front of a plane, the situation studied later in this thesis.

In order to close the system we need a boundary condition for the deformation and the velocity. On Γ_d it vanishes, on $\Gamma(t)$ holds

$$\partial_t \hat{d} = \hat{v}.$$

Altogether we obtain the following equations for the monolithic arbitrary Lagrangian Eulerian fluid structure interaction, see also [Quarteroni (2004)] for more details on the derivation. Note that we pose parts of the equations for the moment on a moving domain and parts on a fixed domain indicated by a hat as before

Problem 4.1 (Monolithic fluid-structure interaction)**.** *Find* $v : \Omega \times \mathbb{R}_+ \to \mathbb{R}^2$, $p : \Omega_f \times \mathbb{R}_+ \to \mathbb{R}$, $u : \hat{\Omega}_s \times \mathbb{R}_+ \to \mathbb{R}^2$, $d : \Omega_f \times \mathbb{R}_+ \to \mathbb{R}^2$ *such that*

$$\begin{aligned}
\rho_f \partial_t v + ((v - \partial_t d)\nabla)\, v - \nabla \cdot \sigma(p, v) = \rho_f f_f \quad &\text{in} \quad \Omega_f(t), \\
\nabla \cdot v = 0 \quad &\text{in} \quad \Omega_f(t), \\
\sigma_f(p, v) n = g \quad &\text{on} \quad \Gamma_N(t), \\
\sigma_f(p, v) n_f = \sigma_s n_s \quad &\text{on} \quad \Gamma(t), \\
\hat{\rho}_s \partial_t^2 \hat{u} - \hat{\nabla} \hat{J} \hat{\sigma}_s \hat{F}^{-T} = \hat{\rho}_s \hat{f}_s \quad &\text{in} \quad \hat{\Omega}_s, \\
\hat{u} = 0 \quad &\text{on} \quad \hat{\Gamma}_d, \\
\Delta \hat{d} = 0 \quad &\text{in} \quad \Omega_f(t), \\
\hat{v} = \partial_t \hat{d} \quad &\text{on} \quad \hat{\Gamma}.
\end{aligned} \tag{4.5}$$

In the subsequent we will derive the weak formulation and show algorithmic details for the numerical approximation of solutions.

4.2 Monolithic weak formulation and discretization

The monolithic method as described above relies on considering fluid-structure interaction as one single system of equations on a common domain. The solution will fulfill a balance of forces at the interface by construction

$$\hat{J}\hat{\sigma}_f\hat{F}^{-T}\hat{n} = \hat{J}\hat{\sigma}_s\hat{F}^{-T}\hat{n}.$$

Indeed this boundary condition is a natural boundary condition for the weak formulation of equations (4.5). We directly show the variational formulation, for further details on the derivation see [Quarteroni (2004)].

Problem 4.2 (Monolithic formulation)**.** *Find* $\hat{u} \in H^1(\hat{\Omega}_s)^2$, $\hat{v}, \hat{d} \in H^1(\hat{\Omega}_f)^2$, $\hat{p} \in L^2(\hat{\Omega}_f)$ *such that*

$$\begin{aligned}
(\rho_f \partial_t v, \phi_f)_{\Omega_f(t)} + (\rho(v - \partial_t d)\cdot\nabla)v, \phi_f)_{\Omega_f(t)} + (\nabla\cdot v, \chi)_{\Omega_f(t)} \\
+ \left(\hat{\rho}_s\partial_t^2\hat{u}, \phi_s\right)_{\hat{\Omega}_s} + (\sigma(p,v), \nabla\phi_f)_{\Omega_f(t)} + \left(\hat{\sigma}_s, \hat{\nabla}\phi_s\right)_{\hat{\Omega}_s} \\
= (\hat{\rho}_s\hat{f}_s, \phi_s)_{\hat{\Omega}_s} + (\rho_f f_f, \phi_f)_{\Omega_f(t)} \\
\sigma_f(p,v) = -pI + \mu D(v), \quad \mu(p) = \mu_0\exp(\alpha p), \\
\hat{\sigma}_s = \hat{J}^{-1}\hat{F}\left(\lambda tr(\hat{E})I + 2\mu\hat{E}\right)\hat{F}^T, \\
v = \partial_t d \quad \text{on} \quad \Gamma(t), \quad u = Ext(d|_\Gamma).
\end{aligned} \tag{4.6}$$

for all $\phi_f \in H^1(\hat{\Omega}_f)^2$, $\phi_s \in H^1(\hat{\Omega}_s)^2$, $\chi \in L^2(\hat{\Omega}_f)$.

Here $Ext : H^{\frac{1}{2}}(\Gamma) \to H^1(\Omega)$ denotes the extension operator which extends a function with known values at the boundary to the interior (for instance harmonically).

Now we consider some details related to discretization and refer to chapter 5 for a definition of finite element spaces and an introduction to discretization. When discretizing the equations the extension operator has to be considered separately. The question arises how to discretize the extension operator, especially on the boundary. In the interior of the domain it is a pure harmonic continuation. On the boundary we have to take care that the unphysical extension does not influence the deformation of the structure. We have to discretize the extension on the boundary as a one-sided Dirichlet condition. Therefore we eliminate, as for

the treatment of usual Dirichlet boundary conditions, contributions from certain test-functions. For the residual all contributions on the interface coming from the extended side of the cell are eliminated. For implementation reasons we also have to extend the pressure to the structure domain. A special treatment for the pressure, which is most critical in this context, can be avoided when using discontinuous finite element spaces for this unknown.
For the matrix all couplings between test-functions on the boundary to the interior of the extension have to be eliminated. By this procedure we achieve the discretization of a Dirichlet-Neumann boundary condition for the structure and the extension. Consequently the extension has no unphysical spoiling effect on the solution of the deformation of the structure. This kind of modification of the integration has to be applied for the pressure as well as the structure. Yet the pressure is, conversely to the structure, a physical variable in the fluid domain and extended on the structure domain. One could also think about different techniques disregarding the pressure on the structure domain completely. Indeed the extension of the deformation of the structure is necessary in order to treat the fluid in its actual transformed configuration. The extension of the pressure carries no information at all and can be considered as merely artificial and a numerical artefact. In the code used for this thesis *GASCOIGNE* [Becker & Braack (1999)], it is difficult to implement a weak formulation for a system of equations with different numbers of components in different parts of the domain. Therefore we use also an extension of the pressure instead of disregarding it completely.

- The treatment of the pressure extension is crucial especially for elastohydrodynamic simulations. Without a separate integration the pressure in the fluid domain will be strongly coupling with the extension especially due to the extreme anisotropy and smallness of the fluid domain. Even when treated accurately as described above the nonlinear character of the boundary condition can have a negative influence on convergence. A change in the value of the pressure leads to a changed residual of the extension so that quadratic convergence may be lost. This effect can in practice be reduced by scaling the extension with a *small* parameter.

- The specific choice of extension of the structure deformation to the fluid *should* have no influence on physical values and functional evaluations of the solution. Via the transformation this extension is entering the equations on the fluid domain, there should be just no net effect when considering

different types of extension or changing parameters of the extension. Yet when discretizing, such parameters as well as the chosen extension operator *do* have some influence in reality which decreases under mesh refinement.

Notice also that the choice of parameters may have a decisive influence on the convergence speed of the nonlinear solver. The monolithic fluid-structure interaction formulation leads to highly nonlinear equations with respect to

- the geometry, that is the deformation,
- the pressure dependent viscosity,
- the nonlinear boundary condition (balance of forces).

When carrying out numerical simulations in principle not all nonlinearities always have to be considered at the same time. Especially when using fixed point iterations or pseudo time iterations, it is possible to linearize e.g. the nonlinearities coming from the transformation by plugging in the value of the transformation at the last iteration. A similar remark holds for the pressure dependent viscosity which is described in chapter 3. When establishing the simulations for this thesis we were experimenting with such linearized models. However the problem turned out to be extremely stiff. Linearization often leads to instabilities or at least to very slow convergence of the outer fixed-point iteration. After all it proved to be more efficient to keep all nonlinearities and solve them in a monolithic way with a nonlinear solver. Again the high stiffness comes from the strong geometrical coupling. Even small changes in the fluid domain lead to a large response in the pressure profile.
When describing different degrees of explicit and implicit treatment we comment shortly on entirely different techniques to solve fluid-structure interaction problems. The most explicit coupling is to consider the fluid and structure problem separately iterating only on the boundary condition until a balance of forces is fulfilled. Such a framework is also often used in theoretical analysis, in [Grandmont (2002)] a similar fixed point iteration is used to prove existence of a solution to the coupled system. But also for numerical algorithms this decoupling is used often and known as the "partitioned" approach to fluid-structure interaction in literature. In engineering science this approach is even more common than the monolithic formulation because it allows to use existing codes for the simulation

of fluid and structure promising an easy implementation. Due to the inherent explicit character of the decoupled algorithm however stability problems frequently arise. Therefore this approach is prohibitive for the simulation of elastohydrodynamic lubrication. Even for simpler problems stability may not always be guaranteed. In particular the coupling of an incompressible fluid with a structure is critical and may lead to an unconditionally instable algorithm which is shown in [Causin *et al.* (2005)]. If a partitioned algorithm does converge it also possesses some advantages. The local systems and elementary matrices are smaller and no degrees of freedom are wasted for extensions without physical meaning like the pressure extension.

4.3 Treatment of pre-loading

Ball bearings are pre-loaded which means that the ball is pressed on the race with a spring-like structure and a defined force. This force changes the initial geometry of the structure and leads to a high pressure between ball and race. The value of the load therefore influences the physical properties of the bearing and it turns out that it cannot be neglected completely.
When disregarding the fluid for the moment there exists an analytical contact theory for simply shaped bodies pressed onto each other. This theory is known as "Hertzian" theory in literature after its originator and can be found in [Hamrock *et al.* (2004)]. As mentioned this theory was developed for pure contact problems. However in elastohydrodynamic lubrication the fluid also plays a role and contact will not happen as long as a lubrication film is present. Nevertheless the Hertzian theory is used to treat pre-loading in most cases when considering ball bearings in literature. We hence also use it to include pre-loading in our model. From a modeling point of view another difficulty related to incompressibility arises: As mentioned in chapter 3 in an incompressible fluid model the pressure does not have to be identical to the thermodynamical physical pressure. Yet this thermodynamical pressure is described in the Hertzian theory. Since modeling of pre-loading in a fundamental way treating fluid as well as structure consistently as a pseudo-contact problem seems out of the scope of this thesis, we stick to using Hertzian theory.
Pre-loading leads to a flattening of the ball, see figure 4.2. Since the ball is more elastic than the race in the experimental situation the deformation of the race

can be neglected.

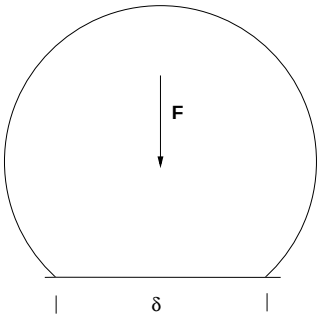

Figure 4.2: Flattening of a ball pressed on an approximately rigid plane, force $F = 130N$, diameter of flattened region $\delta = 400\mu m$

In this situation Hertzian theory predicts a pure flattening of the ball with a diameter of the flattened part of δ and a pressure profile with maximum value p_{max} in two dimensions as

$$p(x) = p_{max}\sqrt{1 - 2\left(\frac{2x}{\delta}\right)^2}. \tag{4.7}$$

These quantities are related to the material parameters and the force in the following way

$$\delta = 2\left(\frac{3FR}{E'}\right)^{\frac{1}{3}}$$
$$\frac{1}{E'} = \frac{1}{2}\left(\frac{1-\nu_{ball}^2}{E_{ball}} + \frac{1-\nu_{plane}^2}{E_{plane}}\right)$$

where E is Youngs modulus and ν the Poisson ratio of the structure. These formulas are derived in [Hamrock *et al.* (2004)].
For the thermodynamical pressure we can make the assumption that the force on the boundary is proportional to pressure. We therefore insert a boundary term in the weak formulation

$$\lambda < \hat{p}_0\hat{n}, \phi >_{\hat{\Gamma}}$$

where $\hat{p}_0$ is the function defined in equation (4.7) and λ is a scaling parameter. With this approach we later show good agreement compared to reference solutions

for the film thickness. However in the simulation of the entire problem with a fluid the results for pressure and deformation are different compared to the Hertzian theory. In particular the pressure tends to be lower than predicted and does not posess the same sharp profile as predicted by equation (4.7).
The influence of pre-loading on film thickness is subject of many publications like [Křupka *et al.* (2005)] and typically the influence is limited. The change in the initial pressure profile can be important for numerical simulations since it prevents contact between ball and race. The high pressure together with the pressure dependent viscosity makes a contact impossible which would otherwise happen as indicated by numerical simulations.

4.4 Rigid body motions in fluid-structure interaction

Compared to the standard formulation of fluid-structure interaction as derived in chapter 4.2, some modifications have to be made for the simulation of ball bearings. First of all we have to deal with rigid body motions in order to treat rotating bodies in the monolithic formulation. Note that a stationary solution in the sense that $v = 0$ holds in the entire structure domain is impossible. In ball bearings ball and race are rotating around different axes and with different frequencies. Therefore for each choice of reference frame at least one of the parts will be moving. This movement will certainly not be arbitrary, neglecting the deformation of the elastic structure it will consist merely of a rigid body motion. A rigid body motion is characterized by the fact that it can be written as follows

$$x = Q(t)\hat{x} + a(t). \qquad Q(t) \in \mathcal{O}(2) \quad \forall t \geq 0, \quad a \in \mathbb{R}^2 \quad \forall t \geq 0$$

where $\mathcal{O}(2)$ denotes the group of orthogonal 2×2 matrices. Hence a rigid body motion is a translation or a rotation or any linear combination of both. When considering rotating bodies one has to keep in mind that a rotating system is no inertial system anymore so that one has to account for fictitious forces. Fictitious forces also arise from translations with non-constant velocity. Details and formulas for fictitious forces can be found in [Scheck (2002)]. Yet in the case of elastohydrodynamic lubrication fictitious forces are usually small and can be neglected.
We will in the subsequent suppose that v in the structure domain is not zero

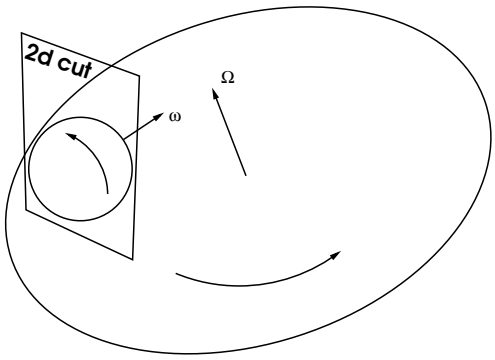

Figure 4.3: Scheme of the experimental setting.

as in the usual stationary formulation but it equals a pure rigid body motion. For the two-dimensional model of the experiments the motion will consist of a rotation in the ball and of a translation in the race.

We now describe the experimental setting in more detail as it is used in [Křupka *et al.* (2005)]. We adopt this benchmark configuration and later compare our own results with the analytical approximation also used in this publication. One kind of experiments consists of a ball rotating in front of an also rotating plane, see figure 4.3 where the rotational frequency of the ball and plane is denoted ω and Ω respectively. In real experiments there is a transparent window in the plane used for light interference measurements of film thickness. More details on the experimental setting as well as different measurement techniques can be found in [Křupka *et al.* (2005)] or [Guangteng *et al.* (2000b)] and the references therein. The rotational frequencies of ball and plane are tuned in a way leading to equal radial velocity in the contact region between them. This is often called "pure rolling" condition in literature and leads to *small* shear rates in the fluid. Therefore no shear-dependent viscosities have to be modeled whereas this type of non-Newtonian fluid behaviour always plays a role for different geometries such as journal bearings.

We now come to the modification of the fluid-structure formulation for treating rigid body motions. For this purpose we recall the monolithic weak formulation derived in chapter 4.2.

The term which causes (in a stationary setting) the velocity to vanish (weakly) in the structure domain is

$$(\hat{v}, \phi)_{\hat{\Omega}_s} .$$

We will instead of requiring $\hat{v} = 0$ require $\hat{v} = \hat{g}$ weakly where $\hat{g}$ is a given rigid-body motion.

$$\left(\hat{v} - \hat{F}^{-T}\hat{g}, \phi\right)_{\hat{\Omega}_s} . \tag{4.8}$$

The term $\hat{F}^{-T}$ is appearing due to transformation and may *not* be neglected in applications, refer to chapter 4.1 for a derivation.
The rigid-body motion for the ball is a rotation with frequency ω and is given as $g = \omega(-y, x)^T$, the translation is $g = (0, \omega r)^T$ if r is the radius of the ball. Recall that in contrast to the fluid tensor the structure tensor does not depend on the velocity v. Since in physical SI-units the coefficients of the differential equation for the deformation in the structure domain are large ($\sim 10^{11}$) we may also scale equation (4.8) with a large parameter. This may lead to better balancing of the terms for deformation and velocity. Alternatively one may also non-dimensionalize all equations if desired. Yet the different order of magnitude of the coefficients for structure and fluid will persist also an non-dimensional formulation.
As aforesaid the value of the velocity does not appear in the structure tensor (conversely to the fluid tensor) so that it does not influence the deformation a role in the structure domain. However it *does* play a role on the boundary where equation (4.8) enforces weakly the continuity of the velocity across the interface. Thus the rotation of the ball carries over to the motion of the fluid by this implicit no-slip boundary condition.
The mechanism of requiring $v = 0$ (without rigid body motion) in the structure weakly by adding equation (4.8) which is also used in [Dunne (2007)] is delicate to analyze theoretically. For a symmetric treatment of velocity and deformation we would prefer to use a harmonic extension of the velocity. Recall that the extension of the deformation in the fluid domain is also harmonic. When doing so we have to replace the L^2 scalar product in (4.8) by its H^1-counterpart

$$\left(\hat{\nabla}\hat{v}, \hat{\nabla}\phi\right)_{\hat{\Omega}_s} .$$

In this case $\hat{v} = 0$ does not hold any more on the boundary by construction but it has to be imposed by an additional boundary condition. Requiring $\hat{v} = 0$ in a

weak sense on the boundary leads after all to the terms

$$\left(\hat{\nabla}\hat{v}, \hat{\nabla}\phi\right)_{\hat{\Omega}_s} + \frac{1}{\epsilon} < \hat{v}, \phi >_{\hat{\Gamma}} .$$

Herein ϵ is a small parameter related to the mesh size in the following way $\epsilon \sim h$. The generalization to non-vanishing rigid-body motions is straightforward and will be omitted.

The different methods of treating the velocity in the structure domain have been implemented for test reasons but there are no clear differences with respect to convergence or accuracy of the numerical approximation.

In this section we have focused on implementing velocity boundary conditions for the fluid. The correct boundary conditions are not trivial to derive. We always use *no-slip* boundary conditions but for fluid flow on a molecular level it is known that a no-slip condition does not have to hold, see [Lauga & Squires (2005)]. Since in the regime of elastohydrodynamics we are at least for small film thicknesses in the range of molecular flow it is not clear without ambiguity if a no-slip condition is valid. A generalization of the no-slip boundary condition is the partial-slip boundary condition presented in [Lauga & Squires (2005)]. In our simulations we stick to the no-slip boundary condition.

Chapter 5

Discretization

In this thesis we exclusively use finite element methods to discretize the partial differential equations under consideration. The following chapter will give an overview of the basic definitions and concepts without any claim to be complete. For a complete detailed textbook introduction we refer to [Braess (2007)]. We will comment on some aspects specific to the discretization of elastohydrodynamic problems.

5.1 Basic definitions

Let Ω be a convex domain with polygonal boundary in $\mathbb{R}^2$ in the following. We remark that practically all domains we will be interested in throughout this thesis in practice are neither convex nor have a polygonal boundary. We stick to the two-dimensional case and remark that some differences appear when considering three dimensions. For example there exist two different types of hanging nodes in three dimensions whereas in two dimensions only one type is possible.
Our goal is to approximate the function space $H^1(\Omega)$ with a finite dimensional space which can be dealt with on a computer. Therefore we subdivide the domain in a set of convex cells of convex quadrilateral shape where each edge is either identical to an edge of a neighbor cell or part of the boundary of the domain $\partial\Omega$. We denote the set of these cells a triangulation $T_h = \{K\}$. The index h indicates

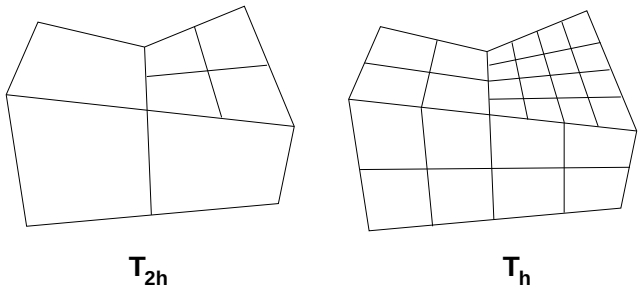

Figure 5.1: Mesh with patch structure.

how fine the triangulation is $h = \max_{T_h} diam(K)$, furthermore we require

$$\bar{\Omega} = \bigcup_{K \in T_h} \bar{K}. \tag{5.1}$$

For practical purpose these definitions have to be weakened twofold

- For the case of curved boundaries of the domain we only require that *nodes* (not edges) lie on the boundary.
- We also allow cells with nodes which are the midpoint of another edge, such nodes are called "hanging".

A global refinement of a mesh is a bisection of each edge of the triangulation thus obtaining four finer cells out of one cell on the coarse original mesh. We require for the triangulation T_h to possesses a patch structure that is it can be obtained by global refinement of a coarser mesh T_{2h}, see figure 5.1.
The formal regularity requirements are more difficult to pose for quadrilateral than for triangular meshes. We refer to [Matthies & Tobiska (2002)] for this technical aspect.

5.2 Finite element spaces

We define the spaces

$$\hat{P}_1 = span\{1, x, y\},$$
$$\hat{Q}_1 = span\{1, x, y, xy\},$$
$$\hat{Q}_2 = span\{1, x, y, xy, x^2y, y^2x, x^2y^2\}.$$

The unit square $\hat{K} = [0,1] \times [0,1]$ is mapped on an actual element by means of a transformation $T : \hat{K} \to K$. We define the finite element spaces now as

$$Q^r(K) = \{u : K \to \mathbb{R} \quad | \quad u\,(T(\hat{x})) \in \hat{Q}^r(\hat{K})\}.$$

In this thesis we exclusively use iso-parametric finite elements that is the transformation itself is in the space $T \in Q^r(\hat{K})$.
Recall also that the domains of interest are neither convex nor have polygonal boundaries. In this case the constructed finite element spaces are not subspaces to $H^1(\Omega)$ and condition (5.1) does not hold. For some problems one may show that this is (under certain conditions) not influencing the order of convergence of the approximation, see [Scott (1973)] for details.
The problems we are interested in are not scalar but possess different variables with different physical meaning. Indeed for Stokes' equations with pressure p and velocity v we require $p \in L^2(\Omega)$, $v \in H^1(\Omega)^2$. These spaces fulfill the following *inf-sup* condition

$$\inf_{p \in L^2(\Omega)} \sup_{v \in H^1(\Omega)^2} \left\{ \frac{(p, \nabla \cdot v)}{||p|| ||\nabla v||} \right\} > C > 0. \tag{5.2}$$

It is known that this condition is essential in order to obtain a well-posed problem [Girault & Raviart (1979)]. Furthermore also the discrete spaces either have to fulfill such a condition independently of h or the discretization has to be stabilized. In the course of this thesis we work with three types of discretization

- Q_1Q_1 Discretization:
  Here we use the same spaces for v_h and p_h $V_h = \{u_h \in \mathcal{C}^0(\Omega) | u_h|_K \in Q_1(K)\}$. This requires stabilization because the *inf-sup* condition (5.2) is not fulfilled. As stabilization technique we either use the *Local Projection* stabilization (LPS) described in [Becker & Braack (2001)] or the *Galerkin Least Squares*-stabilization, see [Hughes *et al.* (1986)].

- Q_2Q_1 Discretization:
  For p_h we use again $X_h = \{u_h \in \mathcal{C}^0(\Omega) \quad | \quad u_h|_K \in Q_1(K)\}$, for v_h we use $V_h = \{u_h \in \mathcal{C}^0(\Omega) \quad | \quad u_h|_K \in Q_2(K)\}$. This discretization is stable which may be favorable if used for free-boundary value problems since at the free boundary unphysical boundary layers in the pressure arise frequently due to stabilization.

- $Q_2P_1^{disc}$ Discretization:
  In this case we use a discontinuous pressure

p_h in $X_h = \{u_h \quad | \quad u_h|_K \in P_1(K)\}$, for v_h we use $V_h = \{u_h \in \mathcal{C}^0(\Omega) \quad | \quad u_h|_K \in Q_2(K)\}$. Also this discretization is stable but solutions to Stokes' equations are also mass-conserving in a cell-wise way which is an advantage for free boundary value problems. For fluid-structure interaction problems it may be advantageous to have a discontinuous pressure along the interface.

The discretization with stabilization on highly anisotropic meshes is not straightforward but we have to take care particularly of the stabilizing terms. We will not go into detail here, instead we refer to [Braack (2008)] for the case of LPS-stabilization and [Apel *et al.* (2008)] for GLS-stabilization.
We remark that all numerical results shown later are established by using anisotropic stabilization. The type of stabilization is crucial when considering pressure dependent viscosities fulfilling for instance Barus' equation, see chapter 3 for details. When employing the LPS-stabilization spurious oscillations in the pressure occur. Furthermore the stabilized discrete system matrix may become singular.
The GLS-stabilization is robust in this case as well as all stable element pairings. Therefore we use these discretizations in these cases. The disadvantage of the GLS-stabilization is the spurious boundary layer in the pressure occurring at Neumann boundaries of the fluid. This is in particular problematic for free boundary value problems.

5.3 Solution of the discrete algebraic equations

Discretization of the studied partial differential equations with finite elements, and as the case may be with the implicit Euler scheme in time, leads to nonlinear algebraic equations. The nonlinear iterative solver used is Newton's method. In practice often damping has to be applied for a more robust convergence. The necessary directional derivatives of the operator are calculated analytically.
In the case of fluid-structure interaction problems the evaluation of these terms is awkward as it leads to complicated formulas, see [Dunne (2007)] for more details. Therefore many people working in this field also use finite differences to approximate the derivatives

$$A'(u)(\Phi)(Z) \sim \frac{A(u_h + \epsilon Z_h)(\Phi) - A(u_h - \epsilon Z_h)(\Phi)}{2\epsilon}. \tag{5.3}$$

This method was also implemented for testing reasons but for use in elastohydrodynamic simulations there are several severe drawbacks. In lubrication flow the pressure can vary up to ten orders of magnitude. Therefore it is delicate to figure out the correct value for ϵ as long as it is taken constant in the domain. Also the order of magnitude for velocity ($\sim 1\frac{m}{s}$) and deformation ($\leq 1\mu m$) is very different and would require an adapted possibly non-constant choice of ϵ. When using analytical derivatives no such problems arise.
To proceed we now consider the solution of the linear problems which have to be solved to determine the update in the Newton iteration. These linear problems consist of large sparse matrices coming from the discretization of elliptic partial differential equations. In principle multi-grid methods are efficient algorithms for such problems as described in many textbooks on numerics, see e.g. [Kanzow (2005)]. In this specific situation there are special reasons degrading multi-grid convergence to an extent that it becomes practically useless. We shortly describe these reasons:

- Elastohydrodynamic fluid-structure interaction typically deals with steel as structure and a viscous fluid. The material parameters for these materials are of highly different order of magnitude. Since there are two sets of dimensional physical parameters for fluid and structure it is difficult to rescale all of them so that they are balanced at the same time. These parameters lead to a badly conditioned of the Newton matrix.

- The anisotropic mesh cells cause very slow, if at all, multi-grid convergence. In [Braack (2008)] it is reported that the anisotropic stabilization leads to improved robustness of the multi-grid algorithm. We however are not able to confirm this observation. In our simulations the underlying mesh has cells with much higher aspect-ratio ~ 1000 compared to [Braack (2008)] where it is at most ~ 80. The lack of robustness of multi-grid methods with respect to anisotropy is a well-known problem but has not been solved completely yet. In [Wienands (2001)] and the references therein some information on robust multi-grid methods is presented. However the proposed solution strategies seem to be quite specialized and it is difficult to estimate their effect under the presence of several pathologies at the same time.

- The pressure dependent viscosity leads to coefficients of the fluid equation which vary strongly throughout the domain. This variation can be more than ten orders of magnitude for the viscosity in the pressure peak compared

to the viscosity at low pressure. This extreme variation in the coefficients results in a bad condition number of the matrix.

- Fluid-structure interaction problems in itself lead to difficulties with multi-grid behaviour, even without non-Newtonian fluid models or anisotropic meshes. If the multi-grid algorithm is not adopted carefully slower convergence is observed on finer grids contrarily to the theoretically desired properties.

In this work we will therefore in practically all cases use direct solvers for the solution of the linear systems. These solvers are *UMFPACK*, see [Davis (2004)] and *MUMPS*, see [Amestoy *et al.* (1998)].
The discrete algebraic equations can not always be solved up to an absolute precision of 10^{-10} when using double precision due to bad conditioning.
The finite element library in use is "GASCOIGNE" and is developed in the numerical analysis group since several years, s. [Becker & Braack (1999)].

5.4 Mesh generation

The generation of a mesh for a realistic ball bearing geometry is involved and only feasible with commercial grid generators. The grid generator used for this thesis is "ANSYS ICEM CFD". The need of commercial mesh generators results from the extreme ratio between radius of the ball and film thickness $\geq 10^4$. The basic geometry in the case of ball bearings consists in a ball of radius $3mm$ with a surrounding fluid flow of $1\mu m$. The surrounding structure is also curved, see figure 5.2. In reality the system is three dimensional without cylindrical symmetry. The races are curved perpendicular to the plane of projection.
In the software package used for this thesis, *GASCOIGNE* [Becker & Braack (1999)], the treatment of curved boundaries works as follows: When a curved boundary is present it is described as an implicit function. For each refinement concerning this boundary each new vertex on the boundary is moved to fulfill the implicit function constraint. Thus *only* vertices at the boundary are moved. This corresponds to the requirement made above in the theoretical section. For curved boundaries vertices shall lie on the curved boundary since it is no more possible for entire edges. The problem is that moving only vertices on the boundary is only practicable if the cells are fairly isotropic. If cells with higher aspect-ratio

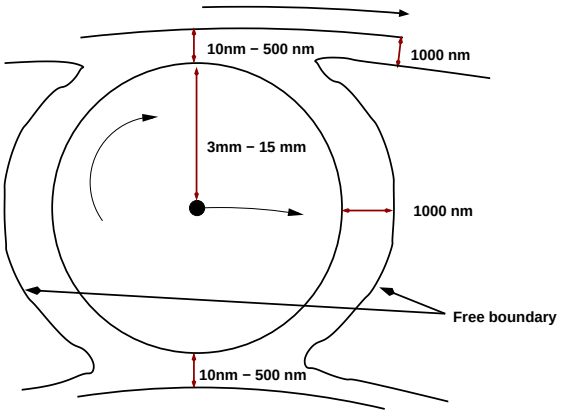

Figure 5.2: Scheme of ball bearing geometry.

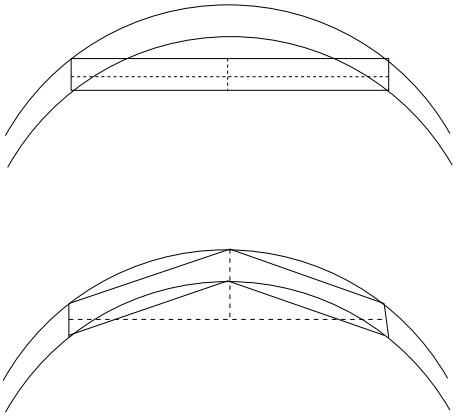

Figure 5.3: When refining anisotropic mesh cells on curved boundaries the refined cell becomes degenerated when only vertices on the boundary are moved.

exist on the boundary, formerly interior nodes will become exterior and the cells become completely distorted, see figure 5.3 for a visualization of this effect.

Treating curved boundaries together with anisotropic cells would need a more elaborate treatment. The displacement at the boundary could for example be extended harmonically to the interior. This was used in parts of this thesis but requires the solution of a partial differential equation for each mesh refinement. In this thesis we do not work with changing meshes in time nor with adaptive mesh refinement, therefore this approach is acceptable. An additional possibility is using locally finer meshes beforehand where a high resolution of the curved boundary is needed. This is most efficiently done with the help of commercial grid generators which treat curved boundaries correctly by themselves. If we were interested in dynamical meshes and very different resolution of curved boundaries on this extreme geometry, the treatment of boundary nodes would pose consid-

Figure 5.4: Typical Mesh: Right and left meniscus of the free boundary of the fluid (above), Fluid film between ball and bearing at $y = -0.0127m$ and overview (below). The fluid film is only recognizable as a line due to its little height, the "dark" regions in the overview in the middle correspond to locally smaller mesh sizes around the tip of the ball.

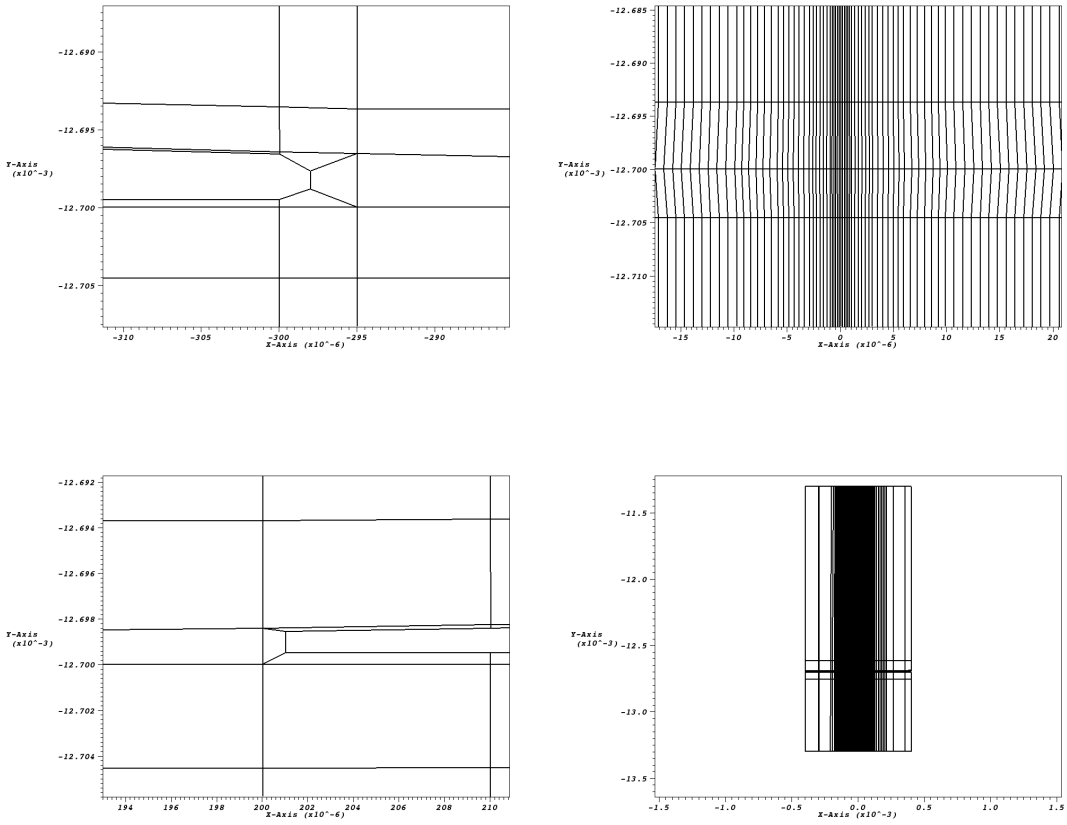

erable problems.

In figure 5.4 a typical mesh is shown comprising the ball, the race and the fluid film with a free boundary. The coarse mesh contains cells with aspect ratio at most ~ 1000. The fluid film in the middle, where the point of closest approach of ball and race $x = 0$ lies, has a thickness of $1nm$. This explains the necessary degree of anisotropy because the dimension of the entire mesh in y-direction is $2 \times 10^{-3}m$ that is 2×10^6 times higher than the minimal film thickness. The minimal film thickness of $1nm$ is indeed smaller than the minimal length scale for which the Navier-Stokes equations begin to hold. In [Szeri (2000)] this length scale is stated $\geq 10nm$. Due to our treatment of pre-loading, see chapter 4.3, the initial film thickness will somehow be higher caused by the additional force. Therefore it will be always larger than the critical distance $10nm$. In figure 5.5 a

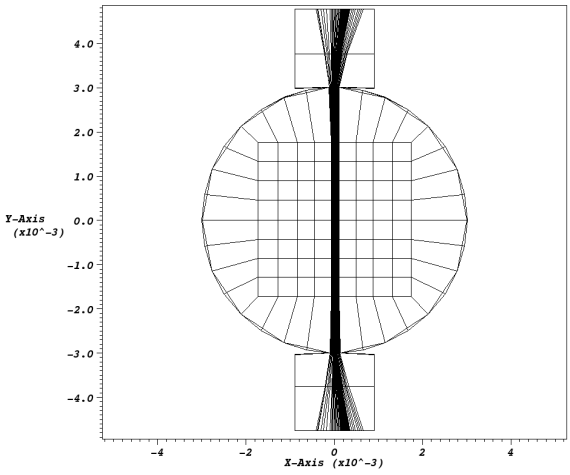

Figure 5.5: Coarse mesh of a ball in a ball bearing.

coarse mesh for a simulation for an entire ball in a ball bearing is shown.
As a last remark concerning this technical point of mesh generation we emphasize the need to reflect the real geometric situation in the mesh accurately. Such a tight coupling of fluid flow and geometry is prevailing that a coarse treatment of the geometry will immediately lead to completely different results. On too coarse meshes also nonlinear convergence becomes slow or there is no convergence at all. This is also the reason why we may not just neglect fluid-structure interaction at all. In simulations it appears frequently that a small change in the geometry of the mesh is leading to a severe change in the solution.
In reality a ball in a ball bearing is also no perfect ball but has a finite surface roughness. In our simulations we neglect this effect but keep in mind that for small film thicknesses surface roughness indeed also plays a role in reality. The exact effect of surface roughness is difficult to estimate. Recently the effect of surface roughness on elastohydrodynamic lubrication has been subject to research. In [Guangteng *et al.* (2000a)] a synthetic 160-nm high asperity ridge is placed on a ball and surface roughness and non-Newtonian fluid-behaviour, see [Chapkov *et al.* (2006)]. In the experimental situation we are considering the root mean square of the surface roughness is stated to be $4nm$, [Křupka *et al.* (2005)]. This would mean a relative precision compared to the radius smaller than 10^{-6} and therefore seems unrealistic. Even in this case some of the measured film thicknesses would be *smaller* than the mean surface roughness.

5.5 Multi-grid algorithm

5.5.1 Introduction to multi-grid methods

When solving the linear systems arising from the discretization of elliptic partial differential equations, multi-grid algorithms are in general, if applicable, the method of choice. An introduction to multi-grid methods as well as some theoretical results can be found in [Hackbusch (1985)]. In this section we broach the issue of problems arising in practice when using multi-grid for somehow pathological situations. Our goal is a greater robustness of the algorithm against such pathological problem aspects. We study a multi-grid smoother with higher complexity but also more robust convergence properties with respect to the presence of anisotropic grid cells. In the end the higher complexity compared to standard smoothers does not pay off and leads to no clear advantage compared to direct solvers. We thus still see an open problem demanding further research in this area.

We consider the linear equation $Ax = b$ with given symmetric positive definite matrix $A \in \mathbb{R}^{n\times n}$ and $x, b \in \mathbb{R}^n$, the defect is then given by $b - Ax$. We will now give a rough introduction to multi-grid, a more precise definition is found below and for more details we also refer to [Hackbusch (1985)]. One method to solve this system of equations iteratively would be the application of a classical Jacobi, Gauss-Seidel or even Richardson iteration. It turns out that these iterations lead to very slow convergence rates when applied directly to the system. However they reduce high frequent components of the defect efficiently. Since by eliminating these high frequent components the residual becomes smooth (but not necessarily small everywhere) this process is called smoothing. The underlying linear operation is denoted "smoother". The smoothing property is exploited by restricting the residual to a coarser mesh. On this coarser mesh the complexity is lower and additional error components have become high frequent and will thus be reduced. In the case of a two-grid algorithm we would prolongate the residual back to the finer mesh, smooth again and obtain an approximation to the solution. In practice we deal with more than two levels in most of the cases. The algorithm will then be applied recursively. In addition we solve the system exactly with a direct solver on the coarsest mesh.

This algorithm will result in an approximate solution with $O(N)$ arithmetic operations (when applied in a nested way) if N is the number of unknowns (on the

finest mesh). For scalar elliptic problems without pathologies this approach is in practice of unrivaled efficiency. Such a situation would be the discretization of a Poisson problem on the unit square. For some moderate difficulties like (small) nonlinearities or saddle-point problems like Stokes' equations it can be still used very efficiently. When a more robust solver is needed multi-grid may also be used as a pre-conditioner for a Krylovspace iteration like CG or GMRES, see [Wienands (2001)].

5.5.2 Description and numerical analysis of a different smoother

We firstly describe the standard approach for multi-grid and show the problems arising on anisotropic meshes and present a variant to achieve greater robustness. In the software package used in this thesis *GASCOIGNE*, see [Becker & Braack (1999)] an incomplete LU-factorization is used as smoother. For scalar problems it consists of a formal LU-decomposition of the matrix A where all elements of the inverse A_{ij}^{-1} are neglected if the coupling does not exist in the matrix itself, that is if $A_{ij} = 0$.
For details of the LU-algorithm see [Kanzow (2005)] or any other basic textbook. Just applying the complete LU-decomposition would in general lead to a dense inverse matrix, this is often called "fill-in" in literature. The amount of fill-in depends intensely on the ordering of the degrees of freedom. Different ordering strategies may lead to very different sparsity patterns and thus to a different number of neglected degrees of freedom in the incomplete LU-factorization. At this point we have to state that the usual ordering of nodes in *GASCOIGNE* is not mathematically motivated but exclusively helpful for simple implementation. Especially for anisotropic problems a lexicographic ordering proves to be useful. It is defined by the following order relation $\tilde{>}$ of the node $n_k := (x_k, y_k)$. It is $n_k \tilde{>} n_l$ if $x_k > x_l$ or, if $x_k = x_l$, there holds $x_k \tilde{>} x_l$ if $y_k > y_l$.
When considering discretizations of saddle-point problems like Stokes' equations with stabilized finite elements we need a further modification of the LU-decomposition. In this case we "block" degrees of freedom in a node-wise way. That is we consider node-wise local matrices as single degrees of freedom and invert them exactly when evaluating formally the elements of the inverse A_{ij}^{-1}. In the case of Stokes' equations in two dimensions there holds $A_{loc} \in \mathbf{R}^{3\times 3}$, for the two dimensional fluid-structure interaction problem $A_{loc} \in \mathbf{R}^{5\times 5}$.

The fluid-structure interaction problem with non-Newtonian fluid contains several problem pathologies which already *individually* lead to a break down of multi-grid convergence. This is explicated in more detail in chapter 5.3. If we consider Stokes' equations and the mesh contains cells with an aspect ratio ≥ 5 multi-grid convergence rates begin to degrade. Convergence results can be found in tabular 5.1. While on the unit square the convergence rates are as fast as for Poisson's equation ≤ 0.1 they become slower with increasing aspect ratio. At an aspect ratio of ~ 1000 no convergence is found at all. Recall that this applies to the system matrix with *anisotropic* (LPS) stabilization, see [Braack (2008)]. For isotropic stabilization the behaviour is even a bit worse but comparable. In the case of ball bearings we need to work with aspect ratios in the region ≥ 1000 so that it lies outside the range of convergence for the multi-grid algorithm as described above. Furthermore for the entire system with pressure dependent viscosities and fluid-structure interaction the application of multi-grid becomes even more delicate.
We now concentrate on the effect of anisotropy on a simple benchmark saddle-point problem without additional difficulties. Therefor we consider Stokes' equations (5.4) on a rectangle $\Omega = [0, L] \times [0, 1]$ with aspect ratio L and global refinement of the mesh.

Problem 5.1. *Find $v_h \in V_h(\Omega)$, $p_h \in X_h(\Omega)$, so that*

$$\begin{aligned} &\nu(\nabla v_h, \nabla \phi) - (p_h, \nabla \cdot \phi) = (f, \phi) \\ &(\chi, \nabla \cdot v_h) + \Pi_{LPS}(\chi, p_h) = 0 \end{aligned} \tag{5.4}$$

$\forall \phi \in V_h(\Omega)$, $\chi \in X_h(\Omega)$.

Here $\Pi(\chi, p_h)$ is the anisotropic LPS stabilization operator as described in [Braack (2008)]. On the boundary $x = 0$ we pose a parabolic inflow, on the boundary $x = L$ there holds $\nu \partial_n v = pn$ (neglecting stabilization) and on the rest of the boundary we pose no-slip boundary conditions $v = 0$. In table 5.1 the number of linear iterations for different aspect ratios and different smoothers is compared. For greater robustness we use one multi-grid(-V-)cycle as pre-conditioner for a GMRES iteration, see [Kanzow (2005)]. Thus one linear iteration as shown in table (5.1) is equivalent to one GMRES step preconditioned by one V-cycle multi-grid iteration with one pre-smoothing and one post-smoothing step.
We applied the nested multi-grid-algorithm, starting on a coarse mesh we solve the problem and use this solution as initial solution on a finer level. In this way three global refinement cycles are conducted. For this algorithm the number of

Number of nodes:	4225	16641	66049	263169
AR 1, ILU	1	5	6	6
AR 10, ILU	4	11	13	13
AR 100, ILU	8	10	22	32
AR 1000, ILU	4	40	2209	*
AR 10,BLOCK 5000	4	6	12	86
AR 100,BLOCK 3000	9	14	14	91
AR 100,BLOCK 7500	8	10	13	15
AR 100,BLOCK 15000	8	10	17	19
AR 1000,BLOCK 500	31	43	63	190
AR 1000,BLOCK 5000	4	21	19	26
AR 1000,BLOCK 15000	4	7	18	25

Table 5.1: Linear iterations on different levels of mesh refinement and for different aspect ratios (AR) with different number of blocked degrees of freedom (BLOCK), * means divergent.

iterations should not increase on finer levels of the mesh but remain constant.
When studying the performance of the ILU-smoother we remark that it is not at all robust against anisotropy. Especially for aspect-ratios larger than ten the number of iterations explodes on finer grids. For aspect-ratio 1000 which corresponds to a realistic value for elastohydrodynamic simulations, the algorithm is no more convergent. At this point we remark that the algorithm also sensitively depends on further numerical parameters. The multi-grid update can for instance be damped with a parameter $\omega \in (0, 1]$. We do not claim that the shown numbers of iterations are *optimal* with respect to variations of all such numerical parameters. What we do assert is that no qualitatively different result can be found with the ILU-smoother. Just by means of variations of these parameters no convergence on fine meshes with arbitrary aspect ratios can be achieved.
The block-smoother is defined as follows: When blocking N nodes we take the lexicographic order defined above and build sub-matrices of N nodes (with all components) and invert them with a direct solver for sparse matrices. Since N is large the resulting sub-matrices will be sparse. In the most simple case we use a block-Jacobi iteration for smoothing with the blocked matrices, in the results presented we used a block-Gauss-Seidel iteration instead.

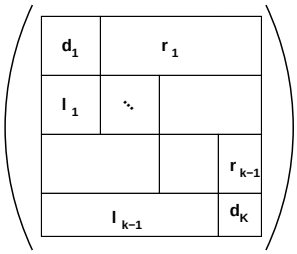

Figure 5.6: Scheme of the definition of sub-matrices for the blocked smoother.

More precisely, for the matrix A we define sub-matrices d_k for $k \in \{1, \cdots, K\}$

$$d_k^{i,j} = A_{i+kN,j+kN}, \quad 1 \leq i,j \leq N \text{ if } k < K$$
$$d_k^{i,j} = A_{i+kN,j+kN}, \quad 1 \leq i,j \leq \overline{N} \text{ if } k = K$$

We do not require that N is a factor of the size n of the matrix A, so that not all sub-matrices need to be of equal size. The size $\overline{N}$ of the last sub-matrix d_K is the remainder of the division of n by N. For the block-Gauss-Seidel iteration we also define rectangular upper and lower matrices

$$r_k = A_{(k-1)N<i\leq kN, j>kN}, \qquad \text{if } 1 \leq k < K,$$
$$l_k = A_{(k-1)N<i\leq kN, j\leq(k-1)N}, \text{ if } 1 < k \leq K.$$

A visualization of these definitions is found in figure 5.6. Furthermore we define the block-diagonal matrix D_K as the matrix consisting of the block-wise inverse matrices $d_k^{-1}, \quad 1 \leq k \leq K$. In addition L_K is the remaining lower block-matrix, R_K the upper block-matrix. With these definitions the block-Jacobi iteration for an initial solution x_0 reads

$$x_0 \in \mathbb{R}^n, \text{ for } \quad 0 \leq t \leq n_{max},$$
$$x^{t+1} = x^t + D_K(b - Ax^t).$$

In a similar manner we define the block-Gauss-Seidel iteration as

$$x^{t+1} = D_K \left(b - L_K x^{t+1} - R_K x^t\right).$$

When implementing this block-smoother the initial motivation was to come to a robustly convergent multi-grid method with as little as possible blocked degrees of freedom $N \sim 100$. For the highest value of the aspect-ratio 1000, this is indeed the case. Here the blocking of 500 degrees of freedom is sufficient. However, also in this case, the exploding number of iterations on the finest grid leads to the

supposition that the algorithm would no more converge when refining the grid once more. In general the number of blocked degrees of freedom has to be so high that there remains no real advantage compared to solving the linear system of equations entirely with a direct method.

Both the block-Jacobi and the block-Gauss-Seidel iterations are in principal equivalent to a direct solver when the number N is greater or equal than the size of the matrix n, of course. However in table 5.1 we see that the entire preconditioned algorithm takes more than one iteration even in cases where N is larger than the number of nodes. An example would be the BLOCK-5000 smoother on the mesh with 4225 nodes which takes four iterations. We remark that due to implementation aspects the GMRES iteration is completely operating on the preconditioned system that means also the residual evaluation results in the residual of the preconditioned system. As stated above one linear iteration is not just the direct solution of the linear system even if the number of blocked nodes exceeds the number of unknowns.

To conclude we state that our numerical experiments confirm that the ILU-smoother is not robust with respect to anisotropy. The block-Gauss-Seidel smoother performs better when the number of blocked nodes is large enough. Unfortunately on finer grids the number has to be so high ~ 10000 that there often is no clear advantage in terms of cost and memory consumption compared to a direct solver.

In our study we focused on the smoother as one part of the multi-grid algorithm. However the grid transfer operations might also be important in this context. Furthermore the benchmark problem using globally refined rectangles with aspect-ratio L might be to pessimistic for real applications. In many applications only a *small* part of the mesh consists of anisotropic cells whereas the rest is more or less isotropic. A typical example is the simulation of turbulent flow with the necessity of resolving boundary layers leading to anisotropic mesh cells only close to the boundary. In such situations it might be useful to divide the mesh into an isotropic and anisotropic part and use blocking only in the anisotropic part. For elastohydrodynamic simulations indeed most of the fluid mesh consists of anisotropic cells.

Chapter 6

Comparison with analytic approximations for elastohydrodynamic lubrication

In this chapter we will use the fluid-structure interaction formulation as well as the methods for non-Newtonian flow and free boundary value problems proposed in the preceeding sections of this thesis for elastohydrodynamic simulations. We compare the results of the simulations to an analytical approximation widely used in engineering literature, the "Hamrock-Dowson" formula for the elastohydrodynamic film thickness. Since these analytical approximations are known to represent experimental data accurately we can conclude that our simulations also match real experiments approximately.
The complexity of the model and the diversity of aspects covered by this model make these simulations unique in the context of elastohydrodynamic research.

6.1 Experimental data and analytical approximations for ball bearings

Due to the immense technical importance of ball bearings there exist a lot of experimental, numerical and also analytical studies. The typical experimental configuration is a somehow simplified model system for ball bearings. Only *one* ball without bearing unit is considered as in [Křupka *et al.* (2005)] or [Křupka

et al. (2000)]. In some publications admittedly also entire ball bearings are studied, see [Olaru & Gafitanu (1997)]. In this thesis we restrict ourselves to considering single balls due to the complexity of the simulations.
The most common quantity measured by experiments is the film height at certain points and the film profile. For reasons of comparability often the *central* as well as the *minimal* film thickness is considered. Anymore the pressure profile can be also measured but apparently with less accuracy as indicated by larger scattering of the experimental results.
The experimental setup consists of a ball race with a transparent window which can be lighted from exterior. The reflected light is analyzed. Since the fluid changes its optical properties under high pressure the pressure can be also figured out. Such measurements are feasible in principle up to a film thickness of $1nm$ which would be far below the film thicknesses we are interested in. An introduction to different experimental techniques is presented in [Spikes (1999)] where the interested reader also finds more details on the physical aspects of measurements for ball bearings.
For central and minimal film thickness there exists an analytical approximation which turns out to be rather precise at least for some situations. In [Křupka *et al.* (2005)] the two quantities are both measured and compared to the analytical theory and are in good agreement. We will also compare our simulations to this analytical formula. In the following we present it as well as the experimental situation with all parameters.
The first difficulty in trying to conduct simulations for elastohydrodynamic lubrication is pre-loading. This process is described in more detail in chapter 4.3. It consists of exerting an external force pressing the ball onto the race. Together with the pressure dependent viscosity only this effect without any rotation of the ball can lead to a remarkable pressure and viscosity. In literature an analytical approximative contact theory is applied often though it is not clear if it is applicable if a fluid is present and no real contact happens. This "Hertzian" theory predicts a maximal pressure in the specific situation described in [Křupka *et al.* (2005)] of $1.54GPa$. The coefficient of pressure-dependent viscosity is stated to be $24.0\frac{1}{GPa}$ and Barus' law is assumed to hold: $\mu = \mu_0 \exp(\alpha p)$. Consequently in such a setting we would have to account for a change in viscosity of $\exp(24.0 * 1.54) \geq \exp(30)$. This makes the difficulties in consistently modeling pre-loading clear. With such an enormous increase in viscosity we could by no means expect that the model equations remain valid. Indeed in [Ohno & Kuwano

(1995)] the point of phase-transition to a glass is stated to be at a value of the exponent $\alpha p \sim 13$. For exponents $\alpha p \sim 25$, which would be exceeded following [Křupka *et al.* (2005)], a further phase-transition to a visco-plastic solid happens. We are thus reasonable in supposing that the oil used in the experiments in [Křupka *et al.* (2005)] will *not* be subject to the pure Barus law for the same constant exponent up to the maximal Hertzian pressure of $1.54GPa$. Either a phase transition will occur indeed or the Barus equation is an approximation up to some intermediate pressure where another material law begins to hold. Besides we would not at all be able to treat a change of coefficients of the differential equation of $\sim \exp(30)$ with any numerical algorithm with double precision. In engineering literature unfortunately such inconsistencies are seldom brought up explicitely. In [Křupka *et al.* (2005)] no comment at all is made on this subject. We treat the pressure dependent viscosity, as described in more detail in chapter 3, by cutting off the exponential function at some value. This can be interpreted as requiring a different pressure-viscosity law at high pressures. If there are phase transitions happening of course the whole type of model equations would change and the models would in these cases be even more dubious than the non-Newtonian fluid models itself. Therefore we refrain from considering phase transitions throughout this thesis.
The field of elastohydrodynamic lubrication research is much older than computers, hence experimental and analytical studies were used exclusively for a long time in this field. This explains why there are so many analytical approximations which are often astonishingly precise approximations at least for certain aspects of experimental data. One of the most important formulas predicts the central and minimal film thickness related to several non-dimensionalized parameters. All details and the derivation can be found in [Hamrock & Dowson (1976)], we will directly show the result.

$$\begin{aligned} H_{central} &= 3.63U^{0.68}G^{0.49}W^{-0.073}\left(1-\exp(-0.68k)\right), \\ H_{minimal} &= 2.69U^{0.67}G^{0.53}W^{-0.067}\left(1-0.61\exp(-0.73k)\right). \end{aligned} \tag{6.1}$$

All physical quantities are non-dimensionalized with the scalings shown in table 6.1. In equations (6.1) H denotes the film thickness, G the elasticity modulus, W the pre-loading and k a geometry parameter depending on the curvature of the bodies and U is the inflow velocity of the fluid. The latter equals the radial velocity of the rotating ball in the case of the experimental benchmark problem considered below.

U	$\frac{\eta v}{E' R_x}$
W	$\frac{F}{E R_x^2}$
G	$\alpha E'$
k	$\frac{R_x}{R_y}$
R_x, R_y $[m]$	Radius of the Hertzian contact ellipsoid
E'	αE, E Elasticity modulus

Table 6.1: Non-dimensionalizing ball bearing parameters.

There are also some variants of this formula for instance to incorporate larger classes of non-Newtonian fluid models, see e.g. [Moore (1997)]. In this publication also the accuracy of formula (6.1) itself is discussed. Indeed for the derivation several approximations are entering. The formula is based on Reynolds' equation, see chapter 3.4, which is itself an approximation of the Navier-Stokes equations. This approximation is supposed to be accurate for small film thicknesses. Non-Newtonian fluid models are delicate to include in the derivation of a formula for the film thickness as this is the case for Reynolds' equation. In [Rajagopal & Szeri (2003)] a consistent derivation is presented but, as stated in this publication, often in literature a somehow contradictory derivation can be found.
In equations (6.1) both central and minimal film thickness tend to zero when α tends to zero which immediately shows the limitations of this approximation. When the pre-load tends to zero, both film thicknesses tend to infinity.
Parts of the experimental data can yet be matched precisely by analytical approximations such as the Hamrock-Dowson formula (6.1). Yet even if these approximations are accurate they only predict some very specific quantities. The advantage of numerical methods is to predict not only film thickness but also for instance drag and lift, film thickness profiles and pressure profiles amongst others for which no analytical formula is available.
Some experiments measure not only the central and minimal film thickness but the entire film profile with its spatial variation. The pressure profile is often depicted as well. Unfortunately it is not common to show error bars in this field even if the experimental data is apparently affected by measuring error. Often experimental results for film thicknesses are scattering considerably, especially for very small values of the film thickness $\sim 1nm$. Also pressure profiles are sometimes measured, see e.g. [Jubault *et al.* (2003)], but evidently these measurements are also not very accurate and scatter. For numerical simulations it can be concluded that modeling and measurement errors are so large that there is no use to seek for

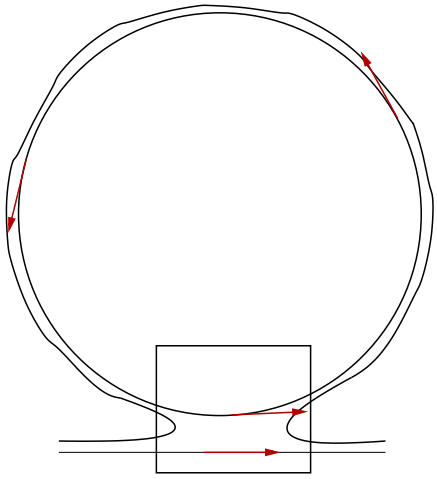

Figure 6.1: Scheme of ball in front of plane. The computational domain consists of the framed region. The tangential velocity on the ball and the race is indicated with arrows.

numerical simulations, which are precisely matching experimental data. Instead our goal is a numerical algorithm showing a qualitatively similar behaviour to the main features observed in experiments. The most important feature is the functional relation between film thickness and rotational speed. This quantity follows approximately a power-law over a wide range of rotational speeds. The numerical simulations will show a very similar behaviour with a similar value for the film thickness as the analytical approximation predicts.

6.2 Numerical results

We will now compare the numerical results with the analytical approximation also used in [Křupka *et al.* (2005)] where it represents experimental data accurately. For this purpose a sketch of the experimental setup is shown in figure 6.1. The material parameters stated in [Křupka *et al.* (2005)] are shown in table 6.2.

	Ball	Race
Poisson number	0.29	0.3
Elasticity modulus GPa	2.1×10^{11}	4.2×10^{11}
Fluid viscosity Pas	0.457	
Pressure-viscosity coefficient GPa^{-1}	24.0	

Figure 6.2: Material parameters for experimental configuration.

Not all material parameters are precisely defined in [Křupka *et al.* (2005)], for instance we find no information about the density of the fluid. For mineral oil it is usually in the interval $850 \pm 100 \frac{kg}{m^3}$ and the numerical approximation does not depend on this quantity sensitively. In addition the diameter of the ball is $25.4mm$ and the pre-loading force is $5N$, $36N$ and $130N$. The process of pre-loading is difficult to treat, we have included it as explained in chapter 4.3.
The viscosity of a fluid strongly depends on temperature as well as the pressure-viscosity coefficient. The experiment was conducted at a temperature of $40 \pm 0.4°C$. We interpret this in the following way: The temperature of the oil and possibly the ball or race at some measuring point was in the stated interval. This does not necessarily mean that the temperature throughout the domain was entirely constant. There could be local sources of heat due to viscous effects in the fluid or the periodic deformation of the ball. Since nothing is reported on that effect we also neglect (local) temperature effects in our simulations. In literature many experiments exist with measurements at different constant temperatures. This mainly causes a change in viscosity and in the pressure-viscosity coefficient and can thus also be treated in simulations by changing these parameters.
In [Křupka *et al.* (2005)] no precise information is given on the relation between pressure and viscosity for the lubricant. Only a "pressure-viscosity coefficient" is stated in a table of material parameters. In such cases we may always assume in engineering literature that Barus' equation $\mu = \mu_0 \exp(\alpha p)$ is postulated implicitly. The Barus model is known to be not applicable for arbitrarily large ranges of pressures, either phase transitions occur or the pressure-viscosity function deviates from the purely exponential behaviour at high pressures, see e.g. [Ohno & Kuwano (1995)]. Since we have no additional information we stick to Barus' law and introduce a cutoff at some high value of the pressure, see chapter 3 for details.
We will now proceed to the comparison of our numerical results with experimental data. We do not compare the results directly with experimental data but with an analytic approximation. In [Křupka *et al.* (2005)] this analytic approximation is also used and shows good accuracy in comparison with experimental data. The analytic theory was explained in chapter 6.1.
For slow rotations and thus low film thicknesses $\leq 10nm$ analytical, numerical and experimental data have to be interpreted with care. First of all in a real bearing the ball has no perfect surface but inevitably some surface roughness will be present. In [Křupka *et al.* (2005)] the surface roughness is stated to

have "a root mean square [...] about $4nm$". To the knowledge of the author such a precision is unrealistic, in [Hamrock & Dowson (1976)] surface roughness is assumed for instance to be $\geq 10\mu m$. In the range of high precision bearing components which might have been used for the experiments, surface roughness is probably particularly small. However any value smaller than $500nm$ seems to underestimate surface roughness. This means that all measured film thicknesses in [Křupka *et al.* (2005)] are smaller than the surface roughness of the bodies. Note however that pre-loading leads to a flattening of the bodies in contact with deformations of several μm so that surface roughness might be equalized by this effect.

Secondly for film thicknesses smaller than $10nm$ the Navier-Stokes equations cannot be considered a valid model anymore. Since simulations and analytical theory somehow depend on the Navier-Stokes equations as basic model we should not expect them to be valid for such ultrathin film thicknesses. From the experimental point of view it also becomes more difficult to measure extremely small film thicknesses. Only recently such studies have become possible, see [Spikes (1999)]. In [Křupka *et al.* (2005)] the authors state that each point on their data sheet below $10nm$ corresponds to three experimental values with maximum difference of $0.6nm$ to the mean value. That is, not all data is shown but some arbitrary mechanism is introduced to drop undesired scattering points. From a scientific point of view this is a doubtable approach, it would be more transparent to keep all data points and let the interpretation up to the reader. We draw the conclusion that all modeling and simulations based on continuum mechanics is not appropriate for very small film thicknesses. This region of parameters and operating conditions has to be treated with models and methods wich do not rely on a continuum description of a liquid, but consider single particle effects. The methods established in this thesis break down at very small film thicknesses.

In [Křupka *et al.* (2005)] three measurements with variable pre-load are presented. In our numerical simulations we have treated pre-loading as described in chapter 4.3. We present three simulations for three different values of the pre-loading force, $0.01N$, $0.1N$ and $1N$. The simulations are compared to the analytical approximation and both are in general not sensitively depending on the pre-loading force. The reasons for taking different values of the pre-loading force than in [Křupka *et al.* (2005)] are diverse: Firstly the modeling error related to this process is considerable as stated in chapter 4.3. This also leads to a lower accuracy of the numerical simulation in comparison to the analytical theory at

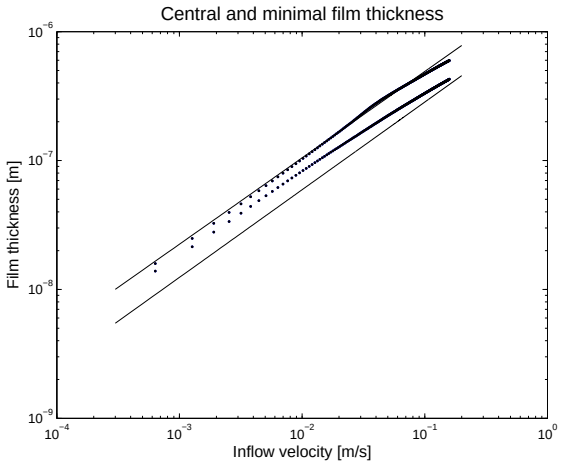

Figure 6.3: Film thickness depending on rolling speed for small pre-load. Solid lines represent the analytical approximation, points simulation results. The upper curve is the central film thickness, the lower the minimal film thickness.

high pre-loads. At the resulting high pressure the pressure-viscosity relation is not known and may not be modeled by the Barus law.
In general the shape of the film thickness function in numerical simulations is a function influenced mostly by the pressure-viscosity relationship and the regularizing parameters described in chapter 3. Another important factor is the initial geometry with the position of the right and left meniscus of the fluid. In the following all simulation results are realized with a fixed boundary for the fluid if not stated otherwise. The reason is that the free boundary value problem introduces a very stiff numerical problem aspect. The transformation at the boundary degenerates quickly for small deformations. Therefore systematic simulations with a free boundary for different parameters require many different meshes with different initial position of the boundary. This is of course awkward and we refrain from systematic studies of the fully coupled system with a free boundary and leave this question open for further research.

In figure 6.3 we depict the film thickness depending on inflow velocity. The solid line corresponds to the analytic formula (6.1), the points are results of numerical simulations. The same applies to figures 6.4 and 6.5. In figure 6.3 which corresponds to a very small pre-loading force of $0.01N$ the central film thickness is in almost perfect agreement with the analytical theory. Only for very small rotational inflow velocity a systematic error exists. This happens in a region of film thicknesses of $\sim 10nm$. In this region the deformation is small, indeed it is always of the same order of magnitude as the film thickness and thus still influenced by

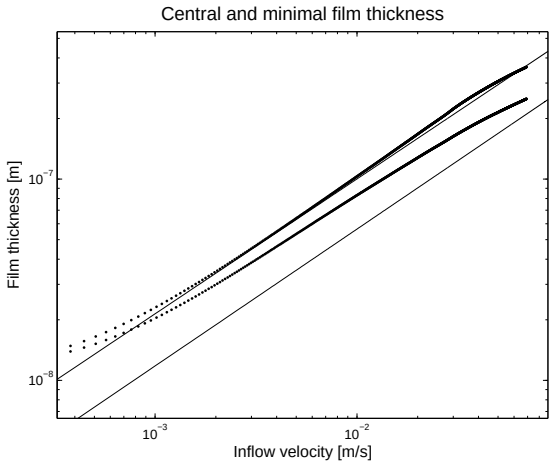

Figure 6.4: Central and minimal film thickness depending on rolling speed for medium pre-load. Solid lines represent the analytical approximation, points simulation results. The upper curve is the central film thickness, the lower the minimal film thickness.

the initial geometry. The treatment of pre-loading described in chapter 4.3 also leads to an initial deformation influencing the results at low speeds. Hence we will remark that the agreement between numerical simulation and analytical approximation is better for low values of the pre-loading force. For higher pre-load the range of values influenced by the initial geometry becomes larger and extends to higher rotational speeds. For a very high inflow velocity the simulation results tend to deviate from a linear behaviour. We may assume that at such high velocity the resulting high pressure leads to a variation of the pressure-viscosity relation.

The minimal film thickness is always represented less accurately in our simulations. It is always larger than predicted by the analytical theory and also has a different slope. For large speeds the agreement is usually better. In [Křupka *et al.* (2005)] the experimental data for the minimal film thickness is also not perfectly matching the analytical theory so that this does not have to be a disadvantage of our simulations. This quantity may also depend strongly on the initial shape of the geometry which is flattened by pre-loading in experiments but not to the same extent in our simulations.

In figure 6.5 the simulations for a pre-loading force of $1N$ are shown and for the reasons stated above the accuracy is slightly worse than in the two examples with lower pre-load. Similar remarks as made above for the examples with smaller pre-load also apply to this situation. For low speeds we see some difference which tends to become smaller as the speed increases. The accuracy for the central film

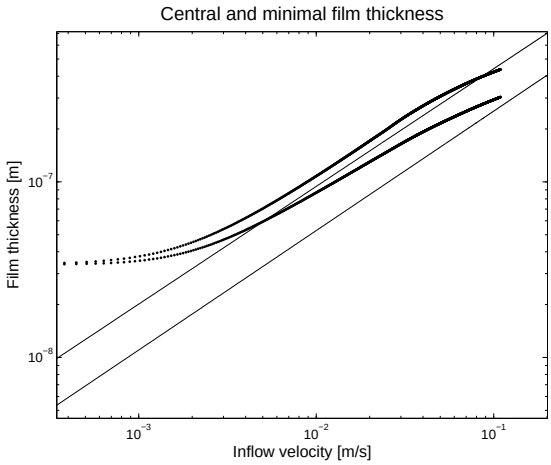

Figure 6.5: Central and minimal film thickness depending on rolling speed for large pre-load. Solid lines represent the analytical approximation, points simulation results. The upper curve is the central film thickness, the lower the minimal film thickness.

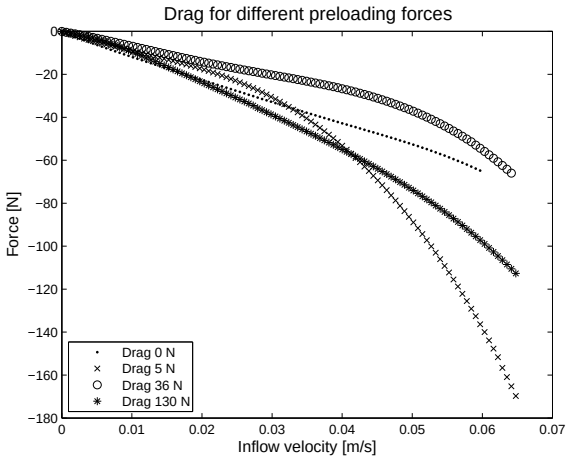

Figure 6.6: Drag depending on inflow velocity for different pre-loads.

thickness is better than for minimal film thickness. At high speeds we remark a deviation from a linear relation.

In figure 6.6 and figure 6.7 the drag and lift depending on different pre-loading forces is shown. For these quantities no analytical approximation exists to compare with. We show these results to illustrate the potential of the method established in this thesis.

In general the numerical results in comparison with the analytic theory are in good agreement, they lie in a reasonably close region and show a qualitatively similar behaviour. Besides we have made no effort to optimize parameters with

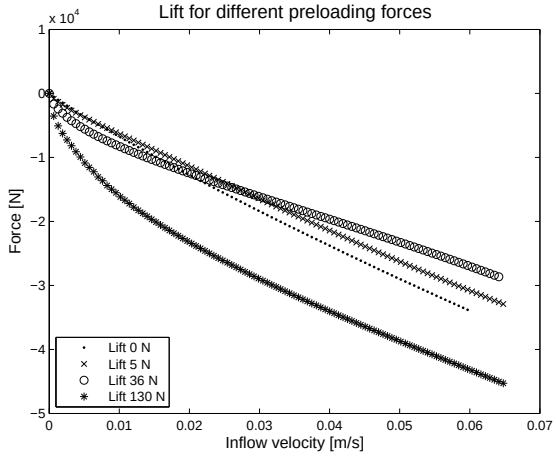

Figure 6.7: Lift depending on inflow velocity for different pre-loads.

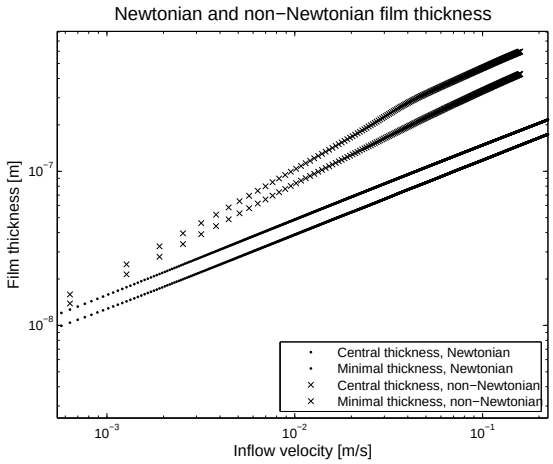

Figure 6.8: Central and minimal film thickness for Newtonian (dotted) and non-Newtonian fluid (crosses). The upper curve represents the central film thickness, the lower the minimal film thickness.

respect to a better approximation. However there is some difference and studying this difference may also help to gain physical knowledge of the relevant processes in a ball bearing.

For a comparison we have also conducted a simulation with constant viscosity and compare it to the Barus' fluid in figure 6.8. It turns out that there is a large difference between the results. Especially it is much larger than the difference between the results with pressure-dependent viscosity and the analytical approximation for these results. Once more we claim that pressure-dependent viscosity itself as well as the exact functional relation is one of the dominating influences

on elastohydrodynamic simulations.
We will now analyze the possible reasons for the partial deviation of the analytic theory and the simulation results.

- The ad-hoc treatment of pre-loading, see chapter 4.3, is perhaps a coarse approximation. Pre-loading consists in pressing the ball onto the race thus involving a contact problem as well as a fluid-structure interaction problem at the same time. For such processes no simple model is available in literature and it is difficult particularly from a modeling point of view to treat it consistently. In our simulations we include the pre-load as an exterior force derived from an analytic contact problem formulation.

- Information on the pressure-viscosity relationship is incomplete. It seems sensible to suppose that the lubricant follows the Barus law for some range of pressures. It is however not clear that the Barus law is valid for the *whole* range of pressures appearing in the simulation. Furthermore we need to introduce regularizing terms in order to be able to solve the discrete equations, see chapter 3. This has considerable influence on the pressure profile and thus the film thickness. Also different material laws as proposed in [Ohno & Kuwano (1995)] or [Bair *et al.* (2006)] would lead to different results.

- Compressibility has been neglected in our simulations (except the regularizations leading to small compressibility). It is known that under very high pressure lubricants become slightly compressible. There is again no lack of models for compressibility, see [Dowson *et al.* (1986)], but since there is also no evidence that compressibility does play an *important* role we neglect it. For further research it would be interesting to study the results of the incompressible case compared to different compressible models.

- Cavitation might happen and influence especially the *minimal* film thickness. The point of minimal film thickness usually lies in a region with negative values of the pressure of the fluid. Such negative pressure is in principle unphysical and a cavitation model would have to be used to guarantee positive pressure everywhere. The main problem in this context is to couple the cavitation model with the fluid-structure interaction formulation. Furthermore cavitation as described in [Nilsson & Hansbo (2008)] leads to variational inequalities for which special numerical algorithms have

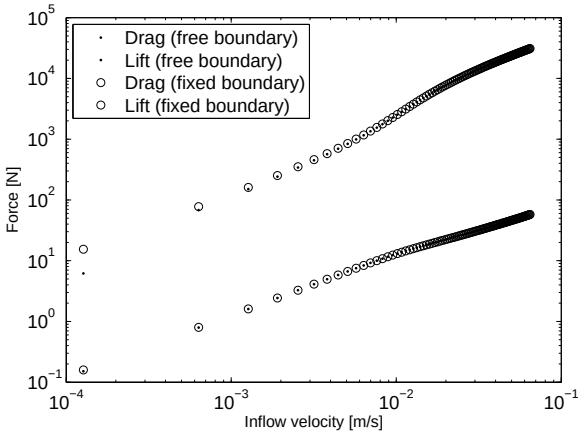

Figure 6.9: Drag and lift coming from simulations with free and fixed boundary.

to be developed. Since positive pressure is dominant and we do not see any numerical hint that cavitation is decisive we refrain from a systematic study.

- All simulation results come from a two-dimensional model. The quality of the two-dimensional approximation of the three-dimensional real system is difficult to estimate. It would indeed be a fascinating task to establish three-dimensional simulations to compare with. Yet even in two dimensions the technical difficulties especially concerning mesh generation are considerable. Furthermore there exists no efficient method of solving the discrete equations, the nonlinear solver takes a lot of iterations due to fluid-structure interaction and non-Newtonian fluid equations. The linear systems have to be solved by means of direct solvers because no efficient working multi-grid algorithm exists. Consequently we face substantial computation times for two dimensions, in three dimensions simulations would be practically restricted to very coarse meshes. Hence numerical errors would be larger and partly countervail the more realistic model.

We can conclude that certain modeling uncertainties exist and often it is difficult for a numerical analyst to judge on the quality and applicability of different material laws, models or simplifications proposed in literature.

In chapter 2 we have established a method to discretize free boundary value problems. We have used this method for the simulation of elastohydrodynamic lubrication and compared the effect of the free boundary to other problem aspects. For this purpose we conducted two simulations with identical initial domain. For

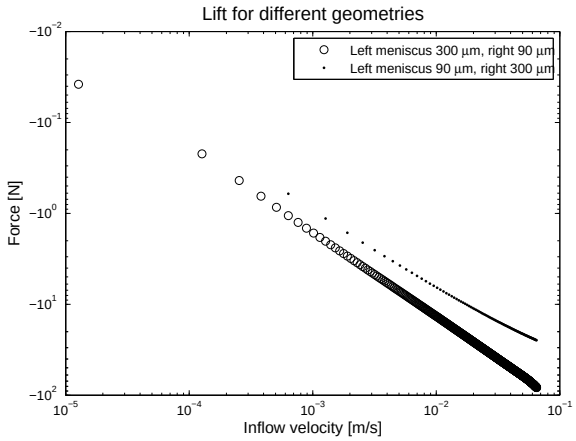

Figure 6.10: Lift for two different initial geometries.

one simulation the boundary remains fixed in time and a *do nothing* boundary condition is posed for the fluid. The other one has a free boundary with surface tension. In figure 6.9 the results for drag and lift are shown and it turns out that there is practically no difference except for very small rotational frequencies. This means that the direct influence of forces related to surface tension can be neglected. However, qualitatively the free boundary shows if the meniscus of the fluid is situated roughly at a physically meaningful place. If not, high normal velocities at the boundary appear, indicating an unphysical position of the meniscus. Indeed the position of the meniscus *does* have a considerable influence on the solution which can be observed in figure 6.10. In this figure two different positions of the initial meniscus and the resulting film thickness is shown, the difference is up to 70%. This effect has also been reported in literature when starvation lubrication is modeled by a smaller distance between the inlet and outlet meniscus of the fluid, see [Hamrock & Dowson (1976)]. In the simulations two extreme cases are compared, for the first simulation the left meniscus is at $-300\mu m$ and the right at $90\mu m$ and conversely for the second simulation. Such a large change in the position of the meniscus seems unrealistic, for simulations with a free boundary the change is always much smaller. We nevertheless present these results to figure out the influence of the initial geometry.

Such a study is one example of the benefit of a fundamental model using full fluid equations instead of the Reynolds equation. Firstly the calculation of drag and lift will always be a crude approximation when based on the Reynolds equation. Recall that only the pressure is kept as variable in the Reynolds equation disregarding all forces related to fluid velocity and shear. Secondly the position

Figure 6.11: Simulation results of x-velocity (right) and deformation (left) of the experimental benchmark problem.

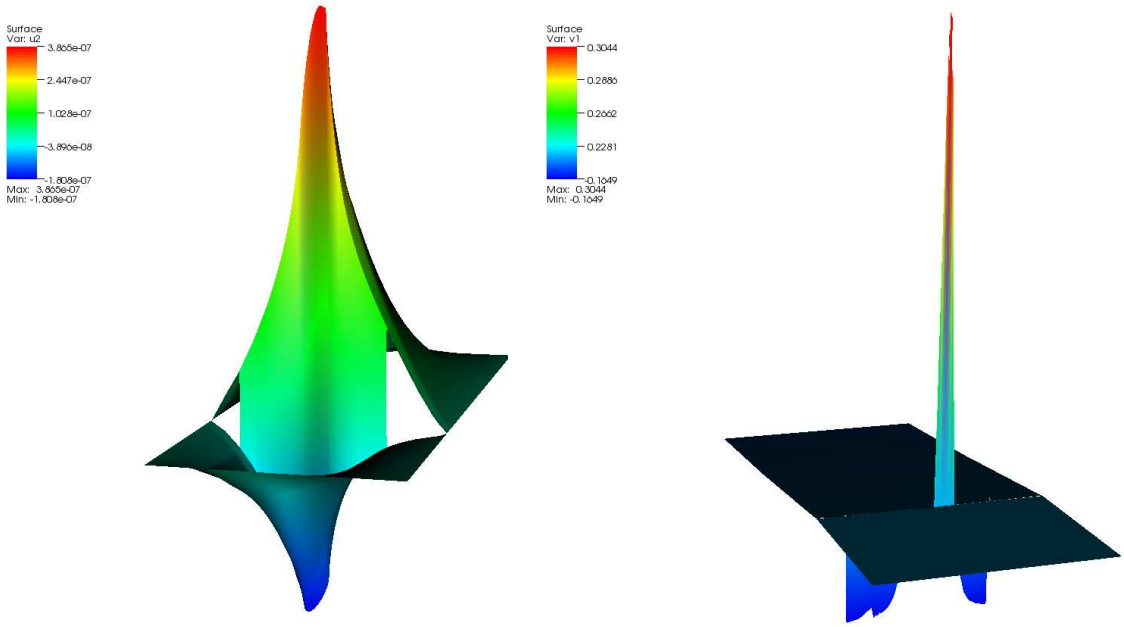

of the meniscus and the free boundary value problem may not be included in the Reynolds equation in a simple meaningful way. To our knowledge the model on which our simulations are based is in this sense the most complete one compared to literature.

An optimal discretization method would be robust so that any set of parameters and operating conditions is compatible to any initial geometry. Since this involves large deformations of the free boundary this robustness is in practice limited. Two further aspects are important in this context. Firstly if mass is not preserved exactly by our discretization, see chapter 2 for a detailed discussion, mass loss or mass gain will cause an additional unphysical boundary movement. This can be overcome by using fine (locally refined) meshes and small time-steps. Secondly we remark that the deformation in the free boundary value problem arises at the boundary. Therefore it is not possible to treat larger deformations with different extensions of the deformation to the interior as it is often the case for instance in fluid-structure interaction problems.

Figure 6.11 and figure 6.12 show simulation results for the experimental benchmark configuration. Notice that the velocity profile can not be determined by using Reynolds' equation since velocity is no independent variable in that case.

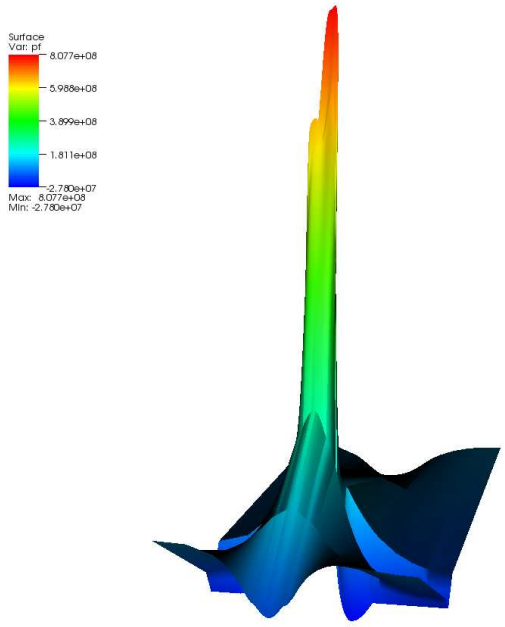

Figure 6.12: Simulation results of the pressure profile of the experimental benchmark problem.

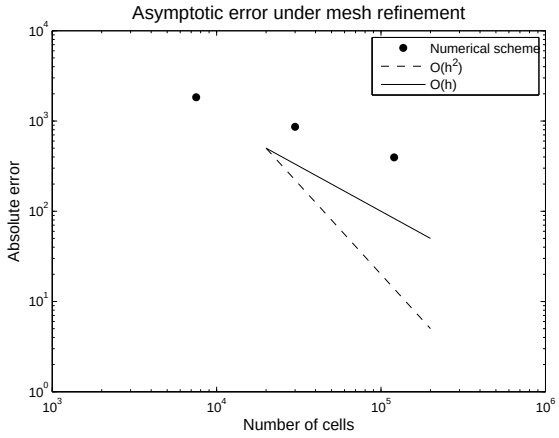

Figure 6.13: Error under mesh refinement the lift of the cylinder.

Since we deal with a compressible material the pressure profile has only a physical meaning in the thin fluid film in figure 6.12. In the structure it is merely an arbitrary harmonic extension of the fluid pressure.

In figure 6.13 the asymptotic error under mesh refinement is shown. It is close to linear compared to the quadratic convergence in the ball bearing example where the lift is evaluated on a *closed* boundary. Therefore a different higher order

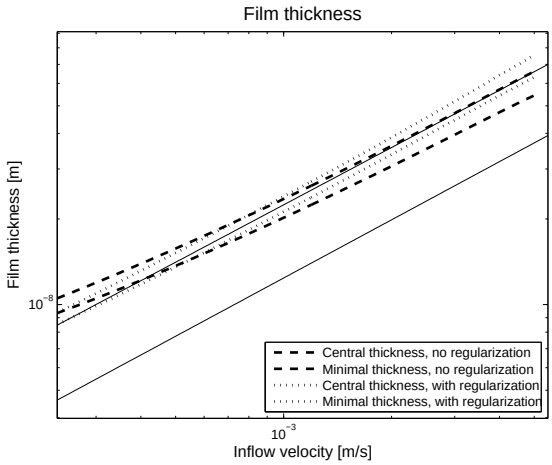

Figure 6.14: Central and minimal film thickness with and without any regularization. The upper curves represent the central film thickness, the lower the minimal film thickness.

evaluation method for the lift can be applied, see [Giles *et al.* (1991)]. It is not directly applicable for a situation without closed boundary as in this geometrical situation.

In figure 6.14 film thickness results with and without any regularization is shown. There exists a difference of approximately 15% for slow rotational speeds. For higher speeds the difference would probably increase but the scheme without any regularization fails. The value for the articial compressibility is $\epsilon = 1.0 \times 10^{-17}$, the cutoff for the viscosity is 1.0×10^5, see chapter 3 for the definition of these regularization parameters. This choice of parameters is also used in the diverse simulation results presented in this and the subsequent chapter. Once more we conclude that the precise non-Newtonian fluid model as well as any regularization leads to a pronounced change in simulation results. The curve without regularization fits the analytical theory more precisely.

6.3 Simulations for ball bearing geometry

The simulation methods presented in the last chapter were adopted in terms of geometry and parameters for the comparison with the situation described in [Křupka *et al.* (2005)]. It consists of a somehow simplified geometry and was implemented for validation reasons. We will now proceed to a ball bearing ge-

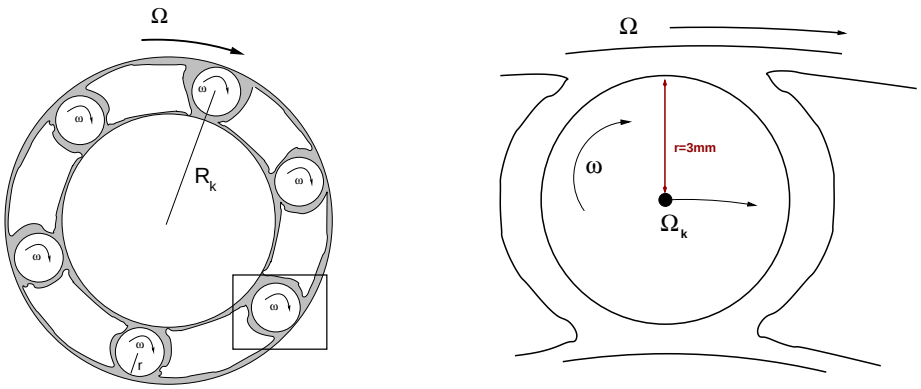

Figure 6.15: Scheme of a ball bearing with several balls. The computational domain corresponds to the box and is sketched in more detail on the right.

ometry as employed in reality. In this case there exist *two* film thicknesses since the ball is confined between inner and outer race which are both curved. We will therefore have an inner and outer film thickness. In reality the races do not possess a cylindrical symmetry but the geometry is fully three dimensional. We restrict ourselves to two-dimensional simulations.
For ball bearings it is reasonable to act on the assumption of "pure rolling", that is the radial velocity of the ball at the boundary equals the velocity of the corresponding race, see figure 6.15.

We have to distinguish three rotational velocities and choose a coordinate system in which the inner race is at rest:

- Ω is the rotational frequency of the outer race.
- Ω_k is the rotational frequency of the center of mass of the ball around the center of the inner race.
- ω is the rotational frequency of the ball around its own center of mass.

If we denote R_k the radius of the circle followed by center of mass and r its radius the pure-rolling condition implies the following relations for the frequencies

$$\Omega_k = \frac{\Omega(R_k + r)}{2R_k},$$
$$\Omega = \frac{2\omega r}{R_k + r}.$$

In reality the pure-rolling condition is not fulfilled exactly and the ball may also experience precession-nutation. When this effect becomes stronger shear-related

changes in the viscosity also have to be considered. We stick to using the pure-rolling condition since precession-nutation can only be accounted for in three dimensions.
Further more we only consider one single ball and neglect all effects related to the coupling of different balls in a ball bearing.
We consider a coordinate system in which the ball is *only* rotating around its center of mass, its center of mass is at rest. In this coordinate system inner and outer race are rotating, in an inertial system outer race and the center of mass of the ball would be rotating. Formally we have to include fictitious forces because we are no more considering an inertial system anymore, these can however be neglected.

	Ball	Race
Poisson number	0.3	0.3
Elasticity modulus GPa	2.1×10^{11}	2.1×10^{11}
Fluid viscosity Pas	0.2151	
Pressure-viscosity coefficient GPa^{-1}	16.5	

Figure 6.16: Material parameters for ball bearing.

All material parameters are given in table 6.16 and we may again assume a Barus' fluid. Note that in ball bearings ball and race are made of the same material in contrast to the experimental situation in the preceeding section. In a ball bearing geometry their exist four distinguished film thicknesses: Outer central and minimal film thickness as well as inner central and minimal film thickness. Results for these quantities for a pre-load of $1N$ are shown in figure 6.17. The accuracy of the outer central film thickness is almost perfect. Both minimal film thicknesses and the inner central film thickness is represented less accurately. However we remark that the analytical theory is unphysical in one detail: In the analytical approximation no coupling between inner and outer film thickness exists at all. Only the different geometry parameters of the ball at the inner and outer race lead to different results for the film thickness. In reality the ball may also undergo a translational rigid body motion. If it rigidly moves in outer direction the outer film thickness becomes smaller to the same extent as the inner becomes larger. Thus the film thicknesses are coupled. This effect exists in our simulations due to the fundamental physical modeling but not in the analytical approximation. It would be hence interesting to compare with real experimental data, but such

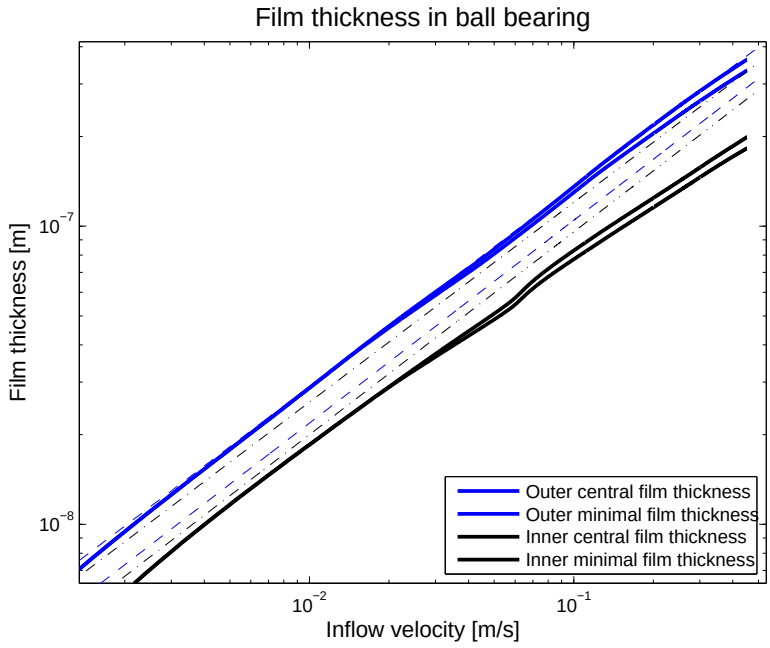

Figure 6.17: Central and minimal, inner and outer film thickness results for ball bearing. Since there are two contact regions of the ball (inner and outer) there are four film thicknesses. The outer film thickness is larger. Dashed straight lines indicate the analytical approximation, solid lines stand for simulation results. These are in ascending order inner minimal, inner central, outer minimal and outer central film thickness.

data for in-situ measurements in ball bearings is rare.

In figure 6.18 we see some simulation results for pressure, deformation and velocity in the ball bearing geometry. Again the pressure spikes due to pressure dependent viscosity are remarkable. Indeed the pressure is approximately constant throughout the entire fluid domain except the contact zone between ball and bearing structure. Consequently, the deformation also reaches its maximal value in the contact zone. However, due to the elastic properties of the structure, there is no spike in the structure, but the deformation field is smoother than the pressure.

In figure 6.19 the asymptotic error under mesh refinement is shown. The order is close to quadratic and thus higher compared to the experimental situation of the previous section because a different method of evaluating the lift is used, see [Giles *et al.* (1991)] for details. It leads to a higher order of convergence but is not easily applicable for the other situation where no closed boundary is present.

Figure 6.18: Simulation results for the pressure profile (top left), y-velocity (top right) and y-deformation (bottom) for a ball in a ball bearing.

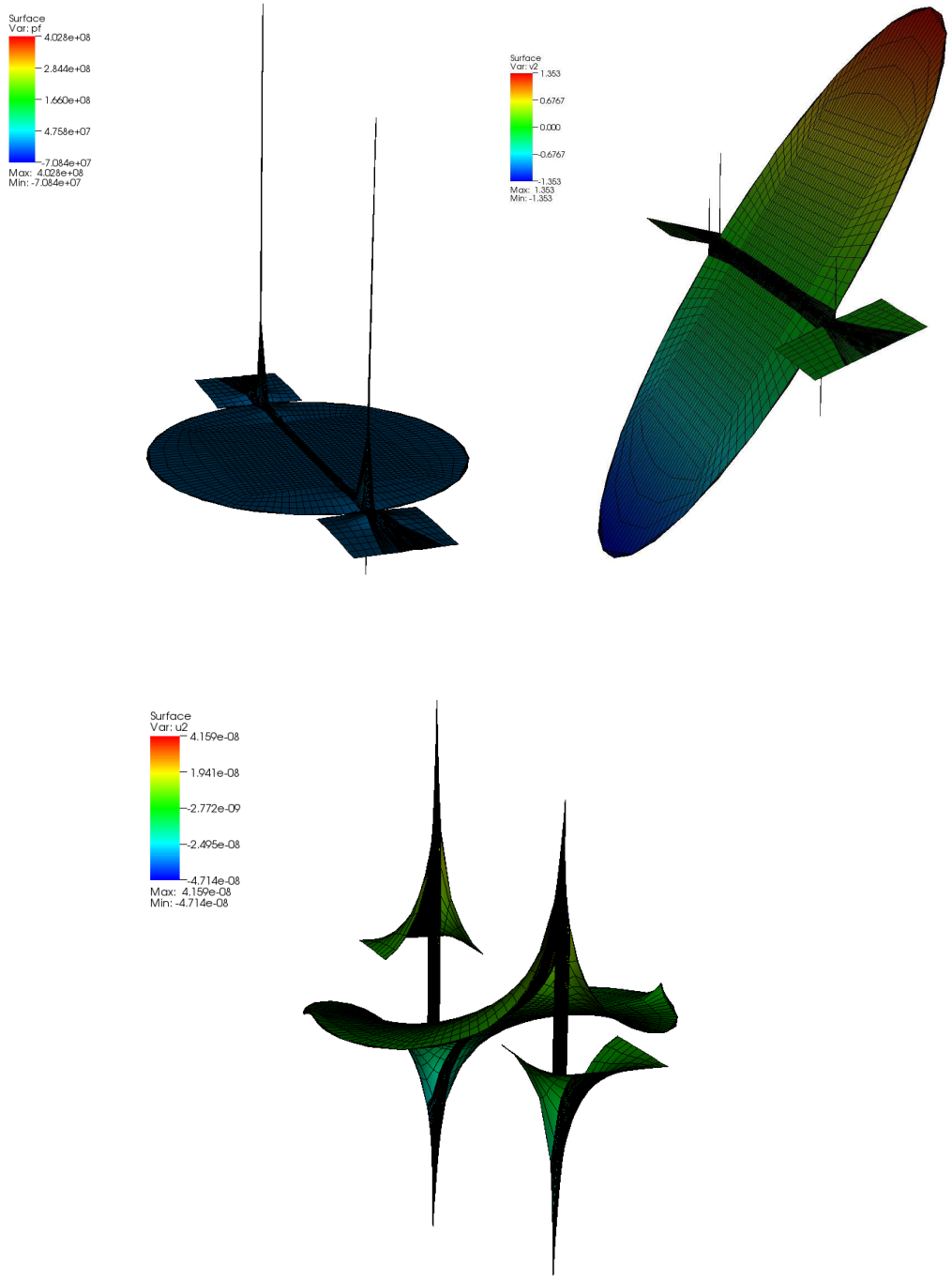

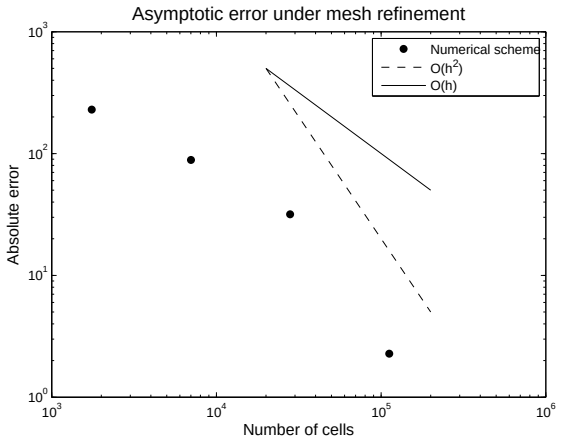

Figure 6.19: Error under mesh refinement the lift of the cylinder.

6.4 Conclusion and discussion of the numerical results

In this chapter we have presented the results of simulations of the elastohydrodynamic film thickness in two experimental situations. It was the main goal of this thesis to derive a validated numerical method for such simulations. A comparison with analytical approximations for elastohydrodynamics shows a resonable degree of consistency.

The film thickness is the most important quantity for lubrication problems since it is an indicator of bearing failure: When the film thickness is close to zero, a collapse of the fluid film is possible. Therefore we concentrated on this aspect. The novel aspect of the presented method is its foundation on basic continuum mechanical models. The method relies on simulation of generalized Newtonian fluids and a complete fluid-structure interaction formulation. It is flexible and robust with respect to fluid and structure models, geometry and parameters. The results presented in this chapter are exemplary and the numerical algorithm easily carries over for different types of lubrication problems with different fluids. It may also be used for the prediction of different quantities such as drag and lift or processes related to the free boundary.

Chapter 7

Conclusion and outlook

In this thesis a novel approach for the simulation of elastohydrodynamic lubrication problems is presented. It relies on modeling the system as fluid-structure interaction problem with free boundary and non-Newtonian fluid. The structure is described as St.-Venant-Kirchhoff material. This kind of modeling is based on much more fundamental physical assumptions than the previously existing work in literature. Often Reynolds' equation is considered instead of the Navier-Stokes equations. The elasticity of the bearing and fluid-structure interaction is often neglected or, if at all, treated with simple ad-hoc approximations. We believe that with the recent evolution of computers and numerical algorithms there is no need any more to base simulations on simple models. In elastohydrodynamics it is often difficult to judge on the quality of approximation of simplified models. In-situ measurements are usually challenging and do not cover the whole range of interesting parameters as for instance for the viscosity. Thus the introduction of further simplifications leads to diverse sources of modeling errors which are difficult to distinguish and to study separately. In our simulations the limits of the underlying models are conversely clear: The Navier-Stokes equations hold for film thicknesses $\geq 10nm$, the elasticity and fluid-structure interaction formulation are widely accepted continuum mechanical models. This thesis gives proof that such complex coupled nonlinear systems can indeed be treated altogether simultaneously on modern computers.

The most important physical prediction in the context of elastohydrodynamics lies in predicting a fluid-film collapse. This may happen whenever the film thickness is close to zero. We have presented a method which is capable of simulating the film thickness. For applications this will therefore constitute the most im-

portant result of this thesis. The potential of the numerical simulations is much larger than this: Generalizations to non-Newtonian fluids, different geometries, parameters and physical effects related to the free boundary can be easily treated with the existing method. The results presented in the last chapter are only exemplary for two experimental situations. There is also an analytical approximation for the film thickness in bearings. This approximation is however only valid for certain parameters and operating conditions. We claim that numerical simulations are much more flexible with respect to variations of such parameters. Furthermore analytical approximations do not exist for all relevant physical quantities such as e.g. drag and lift of a ball in a ball bearing or spatial variations of pressure or velocity.

The overwhelming majority of publications dealing with elastohydrodynamics uses simplified models like Reynolds' equation. We suspect that this fact is more related to the historical development of the field than to any other reason. Reynolds' equation is a scalar equation which admits an analytical solution for some lubrication problems in contrast to the full Navier-Stokes system. This might have been an advantage when engineers began to investigate lubrication problems. At that point no powerful computers existed, of course. Today we state that the numerical solution of Reynolds' equation is by no means far more simple, only the number of unknowns is smaller due to the scalar equation. Also from a theoretical point of view the analysis of a non-Newtonian Reynolds equation is difficult because of the nonlinear expression in the main part of the differential operator. On the other hand Reynolds' equation is a mere simplification of the Navier-Stokes equations. It follows that *the set of problems where Reynolds' equation applies, is a true subset of all problems which can be treated by the Navier-Stokes equations.* This brings us to the conclusion that numerical and theoretical investigations based on generalized Navier-Stokes systems are in this sense more adequate for lubrication problems. We do not see any important disadvantage or additional problem arising when considering such models in comparison with Reynolds' equation.

In such a novel approach presented in this theses as a matter of fact not all arising questions can be answered completely. We will now comment on aspects which came up in the course of this thesis and would be interesting for further investigation. To begin with the comparison between simulation results and analytic approximation yields a qualitative agreement but also some quantitative error. We now state some aspects related to the physical processes in a ball bear-

ing which would be interesting to study in more detail in conjunction with the comparison of simulation and experiments.

- In terms of physical processes in a ball bearing the pre-loading would certainly pose the most important cause for further investigation. For a mathematically consistent treatment we would have to use a contact formulation between two bodies which are somehow separated by a fluid. Since pre-loading changes the initial state considerably this could be a promising approach for an even better insight to fluid-structure interaction in ball bearings.

- The exact functional relation between pressure and viscosity could be studied systematically. Since this function is decisive for the film thickness it would be interesting to consider a parameter estimation problem. In this context we would search for the pressure-viscosity function which leads to the best approximation of experimental data. Different fluid models may also differentiate in their properties with respect to numerical treatment. There could be fluid models which have better properties than the Barus' law in terms of nonlinear convergence of the numerical approximation.

- In this thesis the fluid was assumed incompressible (except a small regularization). Though it is known that lubricants under high pressure are slightly compressible. Similar to the case of pressure-dependent viscosity we could study the effect of compressibility for different material laws and their influence systematically. Also compressibility could lead to better properties of the problem for a numerical approximation.

- In this thesis the ball bearing is considered to be isothermal (at a given fixed temperature). In reality there will be also sources of heat like the periodic deformation of the ball and the shear of the fluid. Hence there will develop a non-constant temperature field in the fluid influencing the strongly temperature-dependent viscosity. Such effects are rarely studied in literature but could be an interesting extension of the existing models.

The numerical discretization we have presented in this thesis allows treating realistic models for ball bearings. We have validated it by comparing to an analytic approximation. This enables to approach even more complex problems such as

dynamic processes related to changes of operating conditions or the effect of surface roughness.
We will in the following state some open problems more related to the numerical algorithm. These are partly known for a long time like the lack of convergence of multi-grid methods on anisotropic meshes. However no fundamental solution seems to be available in literature at least for our specific numerical methods.
When dealing with elastohydrodynamic problems many geometry- and material-parameters are in a problematic range with respect to numerical approximation. The most prominent one is the anisotropic geometry leading to the failure of iterative linear solvers. Further difficulties are caused by the pressure dependent viscosity leading to slow nonlinear convergence as well as linear convergence due to huge variation of coefficients. As a last example we recall that robust iterative linear and nonlinear solvers for fluid-structure interaction systems are by no means easy to design. This brings us to the following concrete suggestions for further studies of numerical algorithms in the context of elastohydrodynamics.

- The linear systems coming from the discretization of elastohydrodynamic problems with finite element methods have a high number of unknowns calling for robust iterative linear solvers. In this context a robust multi-grid method for anisotropic meshes would be indispensable for three dimensional simulations. Our work on this topic could be a starting point for further research in this field. In addition one could work on more robust algorithms for strongly varying coefficients and for fluid-structure interaction.

- As for nonlinear iterations we propose a systematic study of different regularizations and their effect on convergence rates. Especially for the functional relation between viscosity and shear rate there exists a large variety of different models. These are probably not all applicable for elastohydrodynamics but it would however be interesting to find out which models have better properties with respect to convergence rates of the numerical algorithm. Such a study could eventually indicate further regularization methods.

- The ill-conditioned linear systems raise the question to what extent there are differences when using four-fold precision instead of double precision for floating point numbers. Due to the increased cost such an approach would however be only useful for the purpose of testing.

- The discretization of the free boundary value problem leads to a (temporal) accuracy of only first order. When higher accuracy is needed one could work on an improved second-order-accurate discretization scheme.

The present thesis is pointing out a novel possibility to model and simulate elasto-hydrodynamic processes. The numerical solution is robust enough to deal with a realistic system. This allows the validation of models and numerical algorithms. A comparison with a widely accepted analytic approximation shows that in a range of parameters the method leads to reasonable accuracy. Altogether this thesis may serve as basis for numerous further investigations.

Acknowledgments

I would like to express gratitude to Prof. Rannacher for providing me the opportunity to establish this PhD thesis and supervising it. I want to thank Prof. Rannacher for the helpful suggestions and discussions, too. I would also like to thank Prof. Jäger for the opportunity of discussion and interesting remarks and ideas.

During parts of this project I was a member of the International *Graduiertenkolleg* IGK 710 "Complex processes: Modeling, Simulation and Optimization" and I would like to thank for the support. This project was supported by the *Deutsches Zentrum für Luft- und Raumfahrt* (DLR). I want to thank the DLR for this opportunity and especially Reinhold Pietsch for the interest in my work and the good collaboration. This project was a collaboration with the company Rockwell Collins Germany from Heidelberg. I would like to thank Markus Ehinger and Sebastian Meynen for the suggestions as well as the interesting insights offered in the industrial applications of numerical analysis.

In the course of this thesis I had the opportunity to visit the Nečas center in Prague for a collaboration with Prof. Malek and Jaroslav Hron. I also had interesting discussions with Martin Lanzendörfer and I would like to express gratitude to all of them.

This thesis was based on the software packages developed in the numerical analysis group in Heidelberg and I want to thank all the authors and in particular Thomas Dunne for supervising me at the beginning of my thesis. Furthermore I am grateful to all the members of the numerical analysis group, particularly Michael Bézier, Matthias Klinger, Jevgeni, Thomas Richter, Stefan, Matthias Meier, Thomas Wick, Bärbel, Daniel, Adrian, Christian, Christoph, and Rebecca. I also want to thank Winnifried Wollner who has been a remarkable colleague and always made interesting remarks and comments. I owe him a lot of insight into different fields in numerical analysis.

Bibliography

Amestoy, P.R., Duff, I.S., & L'Excellent, J.Y. D. 1998. *Multifrontal Parallel Distributed Symmetric and Unsymmetric Solvers*. Tech. rept. Ecole Nationale Supèrieure d'Electrotechnique, d'Electronique, d'Infomatique, d'Hydraulique et des Télécommunications.

Apel, T., Knopp, T., & Lube, G. 2008. Stabilized finite element methods with anisotropic mesh refinement for the Oseen problem. *Applied Numerical Mathematics*, **58**, 1830–1843.

Bair, S., Yuchuan, L., & Wang, Q.J. 2006. The Pressure-Viscosity Coefficient for Newtonian EHL Film Thickness With General Piezoviscous Response. *Journal of Tribology*, **128**, 624–631.

Bänsch, E. 2001. Finite element discretization of the Navier-Stokes equations with a free capillary surface. *Numerische Mathematik*, **88**, 203–235.

Becker, R., & Braack, M. 1999. *GASCOIGNE High Performance Adaptive Finite Element Toolkit*. http://gascoigne.uni-hd.de.

Becker, R., & Braack, M. 2001. A finite element pressure gradient stabilization for the Stokes equations based on local projections. *Calcolo*, **38**, 173–199.

Braack, M. 2008. A Stabilizied Finite Element Scheme for the Navier-Stokes Equations on Quadrilateral Anisotropic Meshes. *Mathematical Modelling and Numerical Analysis*, **42**, 903–924.

Brackbill, J. U., Kothe, D.B., & Zemach, C. 1991. A Continuum Method for Modeling Surface Tension. *Journal of Computational Physics*, **100**, 335–354.

Braess, D. 2007. *Finite Elemente Theorie, schnelle Löser und Anwendungen in der Elastizitätstheorie*. 4 edn. Springer Berlin Heidelberg.

Causin, P., Gerbeau, J.F., & Nobile, F. 2005. Added-mass effect in the design of partitioned algorithms for fluid-structure problems. *Computer Methods in Applied Mechanics and Engineering*, **194**, 4506–4527.

Chapkov, A.D., Venner, C.H., & Lubrecht, A.A. 2006. Roughness Amplitude Reduction Under Non-Newtonian EHD Lubrication Conditions. *Journal of Tribology*, **128**, 753–760.

Davis, T. A. 2004. A Column Pre-Ordering Strategy for the Unsymmetric-Pattern Multifrontal Method. *Association for Computing Machinery Transactions on Mathematical Software*, **30**, 165–195.

Delfour, Michel C., & Zolésio, Jean-Paul. 2001. *Shapes and geometries*. Advances in design and control ; 4 ; Advances in design and control, no. 4. Philadelphia, PI: Society for Industrial and Applied Mathematics.

Dhunput, A., Teodorescu, M., & Arcoumanis, C. 2007. Investigation of cavitation development in the lubricant film of piston-ring assemblies. *Journal of Physics: Conference Series*, **85**, 1–10.

Dowson, D., & Taylor, C.M. 1979. Cavitation in Bearings. *Annual Review of Fluid Mechanics*, **11**, 35–66.

Dowson, D., Taylor, C.M., Godet, M., & Berthe, D. (eds). 1986. *Fluid film lubrication - Osborne Reynolds centenary*. Elsevier.

Dunne, T. 2007. *Adaptive Finite Element Approximation of Fluid-Structure Interaction Based on Eulerian and Arbitrary Lagrangian-Eulerian Variational Formulations*. Ph.D. thesis, Universitẗ Heidelberg.

Durany, J., G., García, & Vázquez, C. 1996. Numerical computation of free boundary problems in elastohydrodynamic lubrication. *Applied Mathematical Modelling*, **20**, 104–113.

Eschenburg, Jost-Hinrich, & Jost, Jürgen. 2007. *Differentialgeometrie und Minimalflächen*. 2 edn. Berlin, Heidelberg: Springer-Verlag.

Franta, M., Málek, J., & Rajagopal, K. R. 2005. On steady flows of fluids with pressure- and shear-dependent viscosities. *Proceedings of the Royal Scociety A Mathematical, Physical and Engineering Sciences*, **461**, 651–670.

Gallot, Sylvestre, Hulin, Dominique, & Lafontaine, Jacques. 2004. *Riemannian geometry*. 3. ed. edn. Universitext. Berlin ; Heidelberg [u.a.]: Springer.

Giles, M., Larson, M.G., Levenstam, J.M., & Süli, E. 1991. *Adaptive Error Control for Finite Element Approximations of the Lift and Drag Coefficients in Viscous Flow*.

Girault, Vivette, & Raviart, Pierre-Arnaud. 1979. *Finite element approximation of the Navier-Stokes equations*. Lecture notes in mathematics, no. 749. Berlin; Heidelberg [u.a.]: Springer.

Grandmont, C. 2002. Existence for a Three-Dimensional Steady State Fluid-Structure Interaction Problem. *Journal of Mathematical Fluid Mechanics*, **4**, 76–94.

Guangteng, G., Cann, P.M., Olver, A.V., & Spikes, H.A. 2000a. An experimental study of film thickness between rough surfaces in EHD contacts. *Tribology International*, **33**, 183–189.

Guangteng, G.and Cann, P.M., Olver, A.V., & Spikes, H.A. 2000b. An experimental study of film thickness between rough surfaces in EHD contacts. *Tribology International*, **33**, 183–189.

Gwynllyw, D. Rh., Davies, A.R., & Phi, T.N. 1996. On the effects of a piezoviscous lubricant on the dynamics of a journal bearing. *Journal of Rheology*, **58**, 1239–1257.

Hackbusch, W. 1985. *Multigrid methods and apllications*. Springer.

Hamrock, B. J., Schmid, S. R., & Jacobson, B.O. 2004. *Fundamentals of Fluid Film Lubrication*. 2 edn. New York, Basel: Marcel Dekker , Inc.

Hamrock, B.J., & Dowson, D. 1976. *Isothermal Elastohydrodynamic Lubrication of Point Contacts*. Tech. rept. NASA.

Hron, J., & Turek, S. 2006. A Monolithic FEM Solver for an ALE Formulation of Fluid-Structure Interaction with Configuration for Numerical Benchmarking. *In: European Conference on Computational Fluid Dynamics*.

Hron, J., Málek, J., & Rajagopal, K. R. 2001. Simple Flow of Fluids with Pressure-Dependent Viscosities. *Proceedings: Mathematical, Physical and Engineering Sciences*, **457**, 1603–1622.

Hughes, T. J.R., Franca, L. P., & Balestra, M. 1986. A new finite element formulation for computational fluid dynamics: V. Circumventing the babuska-brezzi condition: a stable Petrov-Galerkin formulation of the stokes problem accommodating equal-order interpolations. *Computer Methods in Applied Mechanics and Engineering*, **59**(1), 85–99.

Hysing, S. 2006. A new implicit surface tension implementation for interfacial flows. *International Journal for Numerical Methods in Fluids*, **51**, 659–672.

Jubault, I. 2002. *Application de la microspectrométrie Raman aux mésures in situ dans les contacts dynamiques*. Ph.D. thesis, Université des Antilles et de la Guyane.

Jubault, I., Molimard, J., Lubrecht, A.A., Magnsot, J.L., & Vergne, P. 2003. In situ pressure and film thickness measurements in rolling/sliding lubricated point contats. *Tribology Letters*, **15**(4), 421–429.

Kane, M., & Bou-Said, B. 2005. A Study of Roughness and Non-Newtonian Effects in Lbricated Contacts. *Journal of Tribology*, **127**, 575–581.

Kanzow, C. 2005. *Numerik linearer Gleichungssysteme*. Berlin ; Heidelberg [u.a.]: Springer.

Křupka, I., Hartl, M., Liška, M., Poliščuk, R., & Čermák, J. 2000. Experimental Evaluation of Film Shape and Its Comparison With Numerical Solution. *Journal of Tribology*, **122**, 689–696.

Křupka, I., Hartl, M., & M., Liška. 2005. The Influence of Contact Pressure on Central and Minimum Film Thickness Within Ultrathin Film Lubricated Contacts. *Journal of Tribology*, **127**, 890–892.

Landau, Lev D., & Lifšic, Evgenij Michailovič. 2007. *Hydrodynamik*. Korr. nachdr. d. 5., überarb. aufl. edn. Lehrbuch der theoretischen Physik / von L. D. Landau; E. M. Lifschitz ; 6 ; Landau, Lev D.: Lehrbuch der theoretischen Physik, no. 6. Frankfurt am Main: Deutsch. Aus d. Russ. übers.

Lauga, E., & Squires, T.M. 2005. Brownian motion near a partial-slip boundary: A local probe of the no-slip condition. *Physics of Fluids*, **17**.

Matthies, G., & Tobiska, L. 2002. The Inf-Sup Condition for the Mapped $Q_k - P_{k-1}^{disc}$ Element in Arbitrary Space Dimensions. *Computing*, **69**, 119–139.

Moore, A.J. 1997. The behaviour of lubricants in elastohydrodynamic contacts. *Proceedings of the Institution of Mechanical Engineers J*, **211**, 91–106.

Nilsson, B., & Hansbo, P. 2008. *A Stokes model with cavitation for the numerical simulation of hydrodynamic lubrication.* Preprint.

Nitsche, J. 1971. Über ein Variationsprinzip zur Lösung von Dirichlet-Problemen bei Verwendung von Teilrümen, die keinen Randbedingungen unterworfen sind. *Abhandlungen aus dem Mathematischen Seminar der Universität Hamburg*, **36**, 9–15.

Ohno, N., & Kuwano, N. 1995. Bulk Modulus of Solidified Oil at High Pressure as Predominant Factor Affecting Life of Trust Ball Bearings. *Tribology Transactions*, **38**, 285–292.

Olaru, D. N., & Gafitanu, M. D. 1993. Starvation in Ball Bearings. *Wear*, **170**, 219–234.

Olaru, D. N., & Gafitanu, M. D. 1997. A New Methodology to Estimate Starvation in Ball Bearings. *Tribotest Journal*, **4**, 93–106.

Quarteroni, A. 2004. *Mathematical Modelling and Numerical Simulation of the Cardiovascular System.* Elsevier.

Rajagopal, K.R., & Szeri, A. Z. 2003. On an inconsistency in the derivation of the equations of elastohydrodynamic lubrication. *Proceedings of the Royal Scociety A Mathematical, Physical and Engineering Sciences*, **459**, 2771–2786.

Sahlin, F., Almqvist, A., Larsson, R., & Glavatskih, S. 2007. A cavitation algorithm for abitrary lubricant compressibility. *Tribology International*, **40**, 1249–1300.

Schäfer, M., & Turek, S. 1996. Benchmark Computations of Laminar Flow Around a Cylinder. *Notes on Numerical Fluid Mechanics*, **52**, 547–566.

Scheck, F. 2002. *Theoretische Physik 1 Mechanik Von den Newton'schen Gesetzen zum deterministischen Chaos.* Berlin ; Heidelberg [u.a.]: Springer.

Schweizer, B. 1996. *Weak solutions and a Galerkin scheme for free boundary fluid systems.* Preprint.

Scott, R. 1973. *Finite Element Techniques for Curved Boundaries*. Ph.D. thesis, Massachusetts Institute of Technology.

Spikes, H. A. 1999. Thin films in elastohydrodynamic lubrication: the contribution of experiment. *Proceedings of the Institution of Mechanical Engineers J*, **213**, 335–352.

Szeri, A. Z. 2000. Stokes Flow, Reynolds Flow, Molecular Flow, Restrictions of Modelling Thin Films. *Rheology and Fluid Mechanics of Nonlinear Materials*, **252**, 93–105.

Wienands, R. 2001. *Extended Local Fourier Analysis for Multigrid: Optimal Smoothing, Coarse Grid Correction and Preconditioning*. Ph.D. thesis, Universität Köln.